Towards a unifying model of symmetry breakage in *Xenopus laevis*: serotonin signaling and the cilia-driven leftward flow

Dissertation zur Erlangung des Doktorgrades
der Naturwissenschaften (Dr. rer. nat.)

Fakultät Naturwissenschaften
Universität Hohenheim

Institut für Zoologie

vorgelegt von
Thomas Thumberger

aus Backnang
2011

Dekan:	Prof. Dr. Heinz Breer
1. berichtende Person:	Prof. Dr. Martin Blum
2. berichtende Person:	Prof. Dr. Heinz Breer
Eingereicht am:	20.09.2011
Mündliche Prüfung am:	11.11.2011

Die vorliegende Arbeit wurde am 24.10.2011 von der Fakultät Naturwissenschaften der Universität Hohenheim als „Dissertation zur Erlangung des Doktorgrades der Naturwissenschaften“ angenommen.

für Emma

Danksagung

Herrn Prof. Dr. Martin Blum danke ich für seinen Enthusiasmus mit dem er die Begeisterung für die Entwicklungsbiologie in mir geweckt hat, für die Überlassung des spannenden und breiten Themas, sein Vertrauen in meine Fähigkeiten und deren Förderung und die spannenden Nacht-Sessions vor Einreichung einer Publikation.

Herrn Prof. Dr. Heinz Breer danke ich vielmals für das Interesse an dieser Arbeit und der Bereitschaft, diese zu begutachten.

Ganz herzlich möchte ich mich bei PD Dr. Axel Schweickert bedanken. Einfach für alles und die letzten Jahre. Für das was ich lernen durfte, für Ideen, Balkondiskussionen und Frickeleien. Ein großer Dank gilt seinem dicken Fell, dass einige humoristische Tiefschläge aushalten musste. SNAFU!

Ein ganz besonderer Dank gebührt meinem Ex-Labornachbarn und Muse Dr. Philipp Vick ;) für lebhafte Diskussionen, kulinarische Hypothesen und alkoholisierte Versuche, für Lied Nr.9 auf Geräusch2 und für den Wochentag Freitag, den er erst dazu gemacht hat: „...clap your hands!“.

Bei meiner Laborschwester Dr. Tina Beyer möchte ich mich für 11 sympatisch-symbiontische Jahre bedanken! Es war eine tolle und unvergessliche Zeit inklusive Bock und Ramsch.

Bei allen Kollegen des 'Froschungslabors' möchte ich mich sehr herzlich bedanken! Eine tolle Atmosphäre und Diskussionen haben die Doktorandenzeit für mich unvergesslich gestaltet. Die Untermalung mit Musik, Kuchen, Filmen und Werwölfen eingeschlossen. Ein ganz großes DANKE geht natürlich an das wandelnde Laborlexikon Susanne!

Meiner Familie, meinen Schwiegereltern und Freunden danke ich für das Interesse an meiner Arbeit und den daraus folgenden Diskussionen über die verschiedenen Räume im Elfenbeinturm.

Mein letzter aber größter Dank gilt meiner wunderbaren Frau Anne, die mir den Rücken freigehalten hat, wenn es wieder einmal drunter und drüber herging und Emma für das stetige auffüllen meiner Serotonindepots.

Abstract

Orientation of the three vertebrate body axes anterior-posterior (AP), dorso-ventral (DV) and left-right (LR) is specified during early embryogenesis. Whereas the formation of the AP and DV axes is well understood, it is not finally resolved how and when the left and right sides get molecularly distinct. All deuterostomes analyzed so far, however, display an asymmetric left-sided expression of the TGF-β factor *Nodal* during embryonic development which precedes asymmetric organogenesis. In zebrafish, medaka, mouse and rabbit embryos a cilia-driven extracellular leftward fluid flow was shown to be causal for the left asymmetric induction of the Nodal gene cascade during early neurulation. In *X. laevis*, leftward flow was also shown to be driven by a mono-ciliated epithelium in the posterior part of the archenteron roof (gastrocoel roof plate, GRP). Mechanical blockage of this current resulted in laterality defects. Despite the apparent evolutionary conservation of flow, an earlier mechanism to specify the LR axis during early cleavage stages has been reported in *X. laevis*. Based on mostly inhibitor experiments, the so-called 'ion-flux' hypothesis was put forward which proposes an electrogenic transport and asymmetric accumulation of determinants as early as at the 32-64 cell stage. The monoamine serotonin is the core-effector of this hypothesis and was reported to asymmetrically accumulate at the ventral right blastomeres of early cleavage stage embryos.

The aim of this study was to investigate putative interactions of the two apparently opposing mechanisms for breaking the initial LR symmetry of the *Xenopus* zygote. Re-investigation of serotonin localization could not confirm the initial report. Further, serotonin signaling was shown to be necessary for LR axis formation on the dorsal but not ventral side, more specifically as a competence factor for the canonical Wnt-pathway. Detailed analyses of specimens impaired for serotonin signaling revealed requirement of serotonin signaling for specification of the superficial mesoderm (SM) which gives rise to the GRP and, consequently, to leftward flow. Leftward flow thus indirectly depends on dorsal serotonin signaling.

In a further part of the present thesis, a re-examination of laterality in Siamese twins was performed. It has been known since the earliest experimental investigations of laterality that in induced and naturally occurring Siamese twins the left twin consistently

displays wildtype orientation of the visceral organs whereas the orientation in the right twin is randomized. In experimentally induced conjoined twins, this observation holds true regardless of which twin is the induced. A model of symmetry breakage, in order to be plausible, thus should also be able to account for this phenomenon. When experimentally induced twins were analyzed for leftward flow, in the majority of cases a continuous leftward flow was observed, i.e. both twins shared one GRP. Thus, laterality cue(s) get translocated towards the far left side, i.e. only the left embryo receives the wildtype asymmetric information, regardless if it is the induced or endogenous twin. In rare case *X. laevis* conjoined axes developed far apart from one another such that two separate GRPs and individual leftward flows were observed, a condition that enabled both axes to exhibit a left-sided Nodal cascade. These experiments strongly suggest that Spemann's organizer itself is necessary and sufficient to establish all three body axes.

In conclusion, the present analysis of laterality determination in the frog *Xenopus* supports evolutionary conservation of leftward flow as symmetry breaking event, as previously reported for mouse, rabbit and bony fish.

Zusammenfassung

Die Orientierung der drei Körperachsen anterior-posterior (AP), dorso-ventral (DV) und links-rechts (LR) wird für Vertebraten während der Embryogenese festgelegt. Obwohl die molekularen Mechanismen, die die AP und DV Achse festlegen gut bekannt sind, ist bisher nicht genau geklärt, wann und wie die linke und rechte Hälfte des sich entwickelnden Embryos ihre asymmetrische Identität erhalten. In allen bisher untersuchten Deuterostomiern wurde während der Embryonalentwicklung eine linksseitige Expression des TGF-β Faktors Nodal nachgewiesen, die jeweils der asymmetrischen Organogenese vorausgeht. Im Zebrabärbling, Medakafisch, Maus und Kaninchen wird diese Nodal-Genkaskade durch einen extrazellulären, von Cilien angetriebenen linksgerichteten Flüssigkeitsstrom induziert. Auch für den Krallenfrosch *X. laevis* konnte diese im posterioren Bereich des Archenterondaches ('gastrocoel roof plate', GRP) gezeigt werden. Eine mechanische Störung dieser Strömung verursachte

Lateralitätsdefekte. Neben der augenscheinlichen Konservierung der Flüssigkeitsströmung wurde für die Spezifizierung der LR Achse im *X. laevis* eine zeitlich sehr viel frühere Asymmetrie während der ersten Furchungsstadien berichtet. Die daraus abgeleitete, größtenteils auf Inhibitorexperimenten basierende 'Ionenfluss'-Hypothese setzt einen elektrochemischen Transport und eine daraus resultierende asymmetrische Ansammlung von Determinanten der LR Achse bereits im 32-64 Zellstadium voraus. Die zentrale Rolle in diesem Modell kommt dem Monoamin Serotonin zu, das bereits während der ersten Furchungsteilungen asymmetrisch verfrachtet und in ventralen rechten Blastomeren angereichert werden soll.

Das Ziel der vorliegenden Arbeit war es, eine mögliche Interaktion dieser beiden offenbar unterschiedlich wirkenden Mechanismen in Bezug auf den Bruch der initialen LR Symmetrie der Xenopuszygote zu ermitteln. Eine erneute Untersuchung zur Verteilung von Serotonin konnte die bereits publizierten Ergebnisse nicht verifizieren. Weiterhin konnte gezeigt werden, dass die Wirkung von Serotonin auf der dorsalen aber nicht ventralen Seite wichtig ist für die Bildung der LR Achse. Im Speziellen könnte Serotonin dabei als Kompetenzfaktor für den kanonischen Wnt-Signalweg wirken. Detaillierte Untersuchungen in Embryonen in denen die Wirkung von Serotonin unterbunden wurde ergaben, dass Serotonin die Spezifizierung des superfiziellen Mesoderms (SM), welches das Vorläufergewebe der GRP darstellt, steuert. Der linksgerichtete Flüssigkeitsstrom ist somit indirekt abhängig von der dorsalen Wirkung von Serotonin.

Ein weiterer Teil dieser Doktorarbeit widmet sich der Lateralität von siamesischen Zwillingen. Seit den ersten experimentellen Untersuchungen zum Organsitus von Embryonen ist bekannt, dass in natürlich auftretenden sowie in experimentell induzierten siamesischen Zwillingen ein Phänomen bezüglich des Organsitus auftritt: die Organe des linken Zwillings sind stets wildtypisch angeordnet wohingegen der rechte Zwilling einen randomisierten Organsitus aufzeigt. In experimentellen siamesischen Zwillingen konnte gezeigt werden, dass dieses Phänomen auftritt, egal welcher der beiden Zwillinge induziert war. Daher sollte ein Mechanismus zum Bruch der bilateralen Symmetrie dieses Phänomen eindeutig erklären können. In siamesischen Zwillingen konnte dabei eine linksgerichtete Flüssigkeitsströmung nachgewiesen werden, die sich zumeist über einen gemeinsamen Bereich der

fusionierten GRPs der beiden Zwillinge bewegte. Daher sollte ein transportiertes oder durch die Flüssigkeitsströmung generiertes Signal nur vom jeweils linken Zwilling wahrgenommen werde können, unabhängig davon ob dieser induziert oder endogen ist. In seltenen Fällen entwickelten sich die dorsalen Achsen der siamesischen Zwillinge weit genug von einander entfernt, so dass zwei getrennte, funktionelle GRPs entstanden, die jeweils eine linksgerichtete Flüssigkeitsströmung generierten und somit beide Zwillinge eine wildtypische Nodal-Genkaskade aufzeigten. Diese Experimente deuten stark darauf hin, dass der Spemann-Organisator sowohl notwendig als auch hinreichend ist, um alle drei Körperachsen zu etablieren.

Die vorliegende Doktorarbeit unterstützt daher eindeutig die Hypothese, dass auch im Frosch *Xenopus laevis* der Symmetriebruch durch den linksgerichteten Flüssigkeitsstrom erfolgt und daher evolutionär konserviert ist.

Table of contents

Table of figures

I Introduction

The anatomical Bauplan of all higher organisms is composed by specifically arrange organs, tissues and peripheral body parts along predefined axes. The specification of these axes is the most elementary process during embryogenesis. In many cases, the first axis (animal-vegetal) is maternally determined in the oocyte and represents the anterior-posterior (AP) axis during later embryogenesis. The Radiata (e.g. jellyfishes) keep this sole axis and therefore display radial symmetry. Bilateria in contrast, develop a second body axis after fertilization, i.e. the dorso-ventral (DV) axis. Thus the embryo appears bilaterally symmetrical from the outside. A three-dimensional body, however, is not sufficiently defined by two axes. Like in a Cartesian coordinate system, axes are perpendicular to each other which demands a third, the left-right (LR) body axis. In vertebrates, the necessity to define a third body axis is particularly obvious, as the visceral organs are asymmetrically arranged in a preserved manner. However, as the DV axis is randomly but perpendicularly aligned on the AP axis, left and right sides cannot be predefined but must be specified thereafter. The point in time and the mechanism by which this is achieved is still not satisfactorily solved and may even differ phylogenetically. For vertebrates, development along these axes begins with the cleavage of the zygote and proceeds with gastrulation, neurulation and organogenesis (Wolpert et al. 1997; Gilbert 2006).

I.1 Embryogenesis

Fertilization of the oocyte is followed by cleavage, i.e. rapid mitotic divisions of the zygote, which results in so called blastomeres – the cells of the early embryo. Species with yolk-rich zygotes mostly perform meroblastic (or partial) divisions (e.g. birds). In the majority of eggs with sparse yolk content cleavage furrows, in contrast, extend holoblastically, i.e. throughout the entire zygote (e.g. in mammals). Usually this process produces a spherical embryo, the so-called blastula. Often, the blastula develops a fluid filled cavity (blastocoel) in its center. This fluid spacer separates the germ layers ectoderm, endoderm and – in case of triploblastic species – mesoderm to inhibit tissue

interaction ahead of time. During the subsequent stage of gastrulation, the germ-layers become rearranged such that the ectoderm covers the outer surface of the embryo, the endoderm lines the inside of the forming gastrocoel and mesoderm is placed in between. The gastrocoel, also known as archenteron or primitive gut, is of importance because it will not only give rise to the future digestive tract but also to the majority of the visceral organs which develop by budding off of this structure. Shape conversion during gastrulation is driven by a multitude of cellular forces, e.g. apical constriction, bottle-cell formation and cell migration, epiboly and convergent extension (CE). The latter is a process by which cells rearrange by intercalation which narrows the tissue mediolaterally but elongates it perpendicularly to the plane of cell movement (Wolpert et al. 1997; Gilbert 2006).

Subsequently, neurulation takes place in the dorsal neuro-ectoderm which is obvious by elevation of the neural folds that fuse at the embryonic midline to give rise to the neural tube (e.g. in *Xenopus laevis*). The anterior portion will give rise to the brain, whereas the caudal part will become the spinal chord. Ventral to the neural tube, the notochord forms as dorsal most mesodermal tissue which stretches the embryo along the AP axis by CE. In the paraxial mesoderm, somites are formed on both sides of the developing notochord. With the end of neurulation the phylotypic stage emerges which is known as the pharyngula in vertebrates. At this point in development all vertebrate embryos look most alike, even though earlier and later development is very divergent and derived (Wolpert et al. 1997; Gilbert 2006).

Also, when the germ layers are in correct position, cells interact, rearrange and form precursors for the organs. Often these precursors are composed of cells from different germ layers. Therefore during organogenesis, some cells undergo long migrations like the precursors of blood, lymph or pigment cells to reach their final location (Wolpert et al. 1997; Gilbert 2006).

I.2 *Xenopus laevis* as model organism for early embryonic development

The first embryological experiments performed in the 19th century were based on the easily accessible spawn of wild living amphibians. Plagued with only seasonal availability, all kinds of urodele and anuran species were used at that time. In the 1930s it was discovered that spawning of mature amphibian oocytes could be induced by injecting urine of pregnant women into the dorsal lymphatic sac of the African clawed frog *Xenopus laevis*. With this, not only a first pregnancy test was established, but with purification and injection of the human chorion gonadotropin, accessibility of embryos was now possible perennially. *Xenopus* colonies were established in European and North American laboratories and *X. laevis* was introduced as model organism for early development. The spawnings of hundreds of eggs can be fertilized *in vitro* and the relatively large size (~1mm) of the zygote allows manipulation by microsurgery (ablation or transplantation) or microinjection (reviewed in Gurdon & Hopwood 2000).

I.2.1 Orientation of primary body axes is defined at fertilization

The mature oocyte is pre-patterned with respect to the animal-vegetal axis. The animal pole contains the nucleus and maternally provided mRNAs and proteins. It is pigmented and therefore appears darker than the yolk-rich vegetal pole. After fertilization which can occur anywhere within the animal hemisphere, the vitelline membrane detaches and the zygote is free to get aligned by gravity which is obvious from the vegetal pole facing downwards. With the entry point of the sperm, the orientation of the DV axis is determined with ventral being represented by the point of entry and the dorsal side opposing this position. Re-arrangement of microtubules (MTs) in the cortex of the zygote is organized by the sperm centriole. With the help of these MTs, cortical rotation takes place, i.e. the whole cortical cytoplasm rotates about 30° across the animal pole towards the point of sperm entry. By this, vegetally localized Dishevelled (Dsh) protein and *Wnt11* mRNA gets transported to specify the future dorsal side (see below; Gilbert 2006; Nieuwkoop & Faber 1967; Wolpert et al. 1997).

About 90 minutes past fertilization, the first cleavage furrow starts animally and divides the zygote with some range of deviation along the prospective embryonic midline, i.e. left and right blastomeres are separated (Klein 1987; Masho 1990). The second cleavage furrow forms perpendicularly to the first, also starting at the animal pole dividing the embryo in ventral and dorsal blastomeres. The resulting 4-cell stage can thus already be aligned along the axial coordinate system. Due to the cortical rotation, pigment is shifted along with the cortex towards the ventral side. This segregation is retained by the second cleavage furrow, which renders the animal part of the two prospective dorsal blastomeres slightly lighter than the same region of ventral ones. As the dorsal cells contain the factors re-localized during cortical rotation, the way has been paved for the specification to happen. Also the left and right blastomeres can be deduced logically although they are not yet molecularly distinct from one another. Finally, cleavage leads to the formation of a spherical blastula inside which a fluid filled cavity is generated (Gilbert 2006; Wolpert et al. 1997; Sive et al. 2000).

I.2.2 Gastrulation and patterning of the embryo

The proteins encoded by maternally deposited mRNAs of *vegetal-T* (*VegT),* the *wingless-type MMTV integration site family, member 11* (*Wnt11*) and the member of the transforming growth factor-beta (TGF-β) superfamiliy, the *growth differentiation factor 1* (*gdf1* or *Vg1*) pattern the early embryo (Tao et al. 2005). Vg1 and VegT are found in a vegetal to animal gradient and induce further TGF-β members, the *Xenopus nodal related* (*Xnr*) genes (Heasman 2006). In addition these maternally provided TGF-β factors specify mesoderm formation, therefore, the blastocoel serves as a physical barrier to ensure that the animal cells beyond the cavity are not exposed to these factors and fate stays ectodermal (Wolpert et al. 1997). Thus the blastula is patterned with prospective ectoderm at the animal pole, endoderm is situated vegetally and mesoderm in between at the equatorial region, the so-called marginal zone. In *X. laevis*, this presumptive mesodermal belt is superimposed with a single cell layer of endoderm except for the most dorsal part. Here, mesoderm lies also superficially (superficial mesoderm, SM; Fig. 1A; Shook et al. 2004). Also on this side, in the cells which descended from the subset of the blastomeres that obtained the shifted Dsh

protein and *Wnt11* mRNA during cortical rotation, the canonical Wnt-pathway is activated (Gilbert 2006; Wolpert et al. 1997).

The canonical Wnt pathway

Canonical Wnt-signaling is thought to function as follows: Wnt ligands bind to a transmembrane receptor complex of frizzled and the low-density lipoprotein receptor-related proteins 5 and 6 (LRP5/6). After binding, this ternary complex is internalized into signalosomes and the cytoplasmatic domain of the co-receptor LRP6 is phosphorylated by Casein kinase 1γ (CK1γ). This promotes recruitment of Axin, which in absence of a Wnt ligand would target β-catenin (β-cat) for degradation in a complex with APC (adenomatous polyposis coli) and glycogen synthase kinase-3 (GSK3; Cruciat et al. 2010). In the presence of a Wnt-lignad, β-cat becomes stabilized and can enter the nucleus to form a heterodimer with a LEF or TCF DNA-binding protein. This heterodimer acts as a transcription factor (TF) and activates canonical Wnt responsive genes like the homeoboxgene *Siamois* or the TGF-β gene *Xenopus nodal related-3* (*Xnr3*). The exact role for the scaffold protein Dsh in this newly elaborated context remains elusive (Bilic et al. 2007; Gilbert 2006). Undoubtedly, Dsh has the potential to activate the canonical Wnt-pathway as it does after cortical rotation or upon misexpression (Sokol 1996). In the region where dorsal (Wnt) and vegetal signals (Vg1/VegT) overlap, the Nieuwkoop center is specified. This dorsal signaling center remains endodermal but specifies the most important embryonic signaling center directly animal to itself: the Spemann organizer (Boterenbrood & Nieuwkoop 1973).

The Spemann organizer

The rearrangement of tissue during gastrulation relies on the organization capability of the dorsal lip. It was Hans Spemann and Hilde Mangold who discovered the eponymous organizer in a groundbreaking transplantation experiment in 1924. When they performed heterologous grafting experiments of the dorsal lip of a gastrulating unpigmented newt embryo (*Triturus cristatus*) onto the ventral region of a pigmented newt species (*Triturus vulgaris*) of the same developmental stage, dorsal structures were induced in the host embryo. In the best case, a full secondary axis developed and siamese twins were generated which were ventrally fused. By using two differently

pigmented species, it was further traceable that the cells that gave rise to the second axis were pigmented and thus provided by the host embryo except for the notochord which displayed absence of pigmentation. Spemann and Mangold concluded that the dorsal tissue of the dorsal lip has axis induction ability and induces the surrounding tissue to undergo dorsalization (Spemann & Mangold 1924; Gilbert 2006).

Today it is known that the Spemann organizer expresses a range of different TFs like *Goosecoid* and *Siamois*, different *Xnr* genes and the secreted growth factor antagonists *chordin*, *noggin* and *follistatin* among others. The latter antagonizes the ventralizing bone morphogenic proteins 2 and 4 (BMP2, BMP4) which are released to ventrally pattern the mesoderm. Therefore, the Spemann organizer prevents ventralization of the dorsal side (Gilbert 2006; Wolpert et al. 1997).

The endogenous amounts of the dorsal and ventral antagonizers lead to the formation of the embryo true to type. Disruption of this balance results in misshaped embryos which is evaluated by the dorso-anterior index (DAI; Kao & Elinson 1988). An equilibrium of dorsal and ventral factors lead to wildtype embryos (DAI = 5). In contrast, overrepresented dorsal signaling molecules lead to specimens that develop larger anterior and dorsal structures, i.e. the DAI tends to 10 with increasing dorsalization (Kao & Elinson 1989). On the other hand, absence of dorsalizing factors or higher content of BMP2/4 (Clement et al. 1995) cause ventralization of the embryo which is reprsented by a DAI that tends to 0. If all dorsal structures are lacking, a so-called 'bauchstück' (DAI = 0) is generated (Kao & Elinson 1988). However, these changes to the axial setup are visible only after gastrulation.

Gastrulation and neurulation

Molecularly, gastrulation is initiated only after the midblastula transition (MBT), a temporal border after which the genome of the zygote is being transcribed. All earlier processes were driven by translation of maternally provided mRNAs or maternally deposited proteins (Newport & Kirschner 1982). The organizer initiates gastrulation in the dorsal marginal zone (DMZ) just below the equator. Gastrulation causes one of the most dramatic changes to the early embryo. The concert of tissue specification, rearrangement and shaping of the early body was and is still one of the most investigated processes during embryogenesis. In the words of Lewis Wolpert: *'It is not*

birth, marriage, or death, but gastrulation, which is truly the most important time in your life.' (Wolpert et al. 1997).

In *X. laevis*, onset of gastrulation is visible by so-called bottle cells at the DMZ. These cells undergo a shape-change such that the apical membrane (the membrane facing the outside) becomes downsized and the main part of each cell is displaced into the layer of deep mesoderm. This coordinated apical constriction (AC) termed process is driven by actomyosin contractility (Lee & Harland 2007). In *X. laevis*, AC of the bottle cells is visible as pigment granules in these membranes concentrate and subsequently form a slit like depression, the so-called dorsal blastoporal lip. However, if AC or bottle cell formation is inhibited (Lee & Harland 2010) or bottle cells are ablated surgically (Keller 1981), gastrulation still proceeds. Only if also part of dorsal deep mesoderm is removed, gastrulation does not initiate (Keller 1981).

The bottle cells and deep mesoderm of this region arrest their movement and serve as hinge point for the following gastrulation movements. The tissue animally to the bottle cells is pushed vegetally, thereby passing the arrested bottle cells. Thereby involution, i.e. spreading of internalized cells along the internal surface of the outer layer is started. This movement is further supported by epiboly of the animal cap, the opposite process to CE, as here a thick cell sheet flattens by intercalation of the cells from different layers into a single one. Simultaneously the tissue enlarges mediolaterally. The first cells that involute over the dorsal lip are pushed furthest into the inside of the embryo and will give rise to the prechordal plate. These are followed by the superficial and deep mesodermal cells of presumptive notochord. As gastrulation progresses, the dorsal lip extends to both sides forming a semi-circle and finally the ventral lip emerges and the blastopore now depicts a ring-like groove. Here mesoderm gastrulates that will give rise to the heart or kidneys among contributing to other organs. As more and more cells involute into the embryo, the blastocoel vanishes and the gastrocoel – also known as archenteron – is formed. The ring-like blastopore shrinks until the end of gastrulation when it is merely visible as a tiny slit-like indentation, presenting the opening of the prospective cloaca. Now, the embryo is covered by ectoderm and neuroectoderm, endodermal cells line the gastrocoel or are otherwise internalized completely and mesoderm has found its position in between these layers (Keller 1981; Shook et al. 2004; Lane & Keller 1997; Gilbert 2006; Wolpert et al. 1997).

During neurulation, the notochord and neural tube elongate and stretch the embryo along the AP axis. Simultaneously, the neural tube closes in a zip-like fashion from caudal to rostral. Now, the whole embryo is covered with ectoderm that will give rise to the epidermis. In the paraxial mesoderm, somites are formed flanking the notochord and the trunk-organizer (a remnant of the dorsal organizer) splits from the circumblastoporal collar (cbc) after the body elongated. The tail grows out with its tip still performing gastrulation and neurulation processes. After neurulation, the *Xenopus* embryo has clearly visible DV and AP axes and left and right sides can be distinguished (Gilbert 2006; Wolpert et al. 1997).

I.3 The left-right axis

With organogenesis, the mirror image appearance of the left and right sides is obviously established in all vertebrates. Most organs arrange and form asymmetrically along all three body axes, however, the external appearance of bilateral symmetry is not affected in most cases. In humans for instance, the apex of the heart points to the left, whereas the liver is situated on the right. In addition, the lungs have only two lobes on the left but three lobes on the right side. The heart and pulmonary system also display asymmetrical functions such as direction of blood flow, i.e. pumping of relatively oxygenated blood into the body via the left ventricle and relatively deoxygenated blood into the lungs via the right ventricle and the pulmonary artery (Cooke 2004). The wildtype arrangement of the visceral organs is called *situs solitus* and is not random but evolutionarily highly conserved among vertebrates.

However, there are variations to the organ situs. The terminology 'heterotaxia' covers the phenomena of randomly oriented organs, duplications or deletions thereof. About 3% of neonatal heart diseases in human fetuses are caused by heterotaxia. The most frequent case among these is the transposition of the great arteries in which the connection of the pulmonary artery and the aorta are switched at the ventricles. Nowadays, this can already be cured by surgery *in utero* (Hövels-Gürich et al. 1997). Most of these heterotaxia cause severe pathological effects if not embryological lethality. However, in one of 10.000 humans born, the whole organ situs is a complete

mirror image (*situs inversus totalis*). This often stays undetected until medical care is needed by chance as no pathological effects arise.

Of these observations, two conclusions can be drawn: (1) the orientation of the LR axis has no impact on the physiology as long as all organs are affected and thus are aligned correctly with respect of one another (*situs solitus* or *situs inversus*); (2) as the asymmetric arrangement of the organ situs is predictive in all vertebrates, there has to be a basic principle in symmetry breakage during embryogenesis, i.e. specification of the LR axis before organogenesis.

In *X. laevis*, AP and DV axes are defined with fertilization and the zygote is logically divided into a left and right side. However, as the orientation of the first two axes relies on the sperm entry point anywhere at the animal hemisphere (Sive et al. 2000), left and right sides cannot be predefined maternally. The general question how and when the left and right side get molecularly distinct is not finally resolved and may even underlie different mechanisms in different species. However, common in all deuterostomes analyzed so far is a LR asymmetric expression of the TGF-β factor *Nodal* during embryonic development which precedes asymmetric organogenesis.

I.3.1 The conserved Nodal-cascade

In chick embryos, an asymmetric left-sided gene-cascade was described in 1995 (Levin et al. 1995) which in the meanwhile as been shown to be conserved in all vertebrates (Lowe et al. 1996; Long et al. 2003). It consists of the following major factors: the TGF-β family members *Nodal* (Lowe et al. 1996; Long et al. 2003) and the *left-right determination factor* (*lefty;* Meno et al. 1996; Thisse & Thisse 1999) as well as the *paired-like homeodomain transcription factor 2* (*Pitx2;* Campione et al. 1999; Ryan et al. 1998). During neurulation, *Nodal* is asymmetrically activated in the posterior part of the left lateral plate mesoderm (LPM) and rapidly spreads anterior-wards (Ohi & Wright 2007). Here, Nodal signaling results in transcriptional induction of *Nodal* itself but also initiates expression of its antagonist Lefty. As the diffusion-rate of lefty is higher than that of Nodal, *Nodal* expression is restricted to the left side (Marjoram & Wright 2011). This is further supported by a second *lefty* domain in the notochord and neural tube preventing Nodal from crossing the midline ('midline barrier'). The inhibitory effect of

Lefty on Nodal is mediated by allosteric binding of Lefty to the same TGF-β receptor complex Nodal would bind to to activate its own expression (Bisgrove et al. 1999; Cheng et al. 2000). This receptor complex consists of two type I receptor ALK4 subunits and two type II receptor ActRII units. Activation of this receptor by Nodal depends on a co-factor of the epidermal growth factor-like-cripto/FRL-1/cryptic family 1 (EGF-CFC) class (Shen 2007). Binding of Nodal to this receptor complex leads to the phosphorylation of Smad 2 or 3 which complexes with Smad 4 to form an active TF that enters the nucleus and regulates gene transcription (Shen 2007). In contrast to the transient expression of *Nodal* in the left LPM, the TF *Pitx2* is activated in the left heart field by the Nodal-cascade. Pitx2 stays active during organogenesis and is the mediator of LR asymmetry (Davis et al. 2008; Simard et al. 2009). When the Nodal-cascade is ectopically activated in the right but not left LPM, *situs inversus* results, whereas absent or bilateral Nodal-cascades in the LPMs lead to heterotaxia (Lohr et al. 1997; Mogi et al. 2003).

The Nodal-cascade is very highly conserved among vertebrates, but can also be found in primitive chordates like the cephalochordate *Branchiostoma floridae* (Yu et al. 2002) and echinoderms like the common sea urchin *Paracentrotus lividus* (Duboc et al. 2005). We have previously argued that this asymmetric expression is located on the left side of the larva and thus evolutionarily conserved (Blum et al. 2009b).

I.3.2 Symmetry breakage

Historical observations

In the early 20th century, Spemann and Falkenberg found recurrent aberrant organ situs in siamese twinned newt embryos (*T. cristatus*) which were created by completely or partially ligating cleavage and blastula stage embryos. At this time, this phenomenon was already known from spontaneous human conjoined twins. Interestingly, in human conjoined twins as well as in the newt experiments, it was consistently the left twin which showed *situs solitus* and the right twin which displayed *situs inversus* or heterotxia (Spemann & Falkenberg 1919). Further experiments included 180° inversion of a dorsal roof fragment in neurulating embryos of the yellow-bellied toad (*Bombinator*

variegata) which led to complete situs inversion in more than 80% of manipulated embryos (Wilhelmi 1921). On the other hand, heterotaxia was seen when left but not right tissue was ablated (Wilhelmi 1921). In both cases it can be assumed that with the dorsal fragment, a part of the the left LPM containing the asymmetric *Nodal* domain was manipulated by transplantation in the former or ablation in the latter experiments (Blum et al. 2009a).

The F-Molecule

Lewis Wolpert and Nigel Brown postulated a chiral molecule that, when aligned to the AP and DV axis, points into the same direction. Along this chirality, a morphogen should be distributed or be able to diffuse and would hence accumulate only on one side of the embryo, asymmetrically converting the tissue after interpretation of this signal (Brown & Wolpert 1990).

The Kartagener Syndrome

No such molecule was found, instead evidence that organ situs relied on motile cilia arose and accumulated since the studies of the human Kartagener Syndrome (or immotile cilia syndrome). The affected patients exhibit immotility of cilia due to apparent lack of axonemal dynein arms. This typically leads to chronical inflammation of the upper and lower respiratory tract, infertility and interestingly to *situs solitus* in 50% of cases (Kartagener 1933; Afzelius 1976). From this study it became clear that at one point during specification of the LR axis, motile cilia should play a decisive role

I.3.3 Ciliogenesis and cilia function

Cilia are cellular protrusions on nearly all cells in the animal kingdom. Cells can be mono- or multiciliated. Besides motility for propelling fluids, they act as extended sensors for chemical or mechanical stimuli or they simply prevent the cell from undergoing cell division. The latter is caused by the cilium growing out of the basal body which is formed of one of the centrioles. Once re-entering the cell cycle, the primary cilium is resorbed just to grow out again on each daughter cell. The basal body aligns to the apical cell membrane and the ciliary skeleton (axoneme) is assembled (reviewed in

(Satir et al. 2010)). The axoneme consist of nine doublet MTs circularly arranged around the center which can contain none, two or four single MTs (termed 9+0, 9+2, 9+4, respectively; (Feistel & Blum 2006)). The whole structure is enveloped by the cell membrane. Outgrowth is organized by intraflagellar transport (IFT) where kinesin 2 motorproteins (kinesin superfamiliy, KIF) move cargo to the tip of the cilium (anterograde) and cytoplasmic dynein 2 towards the base (retrograde). This setup is common in immotile as well as motile cilia. Motility in addition is gained by axonemal dynein complexes attached to the outer MTs of which the dynein heavy chain accomplishes the motor function. Motility as the consequence is achieved by exercising force of one axonemal dynein complex onto the neighboring MT. As the MTs are interconnected via Nexins, they do not slide along one another, but force is transformed into bending of the whole cilium. Serial regulation of this process leads to either whip-like beat pattern or rotational propelling. Formation, structure, maintenance and function of axonemal proteins are highly conserved from the green alga *Chlamydomonas reinhardtii* to humans (Satir et al. 2010).

I.3.4 Cilia-driven leftward flow

In 1998, the prediction based on the Kartagener Syndrome that motile cilia should be necessary for LR axis formation could be verified in mouse embryos (Nonaka et al. 1998). At the ventral tip of the neural stage egg cylinder, the notochordal plate grows out of Hensen's node which represents the organizer in mammals (Blum et al. 2007). The notochordal plate can be split in two regions, the posterior part (posterior notochord, PNC) which forms a small pit-like indentation of monociliated cells and the anterior part lining the rostral embryonic midline (Supp et al. 1997). Nonaka et al. demonstrated that the cilia of the PNC were motile and drive a vectorial leftward flow through the extracellular medium (Nonaka et al. 1998). The mouse mutant *inversus viscerum* (*iv*) lacks the functional *left-right dynein* (*lrd*) gene, a dynein axonemal heavy chain with expression in the PNC. Leftward flow was absent in *iv/iv* mice, and the Nodal-cascade was not induced in the left LPM which resulted in aberrant organ situs (Okada et al. 1999). By exposing such mutant embryos to an artificial flow that pointed leftward, the Nodal-cascade was rescued. Intriguingly, when the artificial flow was

inverted to point rightward, the Nodal-cascade was activated exclusively in the right LPM in both, *iv* and wildtype mouse embryos (Nonaka et al. 2002). This clearly demonstrated, that the physical event of the fluid flow and its direction decides on laterality in mice.

At the time, when this extracellular flow was discovered in the mouse, the indentation of the PNC was not discriminated from the posteriorly placed Hensen's node, thus both structures shared the terminology 'node' (Beddington & Robertson 1999) which also led to the designation of 'nodal-flow' (Nonaka et al. 1998). However, in a recent histological approach, our group could demonstrate, that both are distinct structures (Blum et al. 2007). From now on the terminology 'node' is used when Hensen's node, the Spemann organizer or homologous structures are referred to and 'leftward flow' when the cilia driven vectorial leftward flow at the PNC is meant.

A characteristic of the murine PNC is the bilateral expression domain of Nodal in the lateral most PNC cells – the so-called crown-cells. If this very domain is deleted by mutating the node-specific enhancer, the Nodal-cascade is absent from the left LPM, clearly demonstrating that the Nodal domain at the PNC precedes the Nodal-cascade (Adachi et al. 1999; Brennan et al. 2002; Saijoh et al. 2003). It was further reported that the intensity of the bilateral Nodal domain at the PNC is slightly increasing asymmetrical in the left crown-cells as a function of leftward flow (Marques et al. 2004). Simultaneously, the Nodal inhibitor *cerberus-like2* (*cerl-2*) – a member of the Wnt / TGF-β / BMP binding protein family of secreted factors – which is expressed in the very same domain, showed increased expression in the right crown-cells after flow (Oki et al. 2009). Relevance of this factor was demonstrated as the *cerl-2*$^{-/-}$ knockout displayed mostly bilateral expression of Nodal in the LPM of both sides.

The generation of leftward flow is caused by two characteristics of the PNC cilia: (1) the posterior positioning of the PNC cilia on each cell and (2) the clockwise rotational beat pattern. Due to the convex surface of the cells and the characteristic of cilia to insert orthogonally to the membrane, the posterior polarization leads to a posterior tilt of the cilium. Their clockwise rotation thus strikes through the extracellular medium on its way to the left and returns at the level of the cell membrane (Nonaka et al. 2005). As all cilia are aligned likewise, the fluid layer directly above the cilia is pushed leftward. Posterior polarization of the cilia is generated by planar cell polarity (PCP; Hashimoto et

al. 2010; Song et al. 2010). PCP is driven by a variation of the Wnt-pathway, i.e. the PCP- or non-canonical Wnt-pathway which is independent of the APC-complex and β-catenin.

All mutations that affect the formation of the PNC, ciliogenesis or cilia polarization lead to LR defects. In mice mutant for Brachyury for example, mesoderm is not specified properly and the whole PNC is missing (Andre 2009). The immotile PNC cilia of the *iv/iv* mouse demonstrate that ciliogenesis *per se* is not sufficient for LR axis specification, instead motility is a requirement. In PNC devoid of cilia no flow but subsequent LR defects are found like in mutants of the ciliary assembly genes *Kif3a/b* (Okada et al. 1999).

In the meantime, leftward flow was also shown to regulate LR axis orientation at the PNC of rabbits (*Oryctolagus cuniculus*; Okada et al. 2005) or the Kupffer's Vesicle (KV) in zebrafish (*Danio rerio*; Essner et al. 2005; Kramer-Zucker et al. 2005) and medaka (*Oryzias latipes*; Hojo et al. 2007). Recently we described this event also to occur at the dorsal roof plate of the archenteron of neurula stage *X. laevis* embryos (Schweickert et al. 2007), strongly suggesting that leftward flow is evolutionarily conserved.

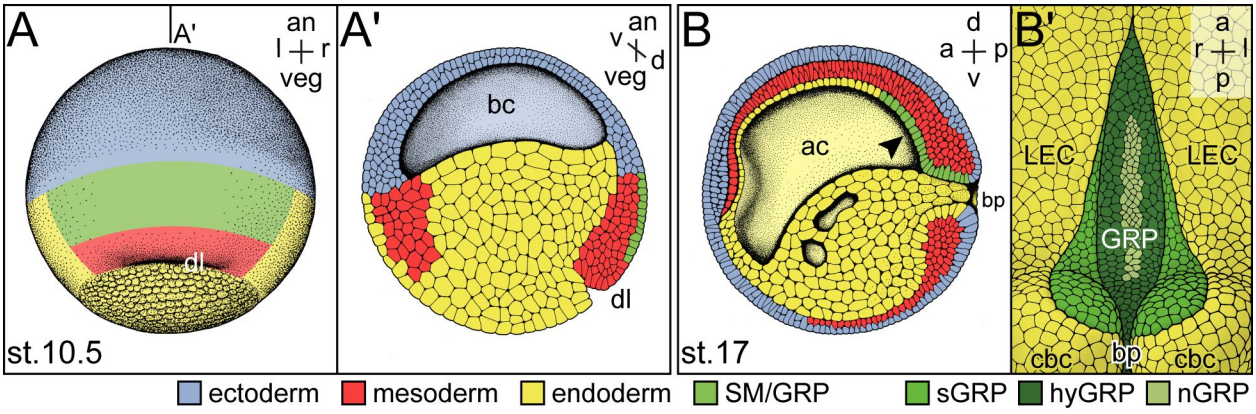

Fig. 1 Superficial mesoderm gives rise to the gastrocoel roof plate during gastrulation
(A) By early gastrula, the embryo is patterned in ectoderm (blue), endoderm (yellow) and mesoderm (red) of which the most dorsal lies superficially (superficial mesoderm, SM; green). **(B)** With gastrulation, the SM cells give rise to the gastrocoel roof plate (GRP) which lines the dorsal midline of the archenteron (ac). **(B')** the GRP is subdivided by different cellular fates in somitic GRP cells (sGRP), hypochordal GRP cells (hyGRP) and notochordal GRP cells (nGRP).
a, anterior; an, animal; ac, archenteron; bc, blastocoel; cbc, circumblastoporal collar; d, dorsal; dl, dorsal lip; l left; LEC, lateral endodermal crest, p, posterior; r, right; v, ventral; veg, vegetal

I.3.5 Leftward flow is crucial for LR axis formation in *X. laevis*

In *X. laevis*, the epithelium that drives leftward flow also lies anterior to the organizer. Due to the complex gastrulation movements and reshaping of the embryo, the epithelium 'anterior' to the dorsal lip is the gastrocoel roof plate (GRP) which involuted to the inside of the gastrula (Fig. 1A-B'; Shook et al. 2004). The GRP is of mesodermal fate as it derives from the dorsal SM (Fig. 1A). It is a transient structure found from stage 13 up to stage 21. By then the GRP cells ingress into deeper mesoderm to contribute to three different structures. The most lateral GRP cells (sGRP) are part of the presomitic mesoderm and will be incorporated into somites when the GRP disappears. The next column of cells will give rise to the hypochord (hyGRP) and the most central cells will intercalate into the notochord (nGRP) above (Fig. 1B'; Shook et al. 2004). Monocilia emerge in central positions on each GRP cell from stage 13 onwards. The subpopulation of hyGRP and nGRP cilia get polarized to the posterior pole of each cell (Fig. 2A, B) by stage 17, whereas the bulk of cilia on sGRP cells stay central (Schweickert et al. 2007). Like in the mouse, GRP cilia are motile (Fig. 2A) and display a rotational beat pattern which drives a leftward flow (Fig. 2B). At stage 15 flow initiates in a turbulent manner due to central orientation of cilia. With lengthening and posterior polarization of the GRP cilia, leftward directionality of flow develops and

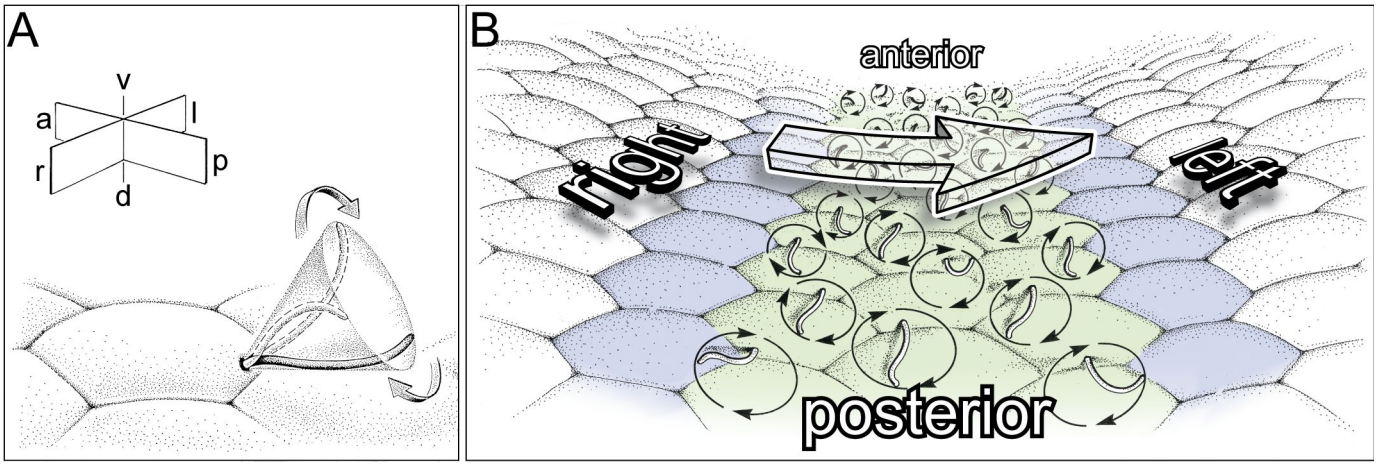

Fig. 2 Posteriorly polarized GRP cilia drive an extracellular leftward fluid flow
(A) Schematic view of posterior positioned monocilium at the GRP. The clockwise rotation thereof drives a vectorial leftward fluid flow in the extracellular medium above the epithelium of the GRP **(B)**. Note: yet unknown positioning of the bilateral midline domain of *Xnr1*/*Coco* relative to the GRP (blue).
a, anterior; d, dorsal; l, left; p, posterior; r, right; v, ventral

velocity increases. At stages 17/18 leftward flow is most robust and from stage 19 onwards, leftward flow breaks down as the GRP vanishes. Relevance of leftward flow for the specification of the LR axis was demonstrated by mechanically blocking the current by increasing the viscosity of the archenteron fluid upon injection of 1.5% methylcellulose into the gastrocoel. Subsequently, flow was abolished, the Nodal-cascade was not induced in the left LPM and situs defects developed (Weber 2006; Schweickert et al. 2007). Hence, the GRP provides the same functionality like the murine PNC for symmetry breakage. Conserved features further entail a bilateral *Xnr1* (*Xenopus Nodal related 1*) expression domain in the posterior paraxial mesoderm. It needs to be investigated if this domain is part of the GRP or if it is flanking the latter. In this very domain also the *Xnr1* inhibitor *Coco* (homolog of the murine *cerl-2* gene) is expressed. Interestingly, Coco – the inhibitor of Nodal – only caused LR defects, when its right but not left portion of the bilateral midline domain was ablated (Vonica & Brivanlou 2007).

I.3.6 Possible perception and transfer of the asymmetric cue

Although leftward flow is necessary for LR axis formation in fish, amphibians and mammals, perception and transfer of the asymmetric information into the left LPM is still poorly understood. As leftward flow takes place at very tiny structures (GRP or PNC), small scale physics applies to this event. The low Reynold's number physics predicts that in such scales inertia has no influence on motion. In other words, as long as a a force acts (GRP/PNC cilia), things are in motion (extracellular liquid) and abruptly halt without coasting once the force is off (Purcell 1977). For leftward flow this means that just a small proportion of the fluid in the archenteron cavity is pushed by the cilia rotational beat pattern and that this motion is restricted to the ciliated epithelium without reaching beyond. Therefore, leftward flow cannot account for transporting an asymmetrical cue all the way through the archenteron. Thus, perception should take place inside or at the borders of the ciliated epithelium. Two models for this perception were postulated: the two-cilia and the morphogen model.

The two cilia model

The two-cilia model (Fig. 3A) favors two different types of cilia, motile cilia which drive the flow and immotile cilia at the periphery for mechanosensation (McGrath et al. 2003; Tabin & Vogan 2003). In mouse, ciliation differences at the PNC were described. Central PNC cilia were reported positive for lrd, whereas the cilia in the periphery were not. These supposedly immotile cilia should act as sensors in this model. In addition, all PNC cilia show localization of polycystin-2 (PC2, encoded by *polycystic kidney disease 2*, *PKD2*), a cation channel known which on kidney cilia measures the discharge pressure of the urine and modulate the diameter of the nephric tubule (Witzgall 2005). Lack of *PKD2* leads to cystic kidneys as a consequence of lacking ability to perceive fluid pressure but in addition also to laterality defects (Pennekamp et al. 2002). In agreement with this notion, a calcium wave at the left border of the PNC/KV downstream of flow was described in mice and fish, respectively (McGrath et al. 2003; Sarmah et al. 2005).

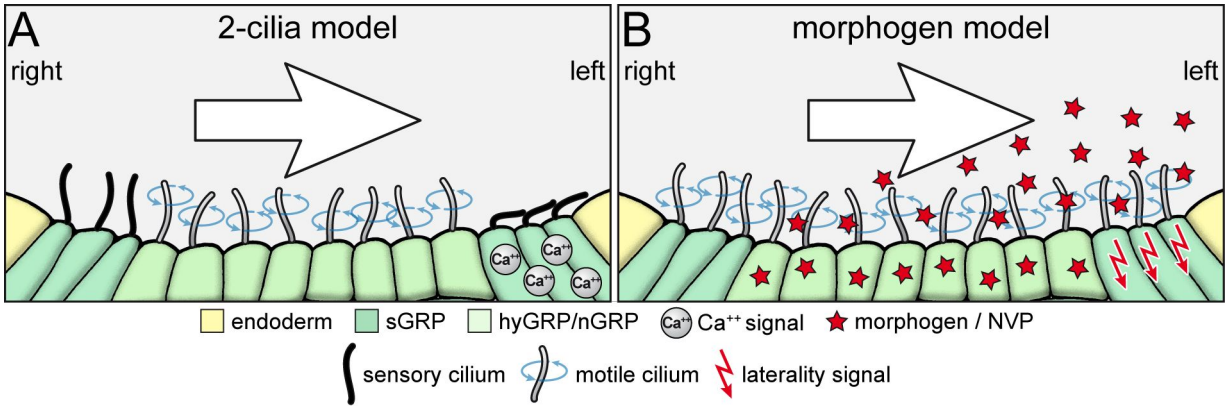

Fig. 3 Perception of leftward flow
(A) In the 2-cilia model, two distinct populations of cilia are postulated. Motile core-cilia that drive the flow and immotile cilia in the periphery sensing the current by mechanosensation that would result in an asymmetric Calcium wave. (B) In the morphogen mode, a morphogen or Nodal vesicular parcels (NVP) is symmetrically (ubiquitously) released from the ciliated epithelium. These are further asymmetric shifted with the current to the left side to signal.

The morphogen model

The morphogen model (Fig. 3B) in contrast comes in two flavors. A morphogen like Nodal itself or other candidates could be released by the PNC/GRP and be asymmetrically transported and accumulate on the left side which would be sensed and interpreted via receptors (Nonaka et al. 1998; Okada et al. 1999). On the other hand in the PNC of mice, vesicles were described to emerge from the ciliated epithelium – so-called nodal vesicular parcels (NVPs) – which should be asymmetrically transported to the left side where they were thought to burst at the elevated crown-cells spilling their content. NVPs were reported to harbor retinoic acid and sonic hedgehog (Tanaka et al. 2005). However, the small Reynold's number physics argues against rupture of vesicles caused by collision, instead a biochemical fusion or integration of the NVPs at the destination seems more plausible (Cartwright et al. 2007).

Anyhow the signal is perceived at the midline and thus has to be passed to the left LPM to activate the Nodal-cascade. As a secreted morphogen, Nodal itself was thought to acquire this long-range signaling. However, mice incubated in recombinant nodal protein did not display laterality defects, therefore it was concluded that Nodal would not signal through the gastrocoel cavity (Kawasumi et al. 2011). Alternative routes for Nodal could be through the paraxial mesoderm, endoderm or the cleft between mesoderm and endodermal cells. Rather unlikely would be a route through the notochord and ectoderm.

I.3.7 Other proposed modes of symmetry breakage in *X. laevis*

Molecular and functional asymmetries have been described in *X. laevis* during cleavage stages and thus much earlier than leftward flow which occurs during early neurulation. These findings have been fit in the so-called 'ion-flux' hypothesis: Here a whole cascade based on pharmacological inhibition experiments was postulated. Asymmetrical localization of the ion pump H^+/K^+-ATPase subunit α protein was found in the right ventral blastomere of 4-cell stage embryos (Aw et al. 2007). This ion pump was proposed to set up a pH-gradient. In concert with Gap junctional communication

(GJC) which interconnect all blastomeres except for the most ventral ones (Levin & Mercola 1998), this gradient is thought to drive an electrogenic mechanism to allow a small molecule or morphogen to travel between blastomeres (Adams et al. 2006). As the gradient should be asymmetric, the morphogen should get asymmetrically localized. The neurotransmitter serotonin is thought to pass GJC and was indeed shown via immunohisto chemistry (IHC) to accumulate in the right ventral blastomeres of 32-64-cell stages (Fukumoto et al. 2005). In addition by specific blockage of serotonin receptors class 3 and 4 from cleavage to gastrulation, laterality could be demonstrated to rely on serotonin signaling. By this asymmetric accumulation of serotonin, the initial bilateral symmetry was thought to be broken already during early cleavage, which would render the later occurring leftward flow dispensable.

I.3.7.1 Serotonin signaling

The monoamine serotonin (5-hydroxytryptamine, 5-HT) is synthesized in two steps from the amino acid tryptophan via the amino acid decarboxylase (ddc) and tryptophan hydroxylase (TPH) which is the rate limiting enzyme (Fitzpatrick 1999). For serotonin signaling in vertebrates, about 20 receptors are known which are grouped into seven classes (5-HT_1 to 5-HT_7). All 5-HT receptors are G-protein coupled except for the ligand-gated Na^+, K^+ or Ca^{2+} channels of class 3 (5-HT_3; Hannon & Hoyer 2008). Serotonin is best known for its neurotransmitter function in the nervous system (Gaspar et al. 2003) but 5-HT also plays a role in non-neural tissues e.g. in the gastrointestinal tract or the cardiovascular system in adult organisms (Sanger 2008). During embryogenesis, serotonin is involved in a multitude of processes from cell divisions of the early embryo (Dubé & Amireault 2007), gastrulation (Colas et al. 1999), neurulation (Lauder et al. 1981), heart (Nebigil et al. 2001) and craniofacial development to bone patterning (Levin et al. 2006) in a diverse range of species. In addition it was shown that serotonin signaling modulates ciliary beat frequency in sea urchin embryos (Wada et al. 1997) and rat brain ventricles (Nguyen et al. 2001) which could hint at a link to the observed laterality defects upon blockage of serotonin signaling (Fukumoto et al. 2005), i.e. serotonin signaling might be required for motility of GRP/PNC cilia driving leftward flow.

I.4 Open questions in left-right axis specification of *X. laevis*

The two major hypotheses for symmetry breakage in *X. laevis* not only differ in time of action but also in localization. Whereas the 'ion-flux' is postulated to take place early during development on the ventral side (Levin 2003; Fukumoto et al. 2005), leftward flow occurs 'late' and is active dorsally (Schweickert et al. 2007). Therefore the question arose if the 'ion-flux' or other yet unknown early asymmetries might precede and therefore be necessary for leftward flow. In the following it is envisaged how an hypothetical early asymmetric determinant in theory could impact on LR axis formation.

I.4.1 LR axis in *Xenopus*: early determinants or leftward flow?

At the four cell stage, orientation of the future body axes is visible and the fate-maps of these four blastomeres is fixed (Vick et al. 2009). Asymmetry of determinants in these blastomeres thus could specify the LR axis by descending and signaling in LR relevant tissues. If early asymmetric determinants would impact on LR axis specification, it is imaginable that these might interfere with the Nodal-cascade in the LPMs or the setup/perception of the leftward flow at the GRP. Therefore one can hypothesize that (1) early left ventral asymmetries should activate the Nodal-cascade or mediate competence for *Xnr1*-signaling in the left LPM, whereas (2) early right ventral asymmetries should repress the Nodal-cascade from the right LPM or inhibit competence for *Xnr1*-signaling. (3) Early dorsal asymmetries could affect the formation of the GRP or impact on the paraxial expression levels of *Coco* or *Xnr1* which are modulators of laterality (cf I.3.5, Fig. 4). Even more downstream interfering with the transfer to the LPM is also imaginable.

Early ventral asymmetries

An early determinant-mediated asymmetry in LPM-competence for Nodal-signaling can be declined as the co-receptor for *Xnr1* – *XCR2* is bilaterally expressed in the LPMs (Onuma et al. 2006). In addition, the Nodal-cascade can be ectopically induced in either LPM (Sampath et al. 1997). Further, if early asymmetric determinants would impact on the Nodal-cascade in the LPMs, this should also be the case when this very tissue is

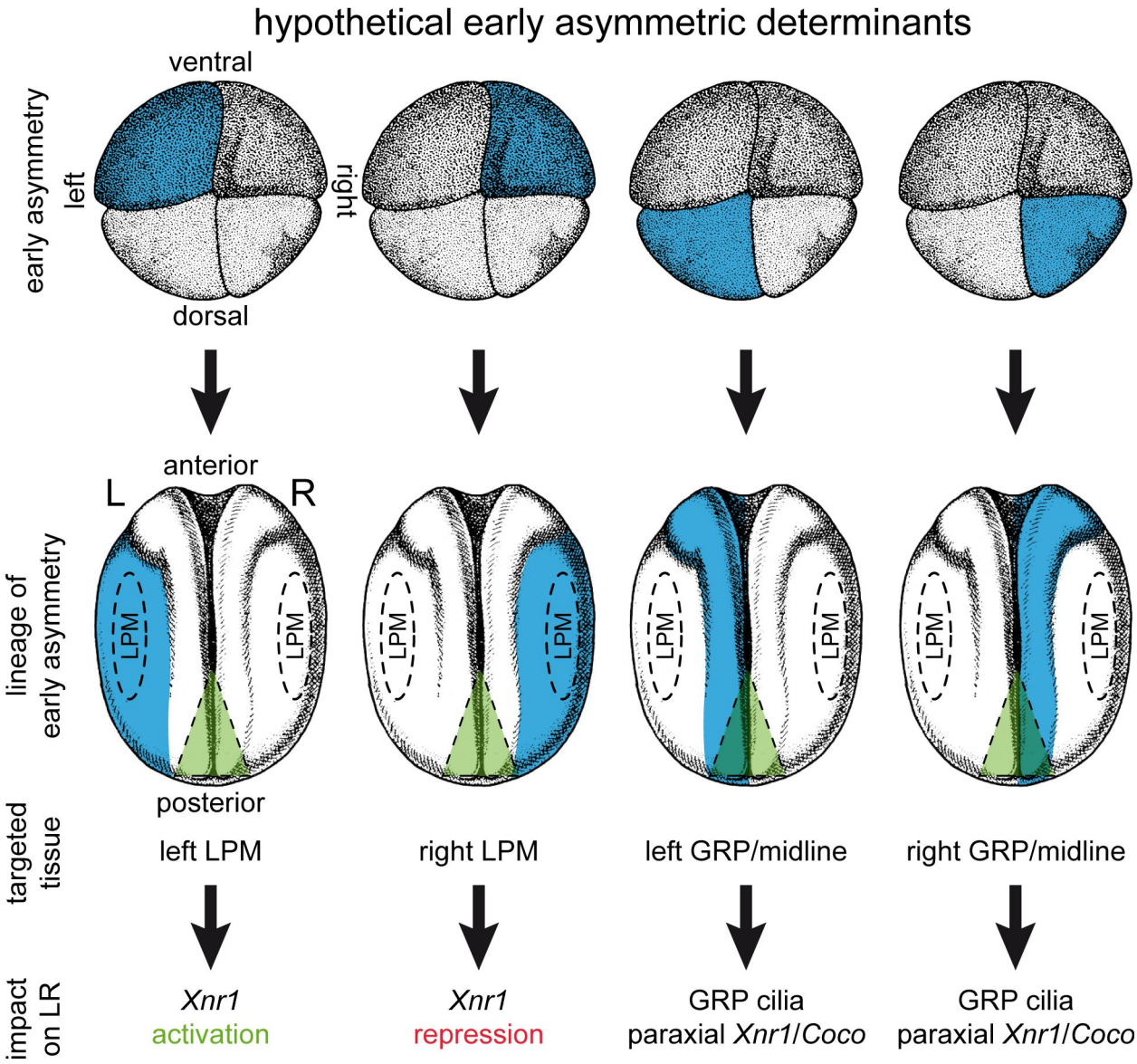

Fig. 4 Impact of hypothetical early asymmetric determinants on LR relevant tissues
(Top row) Four hypothetical early asymmetries in 4-cell stage embryos of *X. laevis:* ventral left; ventral right; dorsal left; dorsal right (blue). (middle row) Based on the restricted cell-lineage asymmetric early determinants could target different LR tissues (LPM, GRP represented by green triangle) superimposed (blue) on neurula-stage embryos. The suggested impact on the LR pathway are indicated. Embryo drawings (4-cell, neurula stage) altered from Nieuwkoop & Faber (1967).

explanted. However, when the LPMs were cut prior to leftward flow (<st.16) and cultivated to about stages 24/25, *Xnr1* was absent from the left and right explants. In contrast, when cut during or post leftward flow, the left but not right LPM expressed *Xnr1* after cultivation (Ohi & Wright 2007). This clearly demonstrated that the default case of the LPM is absence but competence of the Nodal-cascade and that *Xnr1* needs to be induced in the LPM.

In contrast, early right ventral asymmetric determinants would demand inhibition of the Nodal-cascade in the right LPM. This right sided inhibition mechanism would require the default state of the Nodal-cascade to take place bilaterally. This condition again was not seen in the LPM explantation assay (Ohi & Wright 2007).

Early dorsal asymmetries

There are no reports on early dorsal asymmetries, however, it is imaginable that early dorsal asymmetric determinants could impact on the setup of leftward flow. This means it is conceivable that the ciliated epithelium, ciliation, distribution of the hypothetical 'flow-receptor', impact on the paraxial domains of *Xnr1* or *Coco* or the transfer of the flow-generated cue to the LPM could possibly be asymmetrically affected.

For these considerations and findings, an early ventral asymmetric determinant that should be necessary for LR axis formation seems unlikely. In contrast, this theoretical approach turns the attention to investigate if an hypothetical early dorsal asymmetrical determinant might impact on the GRP in terms of providing asymmetric histology or function.

Although unlikely to function in LR axis formation due to the early asymmetric ventral right localization, loss of 5-HT signaling clearly impacted on LR axis formation (Fukumoto et al. 2005). Therefore it seems justified and advised to investigate if and how serotonin signaling and leftward flow might interact during development; three scenarios are conceivable: (1) early asymmetric serotonin signaling and leftward flow could illustrate two pathways independently acting on laterality. (2) Both events could be serially connected with serotonin signaling specifying a subset relevant for leftward flow (asymmetric release of morphogen / perception / transfer). (3) Serotonin signaling

could specify the SM / GRP, however, this would not demand an early asymmetric localization and function of serotonin

I.5 Aims of this work

Starting point of this thesis was the apparent contradiction in time, location and action of leftward flow and 'ion-flux' as possible LR symmetry breaking events in *X. laevis*. As basis for investigations on the impact of factors on leftward flow, first, the setup of leftward flow including morphology of the GRP, ciliogenesis, polarization of cilia and cilia motility should be investigated in detail. Further, it should be investigated if early asymmetries could impact on leftward flow.

Therefore, the following two main questions were examined by descriptive and functional approaches:

(1) Does leftward flow underlie an asymmetric setup of the GRP and are hence early asymmetric determinants necessary for LR axis formation?

(2) Does serotonin signaling and cilia-driven leftward flow interact for LR axis specification in *X. laevis*? Here, three possibilities are considered:
   1. Both events could be serially connected with leftward flow being the amplifier or mediator of an early asymmetric determination process driven by serotonin-signaling.
   2. Serotonin signaling could positively regulate the cilia beat frequency of GRP cilia and therefore be necessary for leftward flow.
   3. Serotonin signaling could specify the SM / GRP, however, this would not demand an early asymmetric localization or function of serotonin.

II Results

II.1 New tools for investigating leftward flow

The main requirement for this work was to analyze leftward flow statistically under wildtype and (molecularly) altered conditions. Therefore, new elaborate and sensitive tools for analysis of leftward flow were required. The new tools should allow for investigating the interplay of ciliogenesis, the morphology of the ciliated epithelium and the directionality of the extracellular liquid current to correlate least changes of the flow setup to LR defects. In addition, an *in vivo* marker to acquire the cilia beat movement of GRP cilia via fluorescence microscopy should be investigated.

II.1.1 The 'leftward flow analyzer' - a universal tool for calculating velocity, direction and directionality of particle motion

To depict fluid motion in *X. laevis* generated by the beat pattern of the GRP cilia, fluorescent latex beads were added to the specimens and time-lapse movies were acquired. In our first publication on leftward flow in *Xenopus*, particle trajectories of the fluorescent latex beads were plotted by summarizing the maximum gray values of each frame following a color gradient over time from green to yellow to red onto a single graph. As time information was provided by the underlying color gradient, the trajectories were named gradient-time-trails (GTTs). The plotted GTTs were manually traced and the velocity of the respective particle was calculated by covered distance over travel time (Weber 2006; Schweickert et al. 2007). As all particle trails were plotted onto the same graph, trajectories were superimposed. This made the manual measurement of trajectories difficult as not all tracks could be selected when timing information provided by the color gradient was concealed by other GTTs. To calculate flow parameters more precisely, a new method that allowed for performing statistic calculations on a larger particle trajectory count was required.

The ParticleTracker plug-in for the open source image analysis software ImageJ provides a solution to this problem (Sbalzarini & Koumoutsakos 2005; Abràmoff et al. 2004). This plug-in tracks particles and links them to yield trajectories. The coordinates

of these trajectories can be saved to process further. By this, every tracked particle can be assessed individually. Further analysis of the trajectories was performed by a custom made program written in statistical R (Ihaka et al. 1996). As all particles in a time-lapse movie are recognized by the ParticleTracker, a mask selecting the field of interest was introduced for calculation. The mask was generated in ImageJ by selecting the GRP or equivalent field of interest (polygonal selection tool) on bright field pictures of the specimen. Next, raw-data of the ParticleTracker was parsed in R to extract the X- and Y-coordinates per trajectory. As the time-lapse movies were acquired with certain frames per second (fps) – 2 fps in *X. laevis* – timing information was provided by the number of coordinates for each trajectory in the logfile. For each particle, the length of the trajectory and the velocity was calculated.

Due to small scale physics (low Reynolds number I.3.6), only the particles which entered the field of force generated by the cilia beat pattern were transported with the fluid flow. As the time-lapse movies of particle motions were acquired on a non-confocal microscope, two artifacts had to be excluded from calculation: (1) beads which were present outside of the focal plane yielded halos which were also recognized and tracked by the ParticleTracker; (2) beads in the plane of focus that were not moved by the fluid but Brownian motion should also be excluded. Therefore, each particle was tested for its directionality to distinguish between the movement generated by the force of ciliar beating in contrast to Brownian motion. This was achieved by performing a Rayleigh's test of uniformity on the angles of the segments of each particle trail. The Rayleigh's test of uniformity results in the dimension-less number ρ (rho) that represents the mean resultant length of the segment angles of the trajectory. The value of ρ equals random movement by tending to 0 and total directedness when tending to 1.

Accuracy of the 'leftward flow analyzer' was verified by re-analyzing the manually examined time-lapse flow movies of our initial publication on leftward flow in *X. laevis* (Weber 2006; Schweickert et al. 2007). It generated comparable results of mean velocity with 4.49 ± 2.88µm/s (stage 17, 13 GRPs, 1670 particles) compared to 4.1 ± 1.9µm/s (828 particles) in Schweickert et al. 2007 plus enabling statistic calculation (Fig. 5A, B). The introduced measure ρ for directionality amounted to 0.83 in these explants, indicating a robust leftward flow for wildtype *X. laevis* embryos of

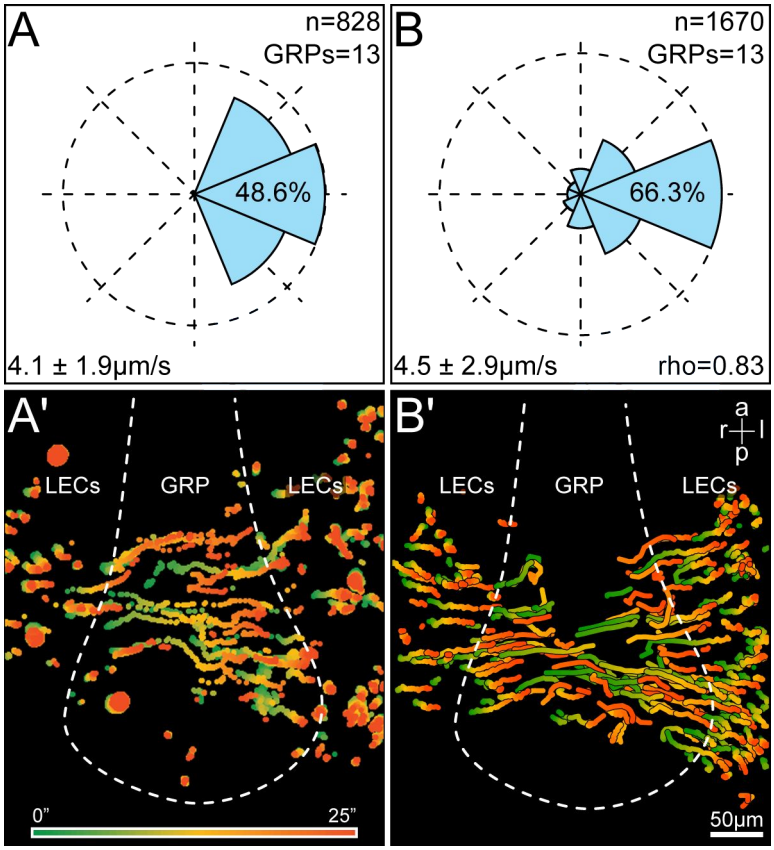

Fig. 5 Comparison of manually and automatically analyzed leftward flows
(A, B) Logarithmic histogram of mean directions of manually (A) and automatically (B) tracked particle trajectories of the same time-lapse movies. Note: increase of tracked particles due to automation allows for calculation of all particles above the GRP. **(A', B')** GTT projections of particles. (A') Old processing resulted in pixelated picture due to collapse of maximum gray levels of the time-lapse movie. (B') Brownian-motion filtered trajectories yields only particles of directed movement. Figure partially adapted from (Schweickert et al. 2007)
a, anterior; l, left; p, posterior; r, right

stage 17 (Fig. 5B), demonstrating that this new analysis tool was suitable for evaluation of further experiments. Projections into GTTs were from now on only used for visualization purpose as by the underlying color gradient, direction of travel is easily visible (Fig. 5A', B'). These projections can also be animated to yield movies of particle trails.

II.1.2 The 'ciliated cell descriptor' – a tool to correlate ciliation and cellular parameters

To investigate the leftward flow underlying properties of the GRP epithelium, a second tool was developed. The morphology of GRP cells and their cilia is best analyzed via scanning electron microscopy (SEM). Here cell-borders and sites of cilia-insertion as well as cilia length are easily measured. To correlate leftward flow phenotypes to morphological conditions, a tool to analyze cell size, ciliation, cilia polarization and length was developed. A macro-based analysis for measuring SEM-raw-data in ImageJ comprised the following steps: the cell borders in SEM pictures were manually traced via the polygon tool. Thereafter, the cilium was manually measured from its insertion site via the segmented line tool and the position relative to the center of the cell was empirically specified, i.e. anterior, posterior, left, right or central. If no cilium was present or the insertion site was unclear, this could be specified separately. The X and Y coordinates of the polygon and segmented line selections were logged as was the number of the cell. Further calculations and statistics were performed in statistical R: cilia length, cell size, ciliation rate and the distribution of cilia insertion points.

The average *X. laevis* GRP consists of ~260 cells (Blum et al. 2009b).These can be subdivided into three cell populations of different fates. The lateral cells are part of the somitic mesoderm (sGRP), the middle GRP cells will intercalate into the notochord (nGRP) and the cells in between those will give rise to the hypochord (hyGRP; Shook et al. 2004). In our initial publication, we noticed aberrant positioning of sGRP cilia compared to the rest of the GRP. To characterize this observations, the SEM pictures of these very GRPs of stages 17/18, i.e. when leftward flow is most prominent, were re-investigated for cilia polarization (Fig. 6). With a mean cilia length of 3.09 ± 0.40µm compared to 4.27 ± 0.46µm, sGRP cilia were very highly significantly shorter than hyGRP/nGRP cilia ($p < 0.001$; Fig. 6D). Very highly significantly ($p < 0.001$) reduced was also the polarization of mostly posterior (88.2%) hyGRP/nGRP cilia compared to 26.5% of sGRP cilia with a likewise increase of central positions (hyGRP/nGRP: 5.9%, sGRP: 58.8%; Fig. 6E). However, mean ciliation rate (hyGRP/nGRP: 87.1, sGRP: 82.5, $p = 0.456$; Fig. 6C) and mean cell surface area (hyGRP/nGRP: 213.98 ± 48.19µm²,

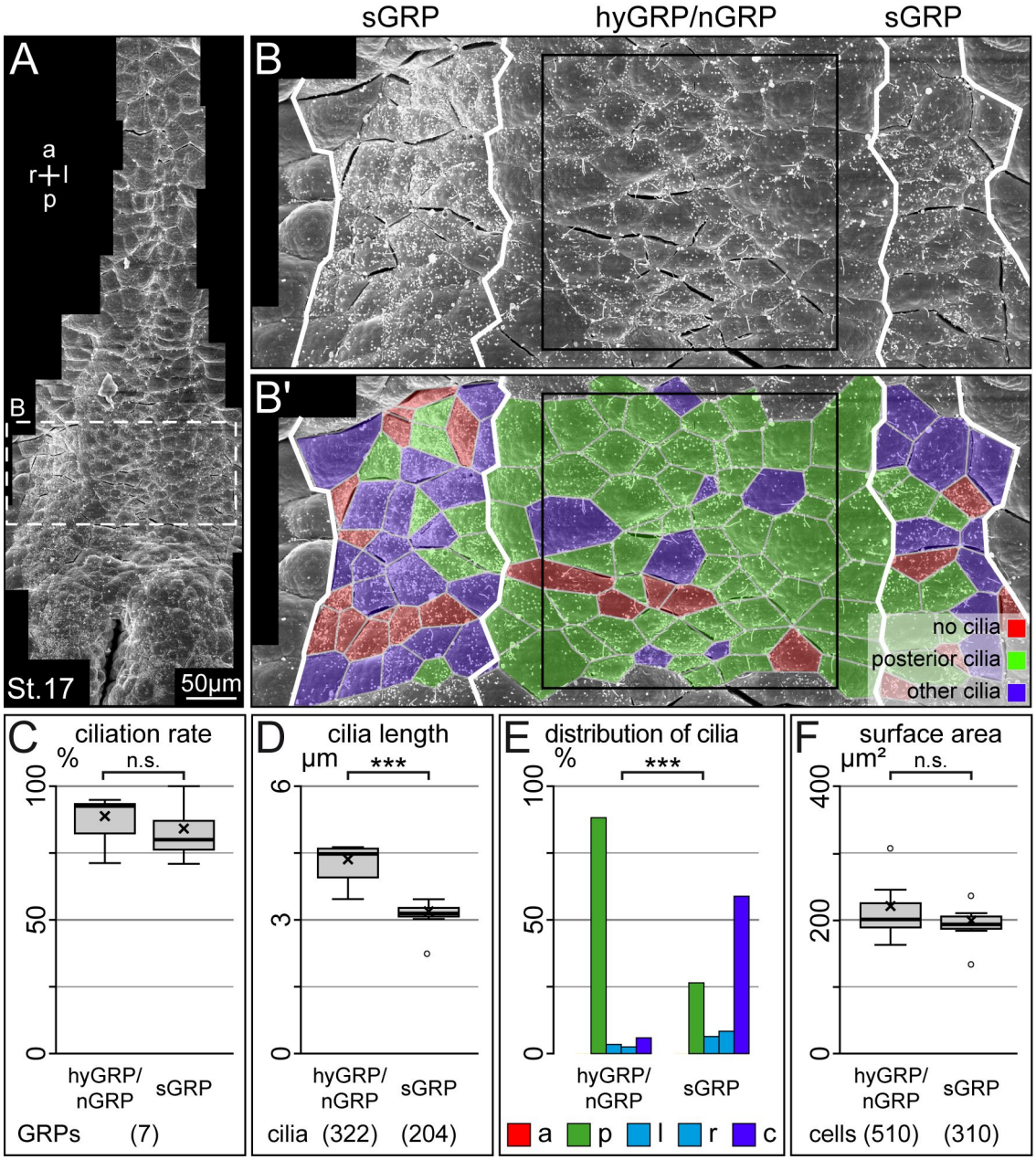

Fig. 6 Cilia on sGRP cells are unique
(A) Exemplary GRP of a st.17 neurula. **(B)** Magnification of GRP anterior to the blastopore. Note: somitic GRP (sGRP) cells appear differently compared to hypochordal (hyGRP) or notochordal GRP (nGRP) cells. **(B')** Analysis of cilia distribution: posterior (green), other positions (purple), no cilium (red). (C-F) Statistical analysis of mean ciliation rate **(C)**, mean cilia length **(D)**, distribution of cilia positions **(E)** and mean cell surface area **(F)** of sGRP and hyGRP/nGRP cells.
a, anterior; c, central; l, left; r, right; p, posterior; 'x' in boxplots represent mean values, whiskers extend to max 1.5×IQR; black squares in B, B' represent center of GRP for further analyses; numbers in brackets represent numbers of embryos (C), cilia (D) and cells (F)

sGRP: 192.41 ± 31.15µm², p = 0.318; Fig. 6F) were not significantly different among these GRP cell subpopulations.

In further experiments in which ciliogenesis or the GRP morphology was targeted (see below), sGRP cilia were excluded from analysis due to their ciliation properties. Therefore, a standard square mask was introduced to the center of the GRP, ranging 1000×1000px in 500×magnifications (86µm side length; black square in Fig. 6B, B').

II.1.3 The *Park2-co-regulated-gene* (*PACRG*)

To circumvent the restrictions of light microscopy on cilia visualization in *X. laevis*, an adequate axonemal candidate gene for fusion to eGFP was investigated.

The *Park2-co-regulated-gene* (*PACRG*), obvious from its telling name, was found to be co-regulated with *PARK2* which in turn is – if affected – the predominant genetic cause of early-onset and autosomal recessive juvenile Parkinson's Disease (PD). The murine *PACRG* (abbreviated *mmPACRG)* is located 204bp upstream of *PARK2*, antisense to the latter on chromosome 17. In addition, the shared promoter contains a site of bi-directional activation. The same arrangement can be found on the human chromosome 6, featuring conserved transcription factor binding sites in both promoter sequences (West et al. 2003). The human *PACRG* (abbreviated *hsPACRG*) could also be found upregulated in Lewy bodies (Imai et al. 2003). Despite a role in PD, *PACRG* is expressed in murine testicles and contributes to the flagelli of spermatozoa. Consequently, *PACRG* deficient mice are infertile and in addition, human patients show a significant association with azoospermia upon mutation of the shared promoter, suggesting a functional role of *PACRG* in the formation of sperm (Lorenzetti et al. 2004; Wilson et al. 2010). Interestingly, *PACRG* has not only been found in mammals, but also in the flagellated protozoan parasite *Trypanosoma brucei* (Dawe et al. 2005) and the green alga *Chlamydomonas reinhardtii* (Ikeda et al. 2007). Here PACRG could be identified as a structural protein of the axoneme, displaying random breaking of this very structure upon loss. However, the ultrastructural positioning and function of PACRG remains controversial. Yet, the axonemal localization and small size of the protein renders PACRG a promising candidate for visualizing cilia *in vivo* when labeled fluorescently. In addition its occurrence in a broad variety of species indicates evolutionary conservation, a condition worth investigating as hypothetical cilia marker.

II.1.3.1 PACRG is highly conserved

For a comparative analysis, the full length coding sequences of mouse (*mmPACRG*), rabbit (*ocPACRG*), chicken (*ggPACRG*) and *X. laevis PACRG* (*xlPACRG*) were cloned and aligned with *PACRG* of *Homo sapiens* (*hsPACRG*) and *Danio rerio* (*drPACRG*; Fig. 7A; cloning of *mm/oc/ggPACRG* was conducted by Nina Tietze Tietze 2008). All *PACRG* full length constructs were of comparable lengths (726bp *mmPACRG*, 726bp *ocPACRG*, 762bp ggPACRG, 722bp *xlPACRG*). The amino-acid sequences showed a significant difference at the N-terminus with increasing conservation towards the C-terminus. Furthermore, alternatively spliced isoforms could be sequenced from rabbit

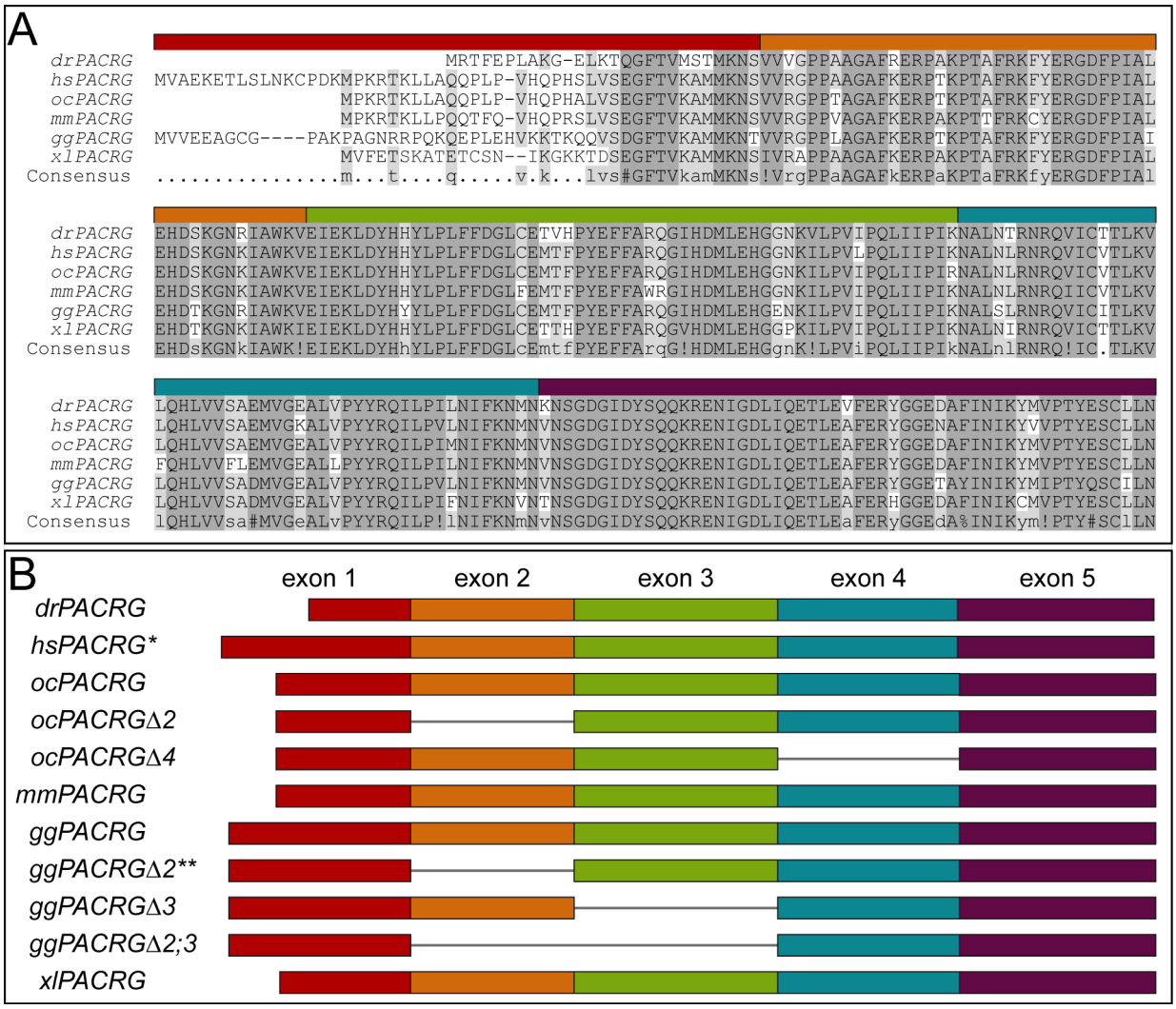

Fig. 7 PACRG is highly conserved among vertebrates and is alternatively spliced
(A) Comparison of amino-acid sequences of PACRG from *Danio rerio* (*dr*), *Homo sapiens* (*hs*), *Oryctolagus cuniculus* (*oc*), *Mus musculus* (*mm*), *Gallus gallus* (*gg*) and *Xenopus laevis* (*xl*). Note the high conservation of the C-terminus. **(B)** Alternatively spliced isoforms of *PACRG*. *****, accession number NM_001080378, **, accession number BU365094.

and the chicken embryonic cDNA in a developmental dependency (Fig. 7B and data not shown). Such alternatively spliced isoforms are also published in human and chicken expressed-sequence-tags databases (www.NCBI.com, Fig. 7B; *ggPACRGΔ2* accession number BU365094), i.e. two isoforms of *hsPACRG*: *hsPACRG* isoform 1 (accession number NM_152410) should comprise six exons whereas *hsPACRG* isoform 2 (accession number NM_001080378) would lack exon 5. However, a recent study could demonstrate that the predicted 5th exon of *hsPACRG* isoform 1 is not expressed, falsifying this transcript (Wilson et al. 2010). Equally, the full length *PACRG* covering five exons could be proven in each investigated model organism used for this analysis (Fig. 7B).

II.1.3.2 Comparative expression analysis of *PACRG* in mouse, rabbit chicken and frog embryos

As PACRG was found to be highly conserved among metazoans, detailed comparative temporal and spatial expression analyses were performed in mouse, rabbit, *X. laevis* and chicken embryos. In mouse, *mmPACRG* was cloned with primers covering the entire coding sequence and a portion of the 5'- and 3' UTR (cf IV.7). A whole mount *in situ* hybridization (WMISH) was performed by Nina Tietze on a time course of early mouse development covering the late headfold stage (E7.5), the 7-somite stage (E8) and specimens of embryonic day 9.5 (E9.5). Besides extra-embryonic tissue (Fig. 8A, A'), *mmPACRG* was expressed at the ciliated indentation of the PNC which forms anterior to the murine node at E7.5 (Fig. 8A'', B). The expression remained there until the PNC vanished. Afterwards, *mmPCRG* transcripts were only detectable in the otic vesicle (Fig. 8D) and the notochord of the head (Fig. 8D') and trunk (Fig. 8C, D'').

The probe synthesized from the cloned full length *ocPACRG* stained the developing PNC during a WMISH in rabbit embryos (conducted by Nina Tietze; Tietze 2008). From stage 5a onwards, *ocPACRG* expression was found in the forming PNC (Fig. 8E, F) with increasing strength during further development of this ciliated structure (Fig. 8G, H). Sections also revealed staining of the floorplate which is known to be ciliated (Fig. 8G', H').

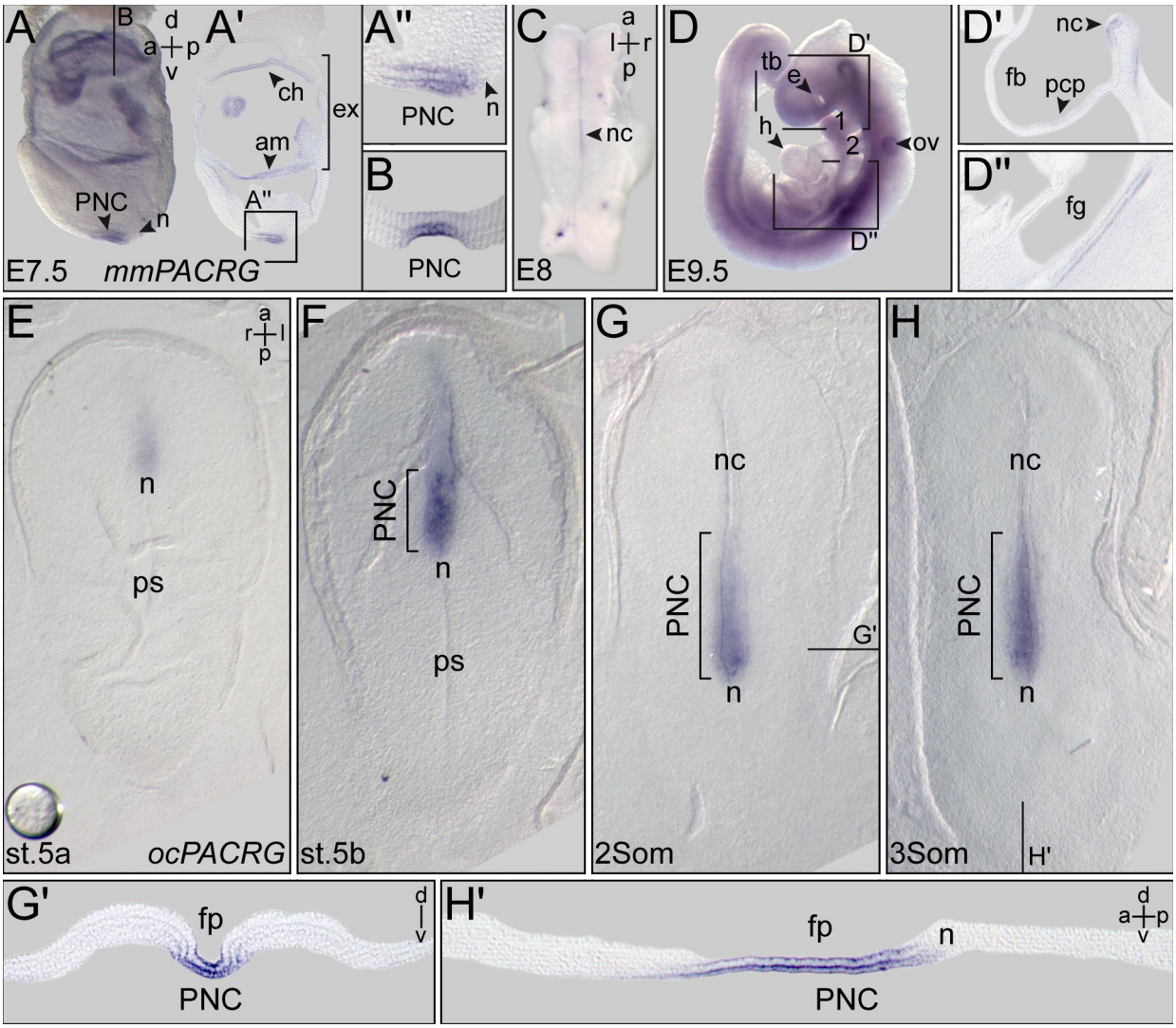

Fig. 8 *mmPACRG* and *ocPACRG* are expressed in the ciliated PNC
WMISH for *mmPACRG* (A-D") and *ocPACRG* (E-H'). *mmPACRG* was expressed in extra-embryonic structures and the PNC in E7.5 embryos **(A)**. Sagittal **(A', A")** and transversal **(B)** section through the PNC. In E8 **(C)** and E9.5 **(D)** the notochord was stained **(D-D")**. *ocPACRG* was exclusively expressed in the forming **(G, H)** and present PNC **(I, J)** as well as in the floorplate (transversal section in **G'**, sagittal section in **H'**) of the presumptive neural tube. Figure partially adapted from (Tietze 2008).
1,2, branchial arches; a, anterior; am, amniotic fold; ch, chorionic fold; d, dorsal; e, eye; ex, extra-embryonic tissue; fb, forebrain; fg, foregut; h, heart; l, left; n, node; nc, notochord; ov, otic vesicle; p, posterior; pcp, prechordal plate; ps, primitive streak; r, right; tb, tailbud; v, ventral

A WMISH with the specific probe synthesized from the full length *xlPACRG* could not detect expression prior (Fig. 9A) to stage 13 where it was found in the dorsal tissue at the dorsal lip (Fig. 9B). Subsequently, expression was found in each cell of the GRP most prominent at stage 17 (Fig. 9C), when most cells of the GRP are ciliated (Schweickert et al. 2007). Here *xlPACRG* was found in the entire GRP (Fig. 9C-C") and the dorsal aspect of the circumblastoporal collar (Fig. 9C, C'"). On the epidermis,

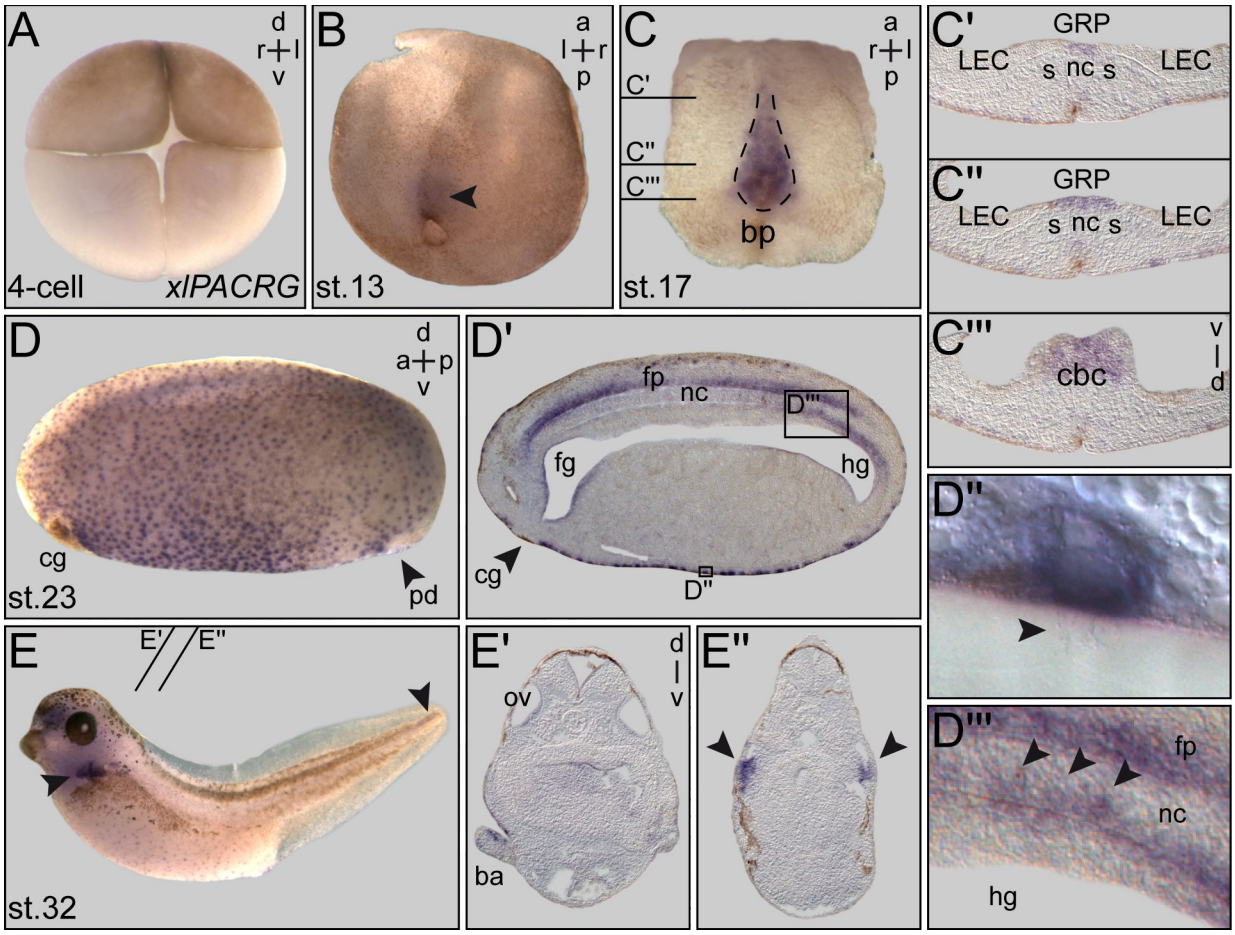

Fig. 9 *xlPACRG* marks the GRP and other ciliated structures during *X. laevis* embryogenesis
WMISH for *xlPACRG* (A-E). **(A)** No expression detectable at the 4-cell stage. **(B)** During gastrulation, *xlPACRG* is slightly expressed in the dorsal lip and dorsal mesoderm (arrowhead). **(C)** Expression in the GRP of a neurula stage embryo. **(C'-C''')** Sequence of transversal sections at levels indicated in C reveals staining of GRP (C'-C") and circumblastoporal collar (C'") as well as few epidermis cells. **(D)** Salt and pepper like distribution of ciliated epidermis cells (magnification in **D"**). **(D')** Sagittal section through (D) discloses *xlPACRG* transcription in GRP remnants at the level of the hindgut, floorplate staining and intercalated nGRP cells into the notochord (magnification in **D'''**, arrowheads). **(E)** *xlPACRG* is expressed in ciliated epidermis cells, the otic vesicle (transversal section in **E'**), branchial arches (arrowhead; E') and the nephrostomes (transversal section in **E"**). Note: slight staining of the trunk organizer region (arrowhead in E). Figure partially adapted from (Tietze 2008).
a, anterior; ba, branchial arch; bp, blastoporus; cg, cement gland; d, dorsal; fg, foregut; fp, floorplate; hg, hindgut; l, left; LEC, lateral endodermal crest; nc, notochord; ov, otic vesicle; p, posterior; pd, proctodeum; r, right; s, somites

xlPACRG expression initiated slightly (Fig. 9C'-C'") and was strongly evident around stage 23 in a salt and pepper like pattern (Fig. 9D). A high magnification picture of the sagittal section in Fig. 9D' revealed that this epidermal expression pattern is in accordance with multi-ciliated epidermal cells (Fig. 9D") which are likewise scattered (Deblandre et al. 1999). At this stage also, nearly all GRP cells have intercalated into deeper mesoderm (Shook et al. 2004) which was visible in the same sagittal section

(Fig. 9D') as some ingressed cells into the posterior notochord were still positive for *xlPACRG* (Fig. 9D'''). Further, *xlPACRG* expression was detectable in the floorplate of the neural tube (Fig. 9D'), the branchial arches, (Fig. 9E, E'), the otic vesicle (Fig. 9E, E'), the nephrostomes (Fig. 9E, E'') and very faintly in the caudal trunk region (Fig. 9E, arrowhead). These expression patterns could independently be verified by Nina Tietze (Tietze 2008). Further, the expression sites of *xlPACRG* are in full concordance with known ciliated tissues in *X. laevis* (Vick et al. 2009).

As *PACRG* contributed to ciliated tissues in mouse, rabbit and *X. laevis* embryos, it was investigated, if a *ggPACRG* expressing field of cells like the PNC or GRP could be found in chick embryos. If this would be the case before the node becomes morphologically asymmetrical around stage 6 (Gros et al. 2009), this could hint to a yet undiscovered and questioned hypothetical leftward flow in chick embryos. Therefore, expression of *ggPACRG* was spatio-temporally investigated. In a semi-quantitative RT-PCR, *ggPACRG* transcripts could be found in stages prior to the asymmetric node, during notochord formation and in later developmental stages. The full length primer pair yielded bands of differing sizes, of which the different spliceforms were sequenced (Fig. 7B). However, one particular band (about 650bp) was expressed in all stages (Fig. 10A). Three independently conducted WMISHs for the full length *ggPACRG* probe in contrast failed to detect cells with *ggPACRG* transcription during chick embryogenesis (Fig. 10B-F).

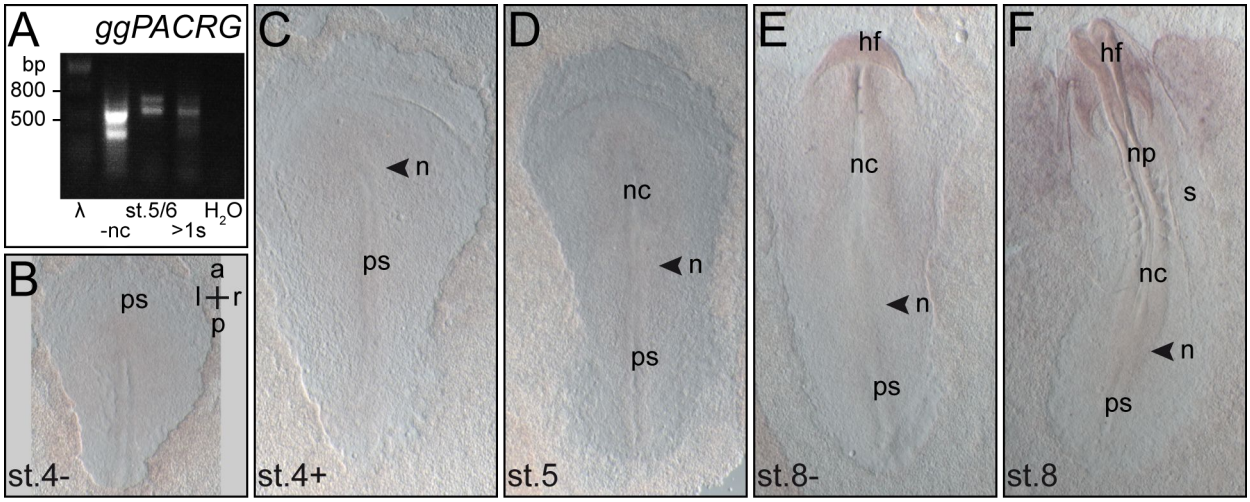

Fig. 10 *ggPACRG* was not detectable via WMISH but RT-PCR
(A) RT-PCR for *ggPACRG* amplified products of different sizes. **(B-F)** WMISH for *ggPACRG* did not detect any signal from pre-gastrula (B) through neurulation (F).
a, anterior; bp, basepairs; hf, headfold; l, left; n, node; nc, notochord; np, neural plate; p, posterior; ps, primitive streak; r, right

Taken together, *PACRG* is very highly conserved among vertebrates and is expressed during early embryonic development in homologous structures which are necessary for the breakage of symmetry (PNC, GRP). Additionally, it is highly likely that *PACRG* can be utilized as a general marker for ciliated cells in vertebrates.

II.1.3.3 *xlPACRG-eGFP* is an *in vivo* cilia marker

Deduced from the expression sites of *xlPACRG* in ciliated tissues and the axonemal localization of PACRG in *T. brucei* and *C. reinhardtii*, an axonemal role of xlPACRG was investigated in *X. laevis*. As PACRG is highly conserved, the epitope which is recognized by the available human PACRG antibody (Rockland Immunochemicals) matches the conserved region of the other vertebrate's PACRGs with a single amino acid mismatch in *X. laevis*. A whole mount co-immunohistochemistry (IHC) was performed in *X. laevis* using this antibody (AB) and the AB against acetylated α-tubulin to co-stain cilia. As predicted, xlPACRG was found to localize to the axonemes of both, the small GRP cilia (Fig. 11A) as well as to the entire axonemes of the multi-ciliated epidermis cells (Fig. 11B, C). Interestingly, xlPACRG was also found at the cell membranes (Fig. 11C), in vesicle like structures in the cytoplasm (Fig. 11D, D') and at the nuclear membrane (Fig. 11C-D') confirming findings in human embryonic kidney and neuroblastoma cell cultures (Imai et al. 2003).

The small size of the encoded xlPACRG protein and its localization to the axoneme allowed to generate a hypothetical *in vivo* cilia marker. Therefore, the full length *xlPACRG* was cloned upstream of *eGFP* into the expression vector CS2+. To prove that the fusion construct *xlPACRG-eGFP* (abbreviated *PACRG-eGFP*) indeed localized to cilia *in vivo*, 0,7pg/µl *PACRG-eGFP* expression plasmid DNA or 80ng/µl mRNA were injected ventral animally at the 4-cell stage. This region will give rise to the majority of the epidermis which provides multi-ciliated cells in great number and is easily analyzable. Indeed, injections stained the axonemes which allowed to visualize the whole bundles of cilia and their beat pattern. The same held true for the cilia on the GRP when injected into the dorsal marginal zone (DMZ) of 4-cell stage embryos. With this treatment, it was possible to visualize the rotational movement of all GRP cilia in *X. laevis* simultaneously. When seen in top-down view, the cilia describe a slight

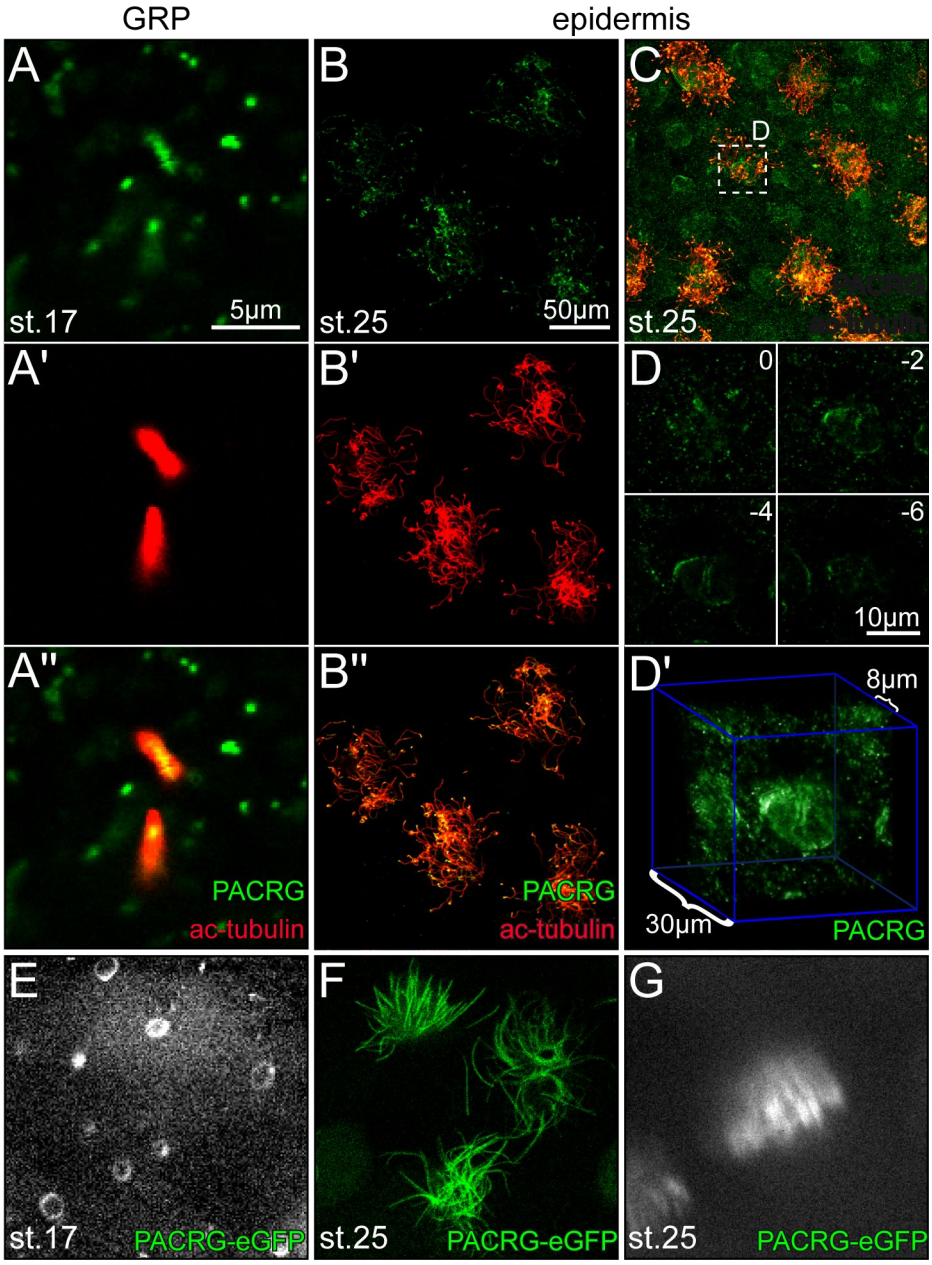

Fig. 11 PACRG and PACRG-eGFP localize to the axonemes of GRP and epidermal cilia, the cell membrane, vesicles and the nuclear envelope
(A-D) IHC against xlPACRG (green) revealed its localization to the axonemes of GRP monocilia **(A)** and multi-ciliated epidermis cells **(B, C)** counterstained with AB against acetylated tubulin (red). **(C)** Maximum-z-projection of stack through cilia bundles and epidermis demonstrated also localization to the membrane of the cell and nuclei. **(D)** Z-stack below the cell membrane revealed localization to vesicles and the nuclear membrane. **(D')** Reconstruction of z-stack in D. **(E-G)** Over-expression of *PACRG-eGFP* mRNA. **(E)** PACRG-eGFP revealed clockwise rotational pattern of GRP cilia (maximum projection of time-lapse movie). Note elliptic appearance due to tilt of cilia. **(F)** *In vivo* still of epidermal cilia bundles. **(G)** Maximum projection of epidermis cilia bundle beat pattern.

elliptical rotation due to their posterior tilt. This setup could be verified in figure 11E which depicts a maximum intensity projection of a 5sec time-lapse movie of PACRG-

eGFP incorporated GRP cilia. In addition, PACRG-eGFP localized to the same subcellular compartments obvious from the IHC, i.e. the nuclear envelope, vesicular structures in the cytoplasm and the apical cell membrane at the epidermis (not shown).

The PACRG-eGFP fusion construct therefore depicted an adequate *in vivo* cilia marker allowing to investigate the beat pattern of the GRP cilia in top-down view for the first time. The axonemal localization further promised a function in ciliogenesis and was therefore interesting to be manipulated with (cf II.2.2).

II.2 dissection of leftward flow

Fundamental to the present work was to investigate the generation of leftward flow in detail. First of all the question arose if the SM and GRP is specified by the organizer, i.e. if the organizer is inseparably connected with LR axis formation. Next, characteristics of the GRP cells and cilia were examined and the interplay of factors present at the GRP was investigated for influence on and establishment of leftward flow.

II.2.1 Connection of the LR axis and the Spemann organizer

II.2.1.1 The superficial mesoderm is not necessary for gastrulation but LR axis formation

In specimens in which only the outer epithelial layer of the organizer – the superficial mesoderm (SM) – was ablated at stage 10.5 via microsurgery (n = 17; Fig. 12A), the AP as well as the DV axes still developed normally (DAI = 5). The LR axis, however, exhibited laterality defects by displaying mostly heterotaxia (n=12/17) but *situs inversus* (n=3/17) and *situs solitus* (n=2/17) in only rare cases (Fig. 12B-C and Blum et al.

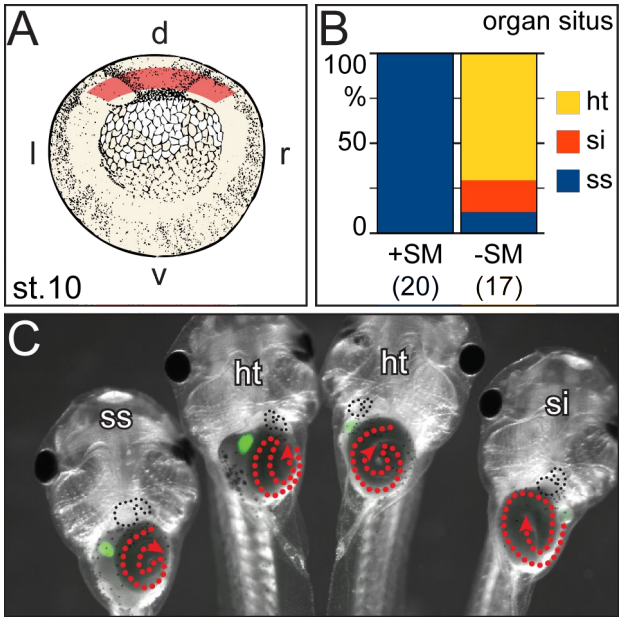

Fig. 12 Removal of the SM impacts on laterality but not on gastrulation
(A) Removal of the SM during gastrulation led to laterality defects (B, C; ht, heterotaxia; si, *situs inversus*) compared to control embryos (ss, *situs solitus*). Figure partially adapted from (Blum et al. 2009a)
d, dorsal; l, left; r, right; v, ventral

2009a). This demonstrated that the SM *per se* is not required for gastrulation and the proper development of the AP and DV axes but it is crucial for specification of the LR axis.

II.2.1.2 The organizer induces the GRP and leftward flow

To investigate, if the organizer is key to instruct the tissue not only to form the AP and DV axes, but also to induce the SM/GRP was approached in a double-axes (DA) assay. When the Wnt-pathway that is endogenously specifying the dorsal side is ectopically activated on the future ventral side just before gastrulation, a second organizer and subsequently a second axis initiates developing a pair of Siamese (or conjoined) twins (Fig. 13A; Lemaire & Kodjabachian 1996). By this induction, there are three random possibilities for the conjoined twins to arrange: in parallel with the (1) left or (2) right twin being induced or (3) fused ventrally, which is a very rare twinning scenario (Fig. 13B; Nascone & Mercola 1997). All reports of DA laterality from the last century revealed that consistently the left twin displayed *situs solitus* whereas organ placement of the right twin was randomized (Spemann & Falkenberg 1919). This observed situs phenomenon holds true for naturally occurring DAs in humans and all other vertebrates as well as for experimentally generated conjoined twins regardless of which one is the induced or endogenous (Fig. 13B; Nascone & Mercola 1997). For studying the formation of a secondary GRP, conjoined twins were generated by injection of 5pg *XSia* mRNA into the equator of a single ventral blastomere at the 4-8-cell stage. The appearance of the conjoined twins varied with respect to the enclosed angle of the axes growing out of the blastopore. Mostly, this angle enclosed about 30°, i.e. the conjoined twins developed 'parallel' with only cranial structures furcating the appearance (n = 142/179, Fig. 13C-D). In fewer cases, the axes developed further apart from one another (designated 'separated'; n = 37/179; Fig. 13E-F). However, the maximum possible enclosed angle of 180° was not seen in this study. As both axes develop over the same blastopore ring by converting the ventral lip into a secondary dorsal fate, dorsal structures were individual for each twin but ventral structures were shared – also was the archenteron. When excising neurulating DAs, the angle between the axes was also reflected by the inner arrangement of the archenteron. Inspecting dorsal explants of stage 17 revealed that

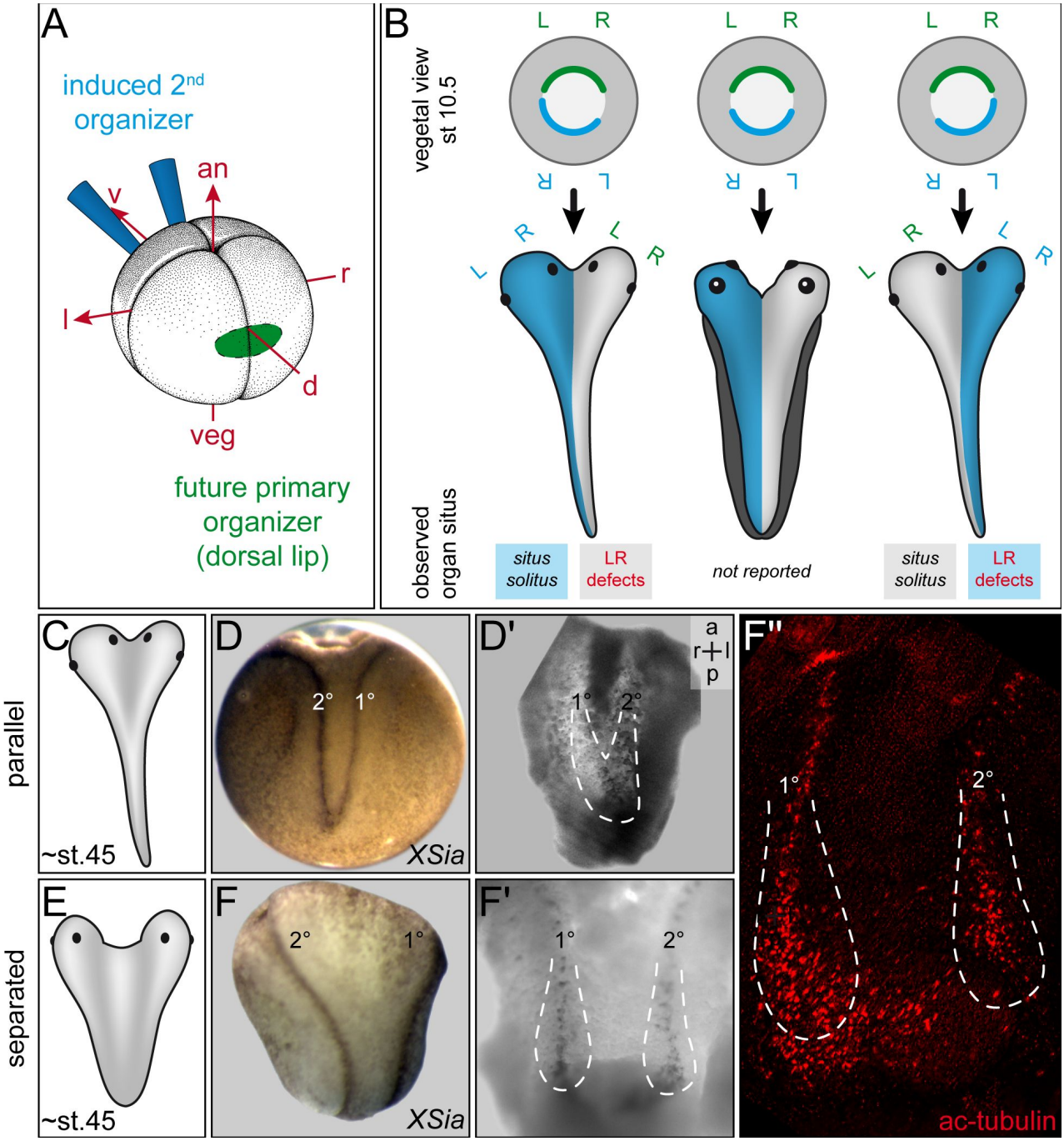

Fig. 13 *Xenopus* conjoined twins developed two ciliated GRPs
(A) Scheme for induction of secondary (2°) axis upon misexpression (blue) of Wnt-pathway components at the VMZ of 4-cell stage embryos. (B) Schematic development of conjoined twins. The endogenous (green) and induced (blue) dorsal lips will oppose one another at stage 10.5. This arrangement leads to three twinning possibilities. The organ situs of the left twin is always wildtype, the right twin demonstrates laterality defects irrespective of which is the induced one. (C, E) Classification into parallel (C) or separated (E) DAs depending on the enclosed angle between the neural tubes. (D, F) *XSia* mRNA induced 2° axes. Parallel (D) and separated (F) DAs developed two fused (D') or separated (F') GRPs which were ciliated (F'').
a, anterior; an, animal; d, dorsal; l, L, left; p, posterior; r, R, right, v, ventral; veg, vegetal; 1° endogenous axis; 2° induced axis

'parallel' developing DAs exhibited a fused GRP (Fig. 13D') whereas 'separated' axes displayed two distinct GRPs (Fig. 13F'). In a staining for acetylated tubulin, IHC revealed ciliation of both GRPs (Fig. 13F''). Both types of DAs developed leftward flow with the 'parallel' axes displaying a fused one reaching from the right side of the right GRP all through to the left side of the left twin's GRP. In contrast, 'separated' GRPs had their individual leftward flows (not shown). Therefore it was analyzed, if this leftward flow defines the left side of each twin individually.

For investigating if laterality in these conjoined twins was a readout of leftward flow, the left-sided marker *Pitx2c* was analyzed at stage 28 via an WMISH. As for singleton embryos, each twin can adopt four *Pitx2c* expression patterns: asymmetric left or right, bilateral or absence of expression. For analysis, the conjoined twins were categorized 'parallel' (Fig. 14A, C) or 'separated' (Fig. 14B, D) and induced left (Fig. 14A, B) or right (Fig. 14C, D). The conditions of *Pitx2c* expression of the left axis was plotted against the conditions of the corresponding right axis (4×4 matrices in Fig. 14). Expression patterns are summarized for each axis with the left twin on the left side of each matrix and the right twin on the top. In case of 'parallel' developing conjoined twins, the right axis mostly displayed absence of *Pitx2c*, regardless if the left (n = 52/62; Fig. 14A) or right (n = 63/80; Fig. 14C) twin was induced. The left twin in contrast displayed an increased amount of wildtype left-sided *Pitx2c* expression with the induced axis (n = 18/62) holding fewer cases than the endogenous one (n = 44/80). The expression patterns of *Pitx2c* hence recapitulated the observed and reported organ situs finding that the left twin exhibits *situs solitus* and the right twin displays heterotaxia.

As in 'separated' DAs two distinct GRPs and leftward flows were found, the question arose if this arrangement might lead to both axes being wildtype, i.e. both displaying *Pitx2c* only on their left sides. For the right twin, the left expression was only rarely achieved in 'parallel' axes. However, this condition could frequently be found in 'separated' axes for both but more often in left (n = 4/14; Fig. 14B) than right (n = 2/32) induced secondary axes. Although the number of 'separated' axes was low, the condition of both twins displaying left-sided *Pitx2c* expression occurred once in right induced DAs (Fig. 14D), demonstrating that this pattern is *per se* possible.

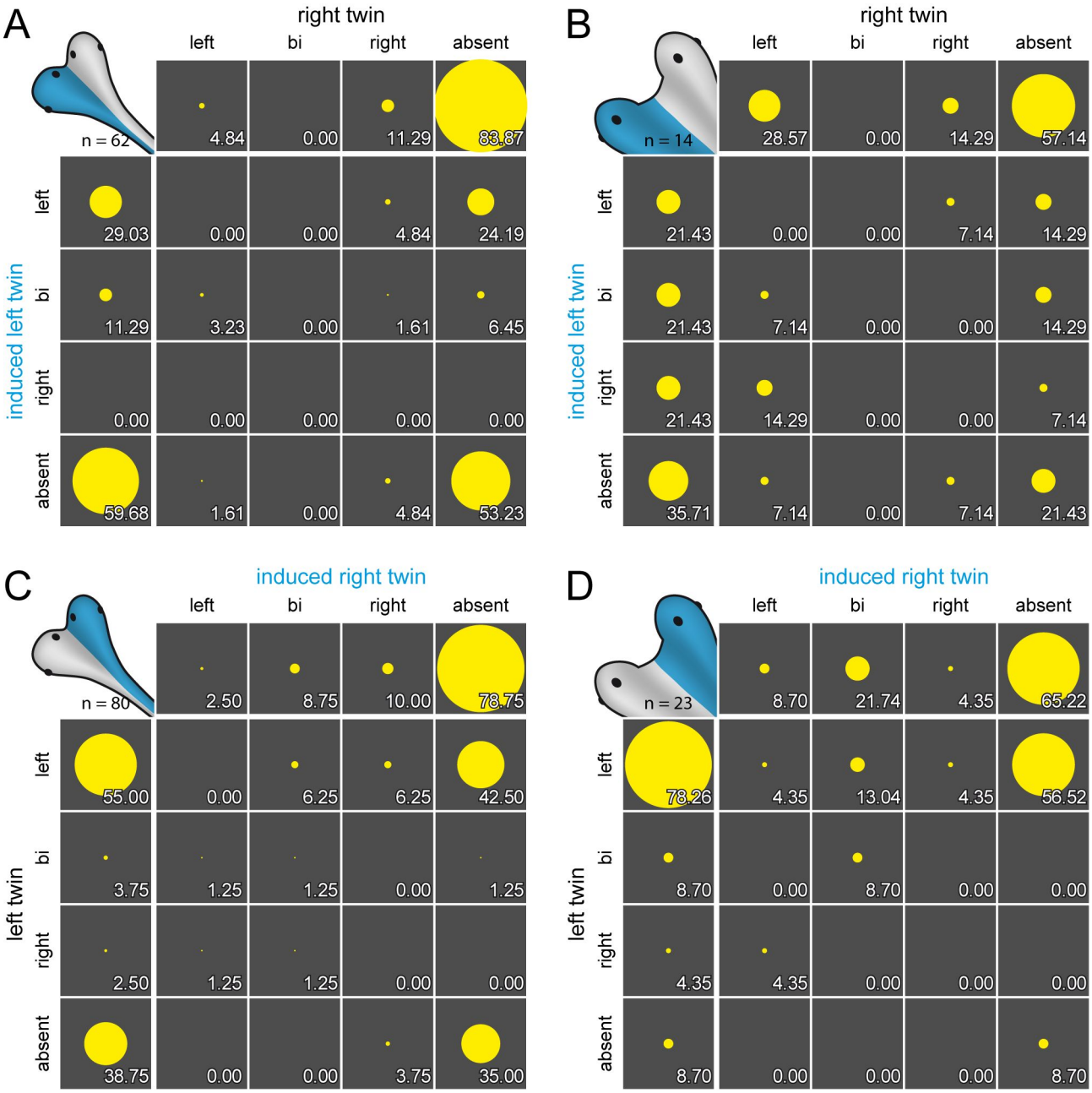

Fig. 14 Aberrant laterality of conjoined twins depends on distance of the dorsal axes
(A-D) Distribution of *Pitx2c* expression patterns in conjoined twins categorized 'parallel' (A, C) or 'separated' (B, D) and induction (blue) of left (A, B) or right (C, D) axes. In each matrix, left four and top four squares represent summary of Pitx2c patterns of left or right twin, respectively. Numbers represent percentages of each condition.
left, wildtype expression; bi, bilateral expression; right, inverted expression; absent, lack of *Pitx2c* expression

It was obvious that laterality in conjoined twins depended largely on arrangement of both axes, like it was predicted from the organ situs reports. However, induction via *XSia* mRNA injection itself impacted on laterality. All induced axes on the left side

displayed fewer wildtype conditions of *Pitx2c* compared to the endogenous left axes (endogen vs. induced: 'parallel': 55.00% vs. 29.03%; 'separated': 78.26% vs. 21.43%).

The DA laterality demonstrated that the organizer indirectly instructs LR axis formation by developing a functional GRP and leftward flow. That the latter mechanical event is crucial for LR axis formation in *Xenopus* was recently demonstrated (Schweickert et al. 2007). Mechanically blockage of the extracellular current upon injection of methylcellulose (MC) into the archenteron of stage 17 neurulae led to absence of the Nodal-cascade from the left LPM. To verify that this absence depended on loss of leftward flow, other experimental inhibitions of this current were investigated (see below). With the 'leftward flow analyzer', the 'ciliated cell descriptor' and the *in vivo* marker for motile cilia *xlPACRG-eGFP* at hand, the setup, function and readout of leftward flow was further analyzed in detail.

II.2.2 Leftward flow depends on motile cilia

To disqualify possible side-effects of the MC treatment on laterality except for blocking leftward flow (Schweickert et al. 2007), it was investigated if the resulting absence of the Nodal-cascade could be mimicked when leftward flow was inhibited molecularly, i.e. by interfering with ciliogenesis or cilia motility at the GRP. In *Xenopus*, molecular inhibition can be achieved by knocking down protein synthesis upon injection of morpholino oligonucleotides (MOs). MOs are synthetic antisense RNA fragments with a morpholine instead of the common ribose backbone (www.gene-tools.com). By binding to the mRNA (preferable to the 5' untranslated region, start codon or splice site), MOs block the binding of the ribosomal initiation complex which results in non- or partial translation of the targeted mRNA, i.e. the gene is knocked down. The axonemal contribution of xlPACRG rendered this protein an adequate candidate for being investigated in ciliogenesis. Accordingly, an ATG binding MO was ordered (cf IV.5). In a second approach, the rotational beat pattern of GRP cilia should be arrested upon blockage of axonemal motor proteins. From the Kartagener Syndrome and embryonic development of mouse and zebrafish, it is known that *dynein axonemal heavy chain genes 5*, *9* and *11* (*dnah5, dnah9, dnah11*) are crucial for ciliar motility and LR axis specification (Essner et al. 2005; Okada et al. 2005; Vick et al. 2009). In a collaborative

study with Philipp Vick (cf IV.1 for detailed contribution), it was analyzed if *dnah* genes accounted for ciliar motility of the GRP cilia and leftward flow in *X. laevis*. The *Xenopus* homologous genes *dnah5*, *dnah9* and *dnah11* were analyzed for expression at the GRP (Vick 2009; Vick et al. 2009). *dnah11*, the frog homolog of the murine *lrd* which is crucial for LR axis formation at the murine PNC (Supp et al. 1997), however, was not expressed at the ciliated GRP but was exclusively found in the caudal region of stage 33 embryos as well as in the gastro-intestinal tract of stage 43/44 tadpoles (Vick 2009; Vick et al. 2009). Instead, the family members *dnah5* and *dnah9* localized to the ciliated cells of the epidermis, the nephrostomes and the GRP (Fig. 15A-C and Vick et al. 2009), thus exactly resembling the expression pattern of *xlPACRG* (Fig. 9). Interestingly, besides transcriptional activity in ciliated tissues, *dnah9* showed strong maternal expression in the animal region of cleavage embryos to blastula stages (Vick et al. 2009; Vick 2009). To investigate the role of the dyneins for cilia motility and LR axis formation, MOs were designed (cf IV.5). To circumvent maternal inhibition of *dnah9* mRNA which caused severe gastrulation defects (Vick 2009), a splice-site-blocking-MO of *dnah9* (*dnah9-SB*-MO) was used (Vick et al. 2009).

In 4-cell stage embryos, it is possible to target the GRP (Fig. 15E) and neural plate (Fig. 15E') exclusively, with injections into the equator that will give rise to the DMZ (Fig. 15D). When injected in this region of 4-cell stage embryos, *dnah5*-MO, *dnah9-AUG*-MO, *dnah9-SB*-MO and *xlPACRG*-MO caused laterality defects (mis-expression of *Pitx2c*) in a concentration dependent manner (Fig. 15F, H and Vick et al. 2009). However, the *dnah9* morpholino that blocks the start codon (*dnah9*-AUG-MO) also caused severe gastrulation and blastopore closure defects from a concentration of 4pmol onwards. The same effect was seen at different doses for the *xlPACRG*-MO. Injections of 1pmol displayed a very highly significant ($p<0.001$) lack of *Pitx2c* from the left LPM. In specimens injected with 1.5pmol *xlPACRG*-MO, expression was nearly absent. However, a good portion of embryos developed neural tube closure defects (NTD). Laterality defects were only scored in embryos exhibiting a DAI of 5. When the MO concentration was raised to beyond 2pmol/embryo, severe gastrulation defects including microcephaly and non-closing blastopores were induced. This interesting effect of the ciliary genes *dnah9* and *xlPACRG* to impact on gastrulation is followed up

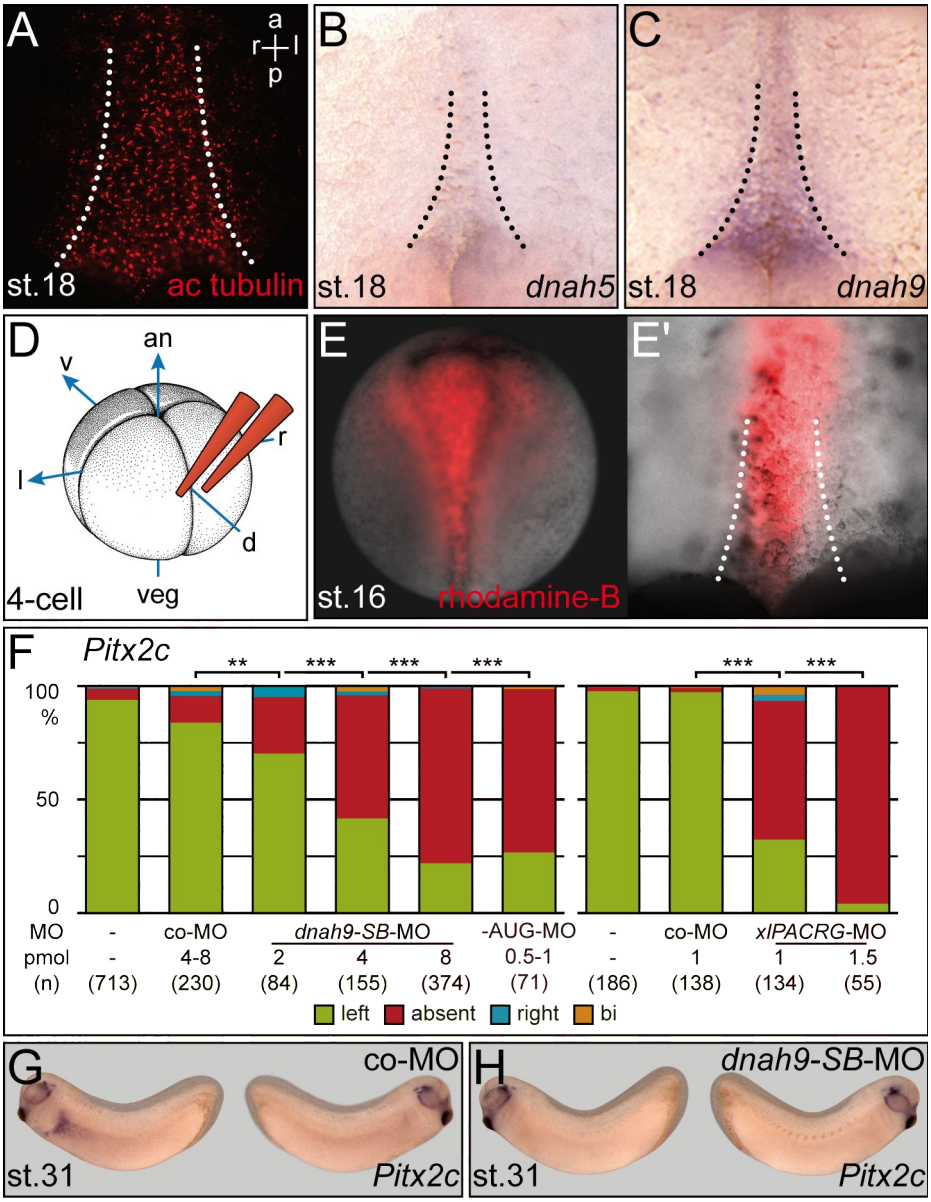

Fig. 15 Laterality defects caused by impairment of the GRP markers *dnah9* and *xlPACRG*
Cells of the ciliated GRP **(A**, IHC against acetylated tubulin**)** were hybridized with specific probes for *dnah5* **(B)** and *dnah9* during WMISH **(C)**. Injections of rhodamine-B dextran into the dorsal marginal zone (DMZ) at the 4-cell stage **(D)** stays in cell-lineage, i.e. the neural tube **(E)** and the GRP **(E')**. Loss of *dnah9* and *xlPACRG* at the GRP led to misexpression of the left marker gene *Pitx2c* **(F)**. Statistical analysis of marker gene expressions (F) of specimens exemplarily depicted in **G** (control) and **H** (*dnah9-SB*-MO). Figure partially adapted from (Vick et al. 2009).
a, anterior; an, animal; bi, bilateral, d, dorsal; l, left; p, posterior; r, right; v, ventral; veg, vegetal; absolut amount of pmol per embryo is given

in a separate chapter (cf II.2.2.1). To investigate if the laterality defects were caused by altered ciliogenesis and impaired motility, 1pmol *xlPACRG*-MO was used further.

Another set of specimens was cultivated to stage 17 when leftward flow is most robust and dorsal explants were prepared (cf IV.3.1). Leftward flow analysis revealed that the laterality defects were caused by impaired leftward flow in *dnah9*-SB (Fig. 16D), *dnah5* (Fig. 16E) and *xlPACRG* morphant embryos which was represented by only few beads that traveled randomly at the GRPs (directionality in exemplary *dnah9-SB* morphant: ρ = 0.31; *dnah5* morphant: ρ = 0.26; *xlPACRG* morphant: ρ = 0.06; Fig. 16A'-D' and Vick et al. 2009). Interestingly, when leftward flow was unilaterally blocked by injection of *dnah9-SB*-MO in either the left or right prospective DMZ in 4-cell stage embryos, only absence of leftward flow from the left side impacted on the Nodal-cascade rendering the right half of this current dispensable (not shown and Vick 2009, Vick et al. 209).

As *dnah* genes code for axonemal motor proteins, it was analyzed if absence of leftward flow was caused by immotile cilia. Therefore, 100ng/µl *PACRG-eGFP* fusion construct mRNA was co-injected with 4pmol *dnah9-SB*-MO into the DMZ of 4-cell stage embryos. Whereas 100ng/µl *PACRG-eGFP* mRNA + 2pmol co-MO injected specimens served as control and displayed wildtype rotational pattern (Fig. 16E), *dnah9-SB* morphant GRPs exhibited altered cilia movements like rotational pattern with

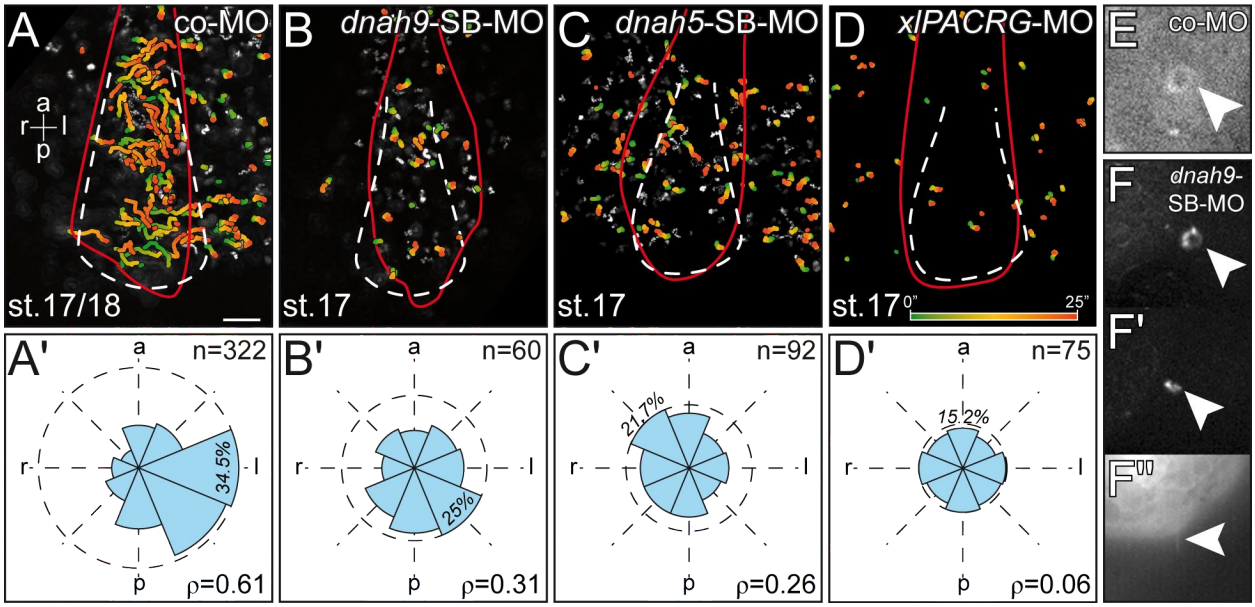

Fig. 16 Loss of *dnah9*, *dnah5* and *xlPACRG* at the GRP led to loss of leftward flow
(A-D) GTT projections of leftward flow analysis revealed wildtype flow in control morphants and absence of leftward flow in *dnah9-SB, dnah5* or *xlPACRG* morphants. Targeted areas represented by limits of lineage tracer (red outline). **(A'-D')** Directionality of leftward flow was likewise affected. **(E-F")** Maximum Z-projection of time-lapse movies of xlPACRG-eGFP labeled GRP-monocilia. Wildtype rotational beat pattern of control morphants **(E)** was altered to whip-like **(F)**, wiggling **(F')** or stalled movement **(F")** in *dnah9-SB* morphants. Figure partially adapted from (Vick et al. 2009).
a, anterior; l, left; p, posterior; r, right; scale bar represents 50µm; gradient bar represents 25".

spontaneous whip-like beating (Fig. 16F), wiggling cilia (Fig. 16F'), or stalled movement (Fig. 16F'') which was present in most cases.

In addition to the *in vivo* approaches of investigating the functionality of the GRP cilia motility and leftward flow, SEM pictures of *dnah9* and *xlPACRG* impaired specimens were analyzed in detail for hypothetical morphological changes. Indeed, analysis of the flow relevant portions (cf. II.1.2) of morphant GRPs disclosed different severity of phenotypes for *dnah9* and *xlPACRG* when knocked down. The GRPs of *dnah9* impaired specimens (n=10) looked well developed at a first glance (cf representative example in Fig. 17A). Unexpectedly, cilia were significantly shorter (2.55 ± 1.02µm) than the control (4.11 ± 0.99µm) and were more often not polarized to the posterior pole of the GRP cells (posterior cilia in *danah9*-SB morphants: 56.1% vs. control: 83.1%, Fig. 17A', A'', E). The appearance of the GRP in *xlPACRG* morphant embryos (n=17) was obviously affected as the triangular shape of this structure was lost in most cases (cf representative example in Fig. 17B). In contrast to the small ciliated cells of wildtype GRPs (112.93 ± 64.5µm²), large (228.7 ± 142.03µm²) and non-ciliated cells inside this structure were found. In addition, most of the remainder small cilia (2.3 ± 1.02µm) were mispolarized and mostly stayed in central positions (51.4%; Fig. 17B', B'', E). Compared to control GRPs (wildtype and co-MO injected), ciliation rate dropped (very) highly significantly (Fig. 17C), cilia length decreased very highly significantly (Fig. 17D) and GRP cell size increased very highly significantly for both treatments (Fig. 17F). Interestingly, most of the shortened cilia were not polarized to the posterior pole in both knockdown approaches. Although being highly significantly different from the control GRPs, morphological defects were far more severe in *xlPACRG* morphant embryos than in *dnah9-SB* ones.

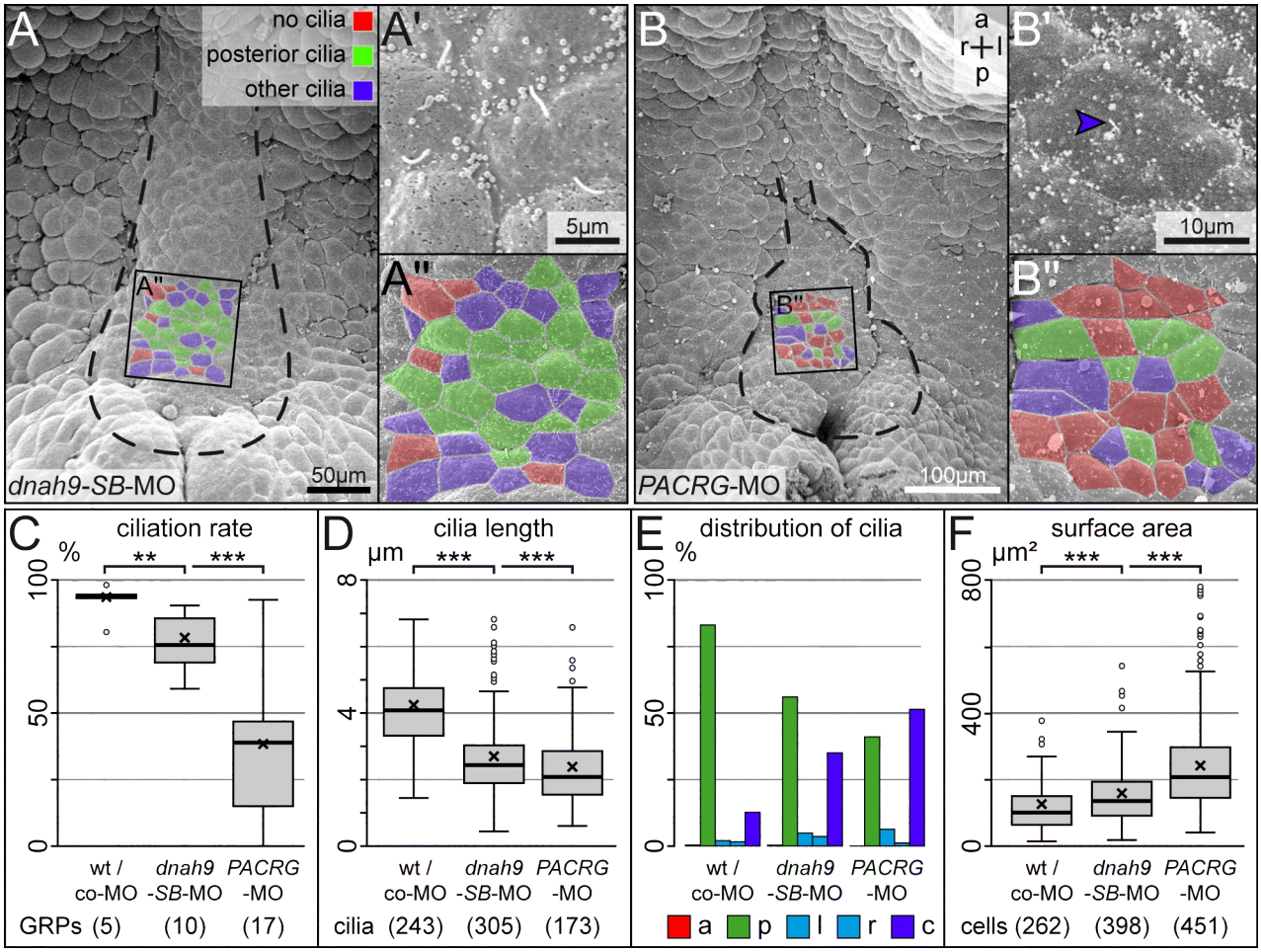

Fig. 17 dnah9 and xlPACRG are necessary for proper ciliogenesis at the GRP
(A-B) Exemplary SEM pictures of *dnah9-SB*-MO **(A)** and *xlPACRG*-MO **(B)** injected specimens revealed distinct phenotypes: proper formed (A) as well as misshaped GRP (B). (C-F) Statistical analysis of GRP and cilia properties in comparison to wildtype/co-MO injected controls.
a, anterior; c, central; l, left; p, posterior; r, right; 'x' in boxplots represents mean value, whiskers extend to max 1.5×IQR

This demonstrated that ciliogenesis of motile GRP-cilia was crucial for driving leftward flow at the GRP. In addition, these experiments verified that leftward flow was essential for specifying the LR axis by mimicking the methylcellulose treatments which blocked leftward flow (Schweickert et al. 2007).

II.2.2.1 Concentration dependent gastrulation defects in *xlPACRG* or *dnah9* morphant specimens

In contrast to the mild effects of low-level loss of *xlPACRG* including absence of leftward flow, shortened and misoriented GRP-cilia (cf II.2.2), higher concentrations of *xlPACRG*-MO led to severe gastrulation defects (Fig. 18). The *xlPACRG*-MO concentration of 0.75pmol/injection caused cranial NTDs when injected into dorsal animal blastomeres of 4-cell stage embryos (Fig. 18A). Co-injection of 100ng/µl *xlPACRG-eGFP* fusion mRNA rescued the NTDs but failed at rescuing the cement gland formation (Fig. 18B). Sole injection of the fusion construct resulted in wildtype embryos.

Dorsal injections with increased morpholino concentration to 2pmol/embryo caused massive malformations of the head and dorsal tissue. The morphant embryos thickened at the ventral side by simultaneously losing head-tissue which is displayed by

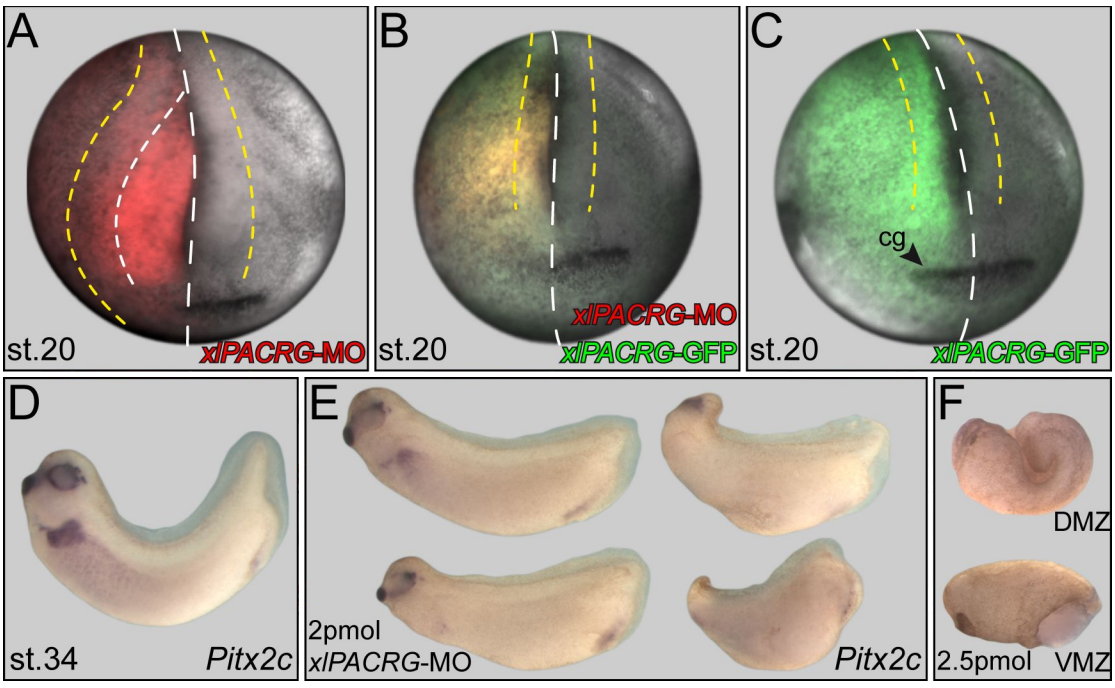

Fig. 18 Loss of *xlPACRG* caused NTD and gastrulation defects in a concentration dependent manner
(A-C) Unilateral injection of 0.75pmol *xlPACRG*-MO caused NTDs **(A)** which were rescued upon co-injection of 100ng/µl *xlPACRG*-eGFP mRNA **(B)**. Note: *xlPACRG*-eGFP injected specimens developed normally **(C)**. (D, E) WMISH for *Pitx2c* in control **(D)** or *xlPACRG*-MO injected specimens with severe gastrulation defects. **(E)** 1.5pmol *xlPACRG*-MO led to microcephaly or absence of cranial structures. **(F)** 2.5pmol *xlPACRG*-MO arrested gastrulation on dorsal (top) or ventral (down) side when injected at the DMZ or VMZ of 4-cell embryos, respectively.
cg, cement gland; frontal views, dorsal side up (A-C); lateral views, anterior to the left (D-F)

microcephaly or even absence of cranial structures (Fig. 18E). Simultaneously the left-sided marker-gene *Pitx2c* was no longer expressed in such affected embryos. Raising *xlPACRG*-MO concentration to 2.5pmol/embryo led to blastopore closure defects. When injected into the prospective DMZ at 4-cell stage, *xlPACRG*-MO caused NTD and lack of cranial structures. Interestingly, specimens injected into the VMZ in contrast developed head and dorsal structures but lacked ventral tissue. It seemed like *xlPACRG* impairment arrested gastrulation movements and blastopore closure at the targeted side.

This very surprising phentoype was not expected to be caused by the lack of an apparent axonemal protein. Interestingly, similar gastrulation defects have been reported by Philipp Vick upon maternal knockdown of the axonemal motorprotein *dnah9*. DMZ injections of 4pmol *dnah9*-AUG-MO per embryo caused arrestment of gastrulation movements. These morphants resembled early gastrulae, when co-MO injected specimens already reached stage 16 and beyond (Vick 2009). To investigate these interesting gastrulation phenotypes, a comparative analysis of the gastrulation performance of *xlPACRG* and *dnah9* morphant embryos was conducted.

II.2.2.2 Knockdown of *dnah9* and *xlPACRG* inhibited gastrulation

To investigate, if the phenotypes observed by high dose *xlPACRG*-MO and *dnah9*-AUG-MO injections were caused by gastrulation defects, long term time-lapse movies (~4hrs) of control and morphant specimens were acquired. In wildtype embryos, gastrulation initiates dorsally with the formation of bottle cells at at stage 10 (Keller 1981). Due to the constriction of the apical membrane and the embedded pigments of these cells, this is visible as a dark crescent vegetal to the DMZ. Subsequently, these cells start to invaginate into the embryo. CE of the involuting marginal zone pushes dorsal tissue vegetal-wards which results in involution (Gerhart & Keller 1986). The dorsal lip extends bilaterally describing a semi circle (st.10.5, Fig. 19A) until the ventral lip itself is formed by cells that contract apically. Before invaginating, the ventral lip twitches mediolaterally (st.11, Fig. 19A'). Afterwards the blastoporal lip equals a circle which shrinks with ongoing involution of tissue (Fig. 19A''). Aligned along these key points of gastrulation, *xlPACRG* and *dnah9* morphant embryos behaved differently.

In embryos which were injected with 2×2pmol *dnah9*-AUG-MO into the DMZ at the 4-cell stage, the dorsal lip began to form in time which was visible by apical constriction of bottle cells (Fig. 19B). However, these cells did not invaginate, consequently, no dorsal tissue gastrulated into the embryo. After 76min – in time with the control embryo – the ventral lip was formed (Fig. 19B'). Subsequently, the dorsal bottle cells relaxed which was visible by the spreading of the crescent's pigmentation, withdrawing the dorsal side's further developed appearance (Fig. 19B''). The ventral lip behaved normally by twitching mediolaterally but as invagination was not initiated, ventral tissues did also not gastrulate into the embryo.

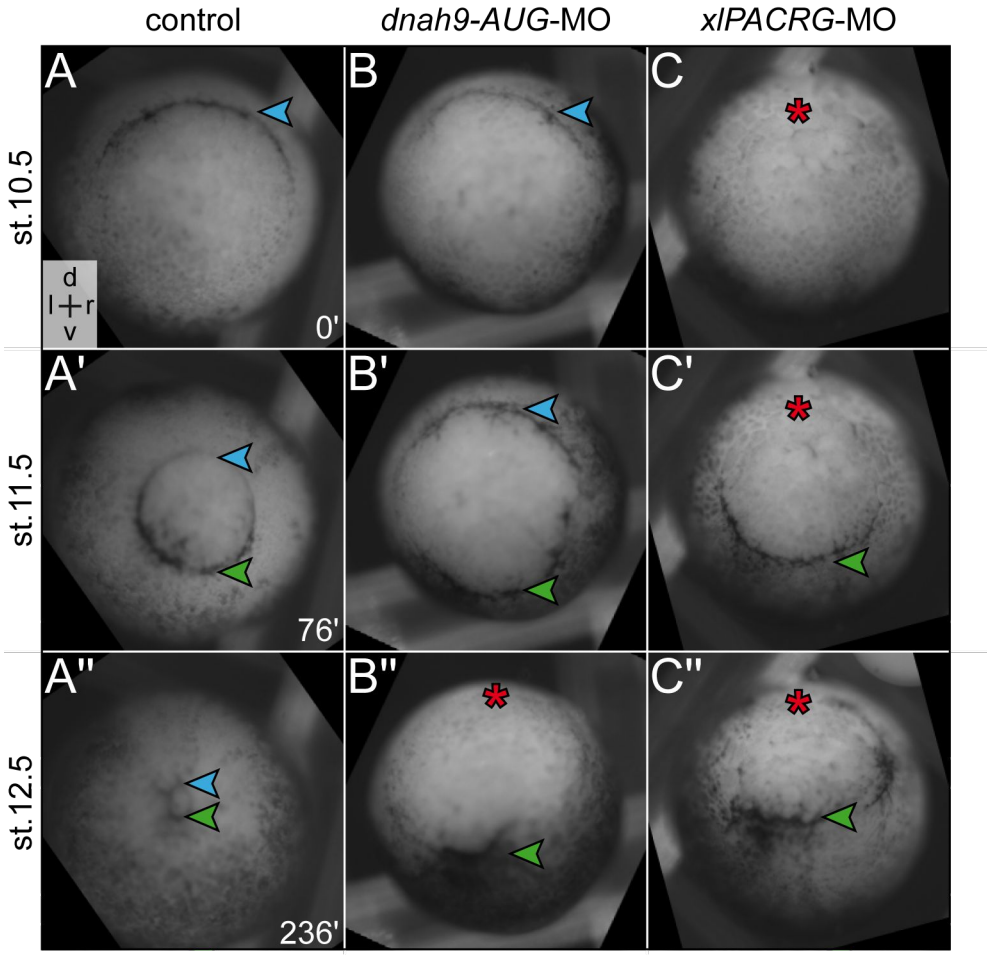

Fig. 19 Inhibition of dorsal lip in *dnah9* and *xlPACRG* impaired specimens
Wildtype time-course (236min) of gastrulation with onset of dorsal lip **(A)**, ventral lip **(A')** and closure of blastopore **(A'')**. Dorsal *dnah9-AUG*-MO injected specimen demonstrated apical constriction at dorsal lip cells **(C)**, proper ventral lip formation **(C')** but relaxation of dorsal lips without invagination **(C'')**. Dorsal *xlPACRG*-MO injected specimen demonstrated no constriction of apical membranes of the dorsal lip **(B)**. Uninjected ventral lip formed in time **(B')** but embryo did not gastrulate **(B'')**.
d, dorsal; l, left; r, right; v, ventral; dorsal lip, blue arrow; ventral lip, green arrow; missing lip, red asterisk; vegetal views, dorsal side up

In contrast, embryos injected with 2×1.25pmol *xlPACRG*-MO at the prospective DMZ in the 4-cell stage even showed no contraction of dorsal pigment at the proper time (st. 10.5, Fig. 19C). With the absence of a dorsal lip, the injected tissue appeared pre-gastrula-like. However, the uninjected ventral lip set up in time (Fig. 19B') and developed normally but failed to invaginate as force from the dorsal lip was lacking (Fig. 19B").

II.2.3 xBic-C is necessary for directionality of leftward flow

As low-dose *xlPACRG*-MO and *dnah9-SB*-MO GRPs tended to grow shortened and unpolarized cilia, the question arose how these cilia are aligned posteriorly. From mouse embryos it is known that the cilia of the PNC are shifted to the posterior pole by the PCP pathway (Antic et al. 2010). One of the effectors thereof is the murine homolog of the *Drosophila Bicaudal C* (*BicC*) gene which is expressed in the PNC of stage E7.5 to E8 embryos (Wessely et al. 2001; Maisonneuve et al. 2009). BicC$^{-/-}$ mutants display aberrant organ situs and randomization of the Nodal-cascade (Maisonneuve et al. 2009). In a collaboration with Daniel Constam (ISREC, Lausanne) the 'leftward flow analyzer' was applied to acquired time-lapse movies of beads traveling the mutant PNC. It was revealed that beads were moving, but a general leftward direction was missing. Particle trajectories were found to project into literally all directions. The clockwise rotational pattern of the PNC cilia was not reported altered but the polarization of these was posterior in only 38% of cases in contrast to 82% of control PNC cilia (cf Fig2 in Maisonneuve et al. 2009).

In the same collaboration, the impact of the frog homolog *xBic-C* on cilia alignment was studied with Philipp Vick and Tina Beyer (for detailed contribution cf IV.1; Maisonneuve et al. 2009). A WMISH using a specific probe for *xBic-C* confirmed expression at the GRP of leftward flow stage embryos (Fig. 20A). However, levels of transcription varied among this structure. The dorsal aspect of the circumblastoporal collar, as well as sGRP cells were significantly stronger stained than the central hyGRP and nGRP subsets (Fig. 20A'). Additionally, *xBic-C* was expressed in the floorplate of the forming neural tube (Fig. 20A'). To investigate the hypothetical role of xBic-C on polarization of GRP cilia, the two published morpholinos *xBic-C*-MO1 and *xBic-C*-MO2

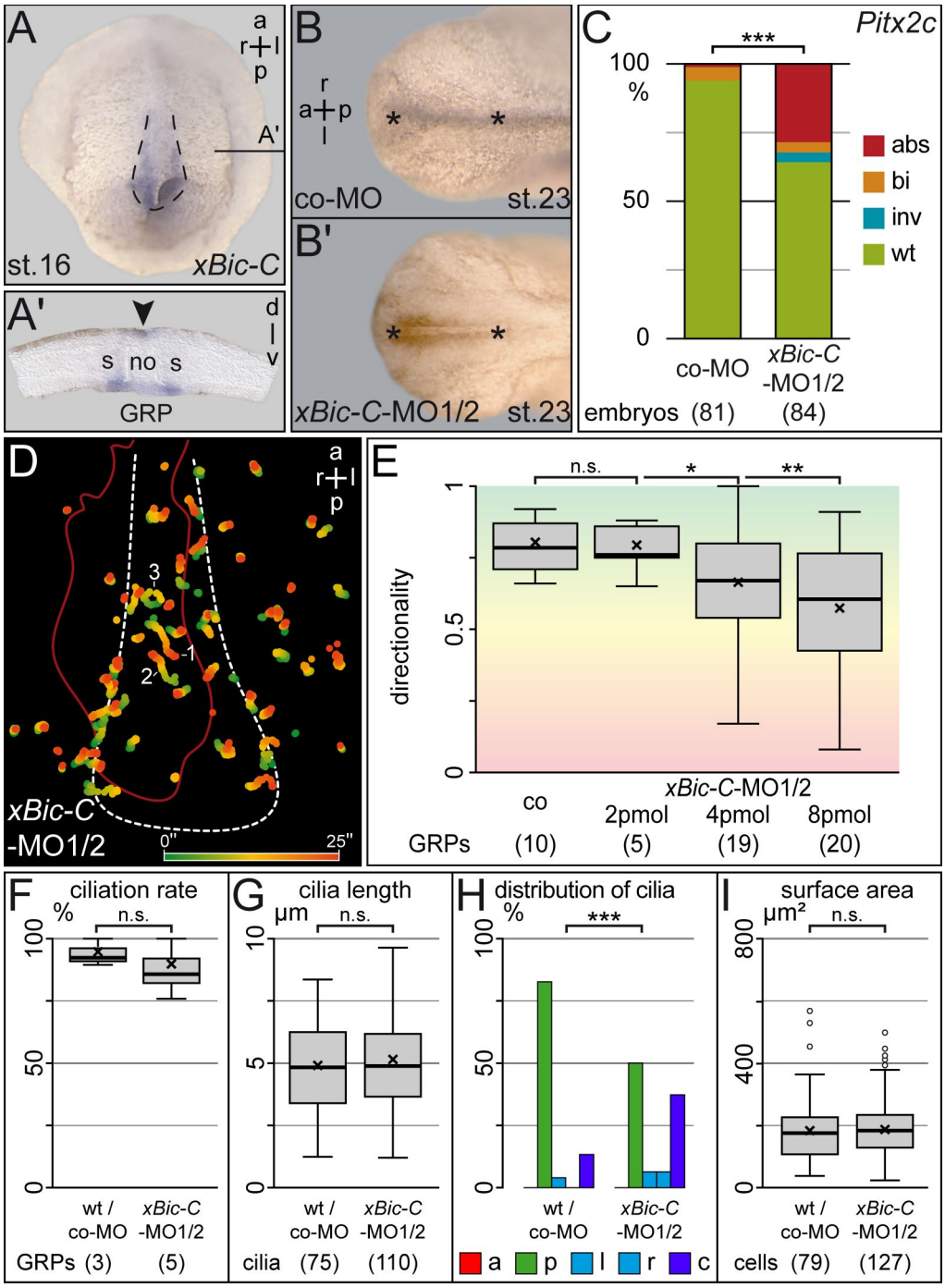

Fig. 20 xBic-C is necessary for posterior polarization of GRP cilia and direction of leftward flow
(A) WMISH for *xBic-C* revealed expression at the GRP. **(A')** Transversal section demonstrates high amount of *xBic-C* transcripts in sGRP and lower amount in other GRP cells. Note also expression in floorplate of neural tube (arrow head). **(B, B')** Neural tube closure delay in *xBic-C* morphants. **(C)** LR axis defects upon knockdown of *xBic-C* are evident from *Pitx2c* misexpression. **(D)** Randomly driven particle trails in *xBic-C* morphant. Direction of travel of particle 1: leftward, 2: top-rightward, 3: trapped in ciliar rotation. **(E)** Directionality of leftward flow decreased with increasing *xBic-C*-MO1/2 concentrations. **(F-I)** Statistical analysis of ciliation properties and cell size in flow relevant GRP areas. Note: no difference from control except for distribution of cilia. Figure partially adapted from (Maisonneuve et al. 2009)
a, anterior; abs, absent; bi, bilateral; c, central; inv, invers; l, left; no, notochord; p, posterior; r, right; s, somite; wt, wildtype; 'x' in boxplots represents mean value, whiskers extend to max 1.5×IQR

were used in combination (Tran et al. 2007). When injected into the DMZ of 4-cell stage embryos, *xBic-C*-MO1/2 caused delay of neural tube closure from stages 12-22 (Fig. 20B) as well as laterality defects revealed by a WMISH for *Pitx2c* at stages 28-32 *(*Fig. 20C; cf (Maisonneuve et al. 2009; Vick 2009). Like in *BicC*$^{-/-}$ mice, fluorescent beads were found to travel randomly at the GRPs of stage 17 *xBic-C*-MO1/2 morphant embryos with trajectories projecting in all possible directions or beads getting trapped by local cilia vortices (Fig. 20D). The latter is also observed at the condition of outgrowing but not yet polarized cilia at wildtype stages 15/16 (Weber 2006; Schweickert et al. 2007). Directionality of leftward flow decreased in *xBic-C*-MO1/2 in a concentration dependent manner (Fig. 20E). In detail SEM analysis of the flow relevant portion of morphant GRPs (cf II.1.2) revealed that ciliation rate, length of cilia and GRP cell surface area was not affected upon *xBic-C*-MO1/2 injections (Fig. 20F, G, I). Solely the polarization of GRP cilia was very highly significant different from wildtype GRP cilia (Fig. 20H) with a decreased portion of posterior cilia from 83.2% to 49.8% in benefit of central cilia.

II.2.4 Downstream targets of leftward flow – *Nodal* and *Coco* are relevant for laterality but not leftward flow

The above experiments demonstrated that absence or immotility of GRP cilia and misalignment thereof led to laterality defects as in all cases leftward flow was impaired. It is known that the bilateral expression domain of Nodal in the posterior paraxial mesoderm is necessary for the induction of the asymmetric Nodal-cascade in the left LPM . Also does the blockage of its co-expressed inhibitor *Coco* on the right side of this domain lead to LR axis defects (Vonica & Brivanlou 2007). This raised two questions which were addressed in a collaborative project of our group (Philipp Vick, Tina Beyer and Isabelle Schneider; for detail cf IV.1): (1) Are the cells that express *Xnr1* and *Coco* part of the GRP like the murine crown-cells which express *Nodal* and c*erl-2* (Marques et al. 2004)? (2) Are the laterality defects of these factors when knocked down caused by inhibition of leftward flow?

WMISHs for *Xnr1* and *Coco* demonstrated a comparable expression in the posterior part of the archenteron of neurulating embryos (Fig. 21A-B). Histological analysis by

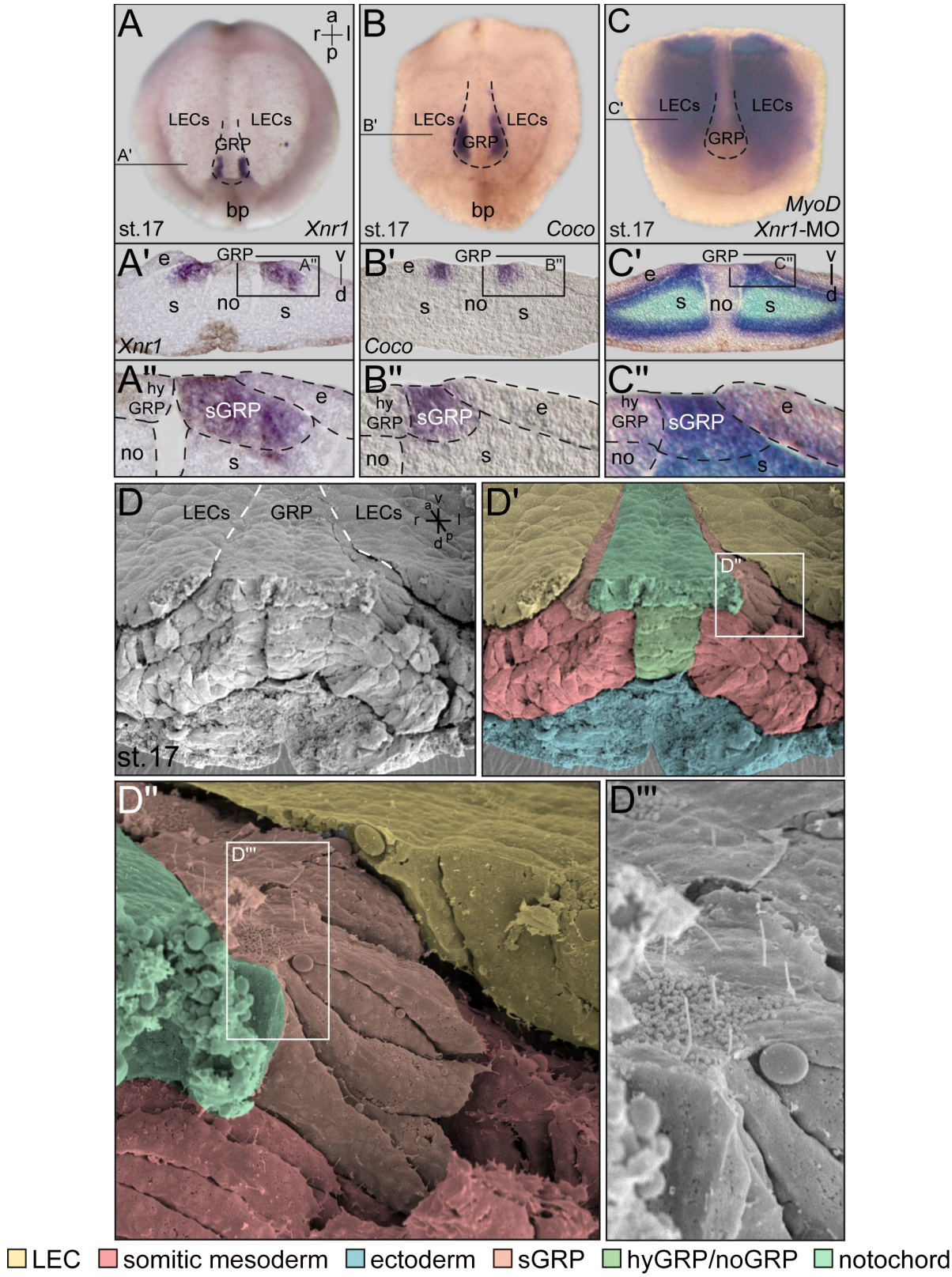

Fig. 21*Xnr1* and *Coco* are expressed in sGRP cells
o **(B)** and *MyoD* **(C)**. *MyoD* positive cells were still existent after injection of *Xnr1*-MO. **(A'-C')** Transversal sections revealed contribution of *Xnr1*, *Coco* and *MyoD* positive somitic cells to the GRP. **(A"-C")** Higher magnification of left sGRP region. **(D)** SEM of posterior dissected neurula.Higher magnifications **(D")** demonstrated ciliation of these cells **(D"')** and identified

vibratome sectioning revealed that the posterior paraxial domains of *Xnr1* and *Coco* were part of the GRP (Fig. 21A'-B'). In comparison with the presumptive mesoderm marker *MyoD* (Fig. 21C), it could be deduced that the very cells of this domain are of somitic fate (Fig. 21C') and mark the sGRP cells (Fig. 21A''-C''). Also after injection of *Xnr1*-MO that caused laterality defects (Fig. 22D), the sGRP cells were still present and part of the GRP (Fig. 21C'-C''). In addition, correlation with a SEM photograph of a posterior transversally dissected embryo (Fig. 21D) supported the assumption that the *Xnr1* and *Coco* positive cells represent the somitic subset of the GRP epithelium (Fig. 21D'-D''). In addition, ciliation of mostly central cilia at these cells was obvious from higher magnification (Fig. 21D''').

Interestingly, *X. laevis* specimens injected with the MO against *Xnr1* at the 4-cell stage (*Xnr1*-MO, 2×0.3pmol, 2×DMZ) displayed wildtype leftward flow (Fig. 22A, C) with a mean velocity of 3.2 ± 1.9µm/s (n=8) and a mean directionality of ρ = 0.62 ± 0.17 which was not significantly different from wild type conditions of co-MO injected specimens (p = 0.194). However, the asymmetric Nodal-cascade was mostly absent from the LPMs (data not shown and Schweickert et al. 2010). In detail, unilateral ablation of the *Xnr1*-domain only led to absence of the Nodal-cascade in the left LPM when ablated from the left side of the GRP which can be achieved by injection of the MO unilaterally into the left DMZ of 4-cell stage embryos (Fig. 22D). Right sided knockdown in contrast, did not alter wildtype conditions (Fig. 22D). Inhibition of the *Xnr1*-antagonist *Coco* upon injection of *Coco*-MO (2×0.5pmol) into the DMZ of 4-cell stage embryos also did not alter leftward flow (Fig. 22B). Leftward flow analysis yielded comparable parameters of mean velocity (3.4 ± 1.8µm/s; n=9) and a mean directionality of ρ = 0.73 ± 0.15 which again was not significantly different from co-MO injections (p = 0.73; Fig. 22C). Interestingly, and in contrast to the *Xnr1* morphants, *Coco* depleted specimens displayed bilateral induction of the Nodal-cascade, i.e. expression in both left and right LPMs (data not shown and Schweickert et al. 2010). Likewise, this effect was unilateral, however, only impacting on the Nodal-cascade when ablated from the right but not left side of the GRP (Fig. 22D).

identified these as sGRP cells. Figure adapted from (Schweickert et al. 2010).
a, anterior; bp, blastoporus; d, dorsal; e, endodermal cells ; l, left; LECs, lateral endodermal crest cells; no, notochord; p, posterior; r, right; s, somite

As leftward flow was not altered by loss of *Nodal* and *Coco* but laterality was antithetically, this offered the opportunity to further analyze how leftward flow, Nodal and Coco interact. Epistasis experiments to analyse this cascade were performed by Philipp Vick, Maike Getwan and Melanie Eberhardt and are thus reported here in short (Vick 2009; Schweickert et al. 2010): Under wildtype conditions, the transcription level of

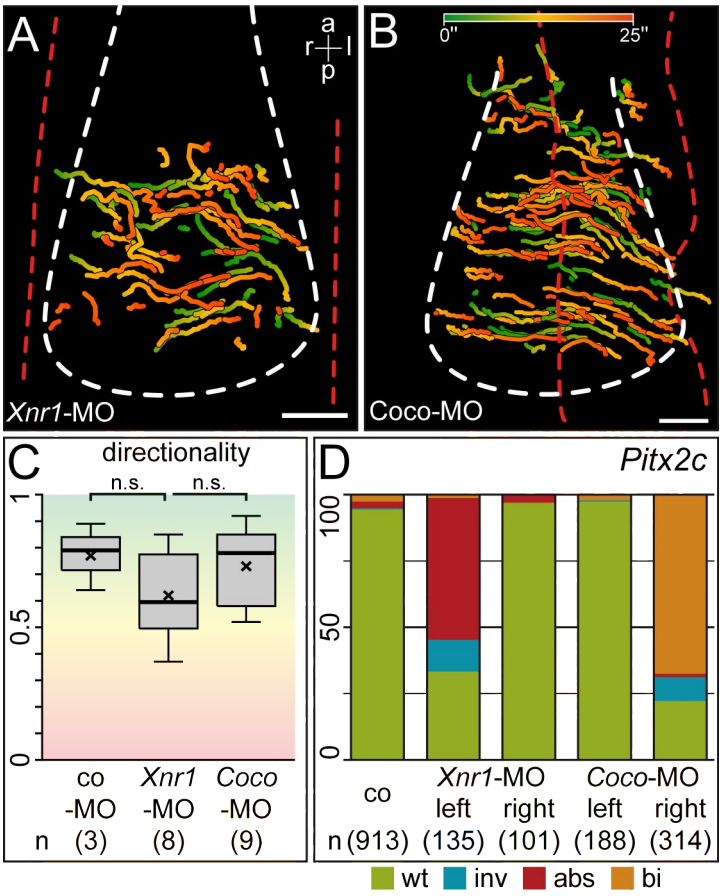

Fig. 22 Loss of *Xnr1* and *Coco* does not impact on leftward flow but laterality
(A-B) GTT projections of leftward flow in *Xnr1* **(A)** or *Coco* **(B)** morphants. Note: *Xnr1*- (2xDMZ) and *Coco*-MO (unilateral left DMZ) injected specimens did not demonstrate altered particle transport. Directionality of leftward was also not altered significantly **(C)** but *Pitx2c* expression was upon left inhibition of *Xnr1* or right inhibition of *Coco* **(D)**. Figure partially adapted from (Schweickert et al. 2010).
a, anterior; abs, absent; bi, bilateral; inv, inverse; l, left; p, posterior; r, right; scale bars represent 50 µm; 'x' in boxplots represents mean value, whiskers extend to max 1.5×IQR

Coco but not *Xnr1* gets asymmetrically downregulated in the left sGRP cells after leftward flow. When leftward flow is blocked molecularly (*dnah9*-MO) or mechanically (1.5% MC treatment), the extent of *Coco* expression stays bilaterally symmetrical and the Nodal-cascade is not induced in neither LPM. When *Coco* is unilaterally left knocked down under no-flow conditions, this rescues the Nodal-cascade in the left

LPM. In contrast, when *Coco* is ablated from the right in no-flow conditions, the Nodal-cascade is activated in the right LPM. A triple knockdown of *Coco*, *Xnr1* and leftward flow depletes the Nodal-cascade from the LPMs again. Therefore it can be summarized that leftward flow is required for release of Xnr1-repression by Coco. Both factors are thus downstream of leftward flow and the downregulation of *Coco* mediates LR axis specification.

The above experiments demonstrated that the event of the leftward flow can be categorized into three main developmental steps: (1) proper formation of the GRP which depended on the organizer, (2) ciliogenesis of motile monocilia that were posteriorly polarized on each GRP cell and (3) the downstream interaction of Coco and Xnr1 which modulated the LR axis in a release of repression mechanism. If intervened at any of these levels, LR axis defects are to be expected. This offers the opportunity to investigate yet unclassified factors impacting on LR axis formation.

II.3 Conservation of the ciliated archenteron and leftward flow

The 'leftward flow analyzer' tool and the 'ciliated cell descriptor' allowed to investigate and compare leftward flow events and the morphology of the flow generating epithelium in different species. Therefore, different model organisms, i.e. such known for leftward flow and such with leftward flow in question, were (re-)analyzed for this event. As the asymmetric Nodal-cascade is conserved in all deuterostomes looked at to date (Lowe et al. 1996; Duboc et al. 2005), it was investigated if leftward flow is present upstream of the occurrence of this gene cascade in each case.

Echinodermata

The common sea urchin *Paracentrotus lividus* as an echinodermate and member of the most basal group of deuterostomia already exhibits the asymmetric Nodal-cascade. In contrast to the asymmetry-preceding midline *Nodal* domain in vertebrates, *P. lividus* displays a single broad expression of *Nodal* at the dorsal midline. Asymmetry is established as this expression is shifted towards the right side (Duboc et al. 2005). To analyze if this asymmetry also depends on a cilia driven fluid flow, embryos were

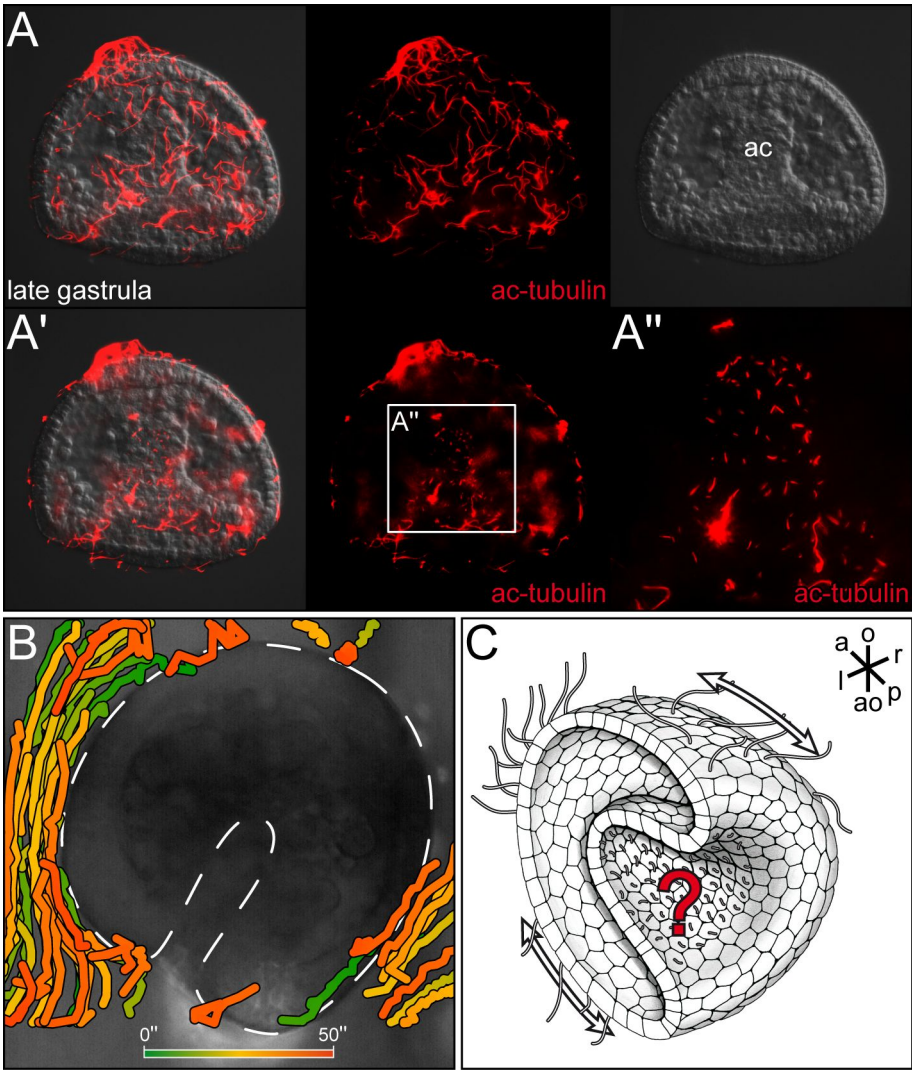

Fig. 23 Ciliation in the late gastrula of *Paracentrorus lividus* and fluid flow at the outer surface
(A-A") IHC against acetylated tubulin. **(A)** Cilia on the outer surface of *Paracentrotus lividus* late gastrula stage. **(A'-A")** Short monocilia inside the archenteron (ac) cavity of same embryo (magnification in **A"**). **(B)** GTTs of vectorial fluid flow on the outer surface of a late gastrula. **(C)** Schematic drawing of ciliation in *P. lividus* and fluid flows (arrows). Motility of cilia inside the archenteron is still unknown.
a, anterior; ao, ab-oral; l, left; o, oral; p, posterior; r, right

fertilized *in vitro* and analyzed for cilia during different developmental stages (cf IV.2.5). Besides cilia on the outer surface (Fig. 23A), the immune histochemistry (IHC) against acetylated α-tubulin indeed revealed monocilia bearing cells in the archenteron of late gastrula embryos (Fig. 23A'). However, motility of the these cilia and a vectorial fluid flow inside the archenteron could not be verified as no fluorescent beads from the medium entered the cavity (not shown). This was likely caused by the fast beating cilia on the outer surface of the embryos that generated a strong current along the AP axis. Although a vectorial flow could not be validated inside the archenteron, the presence of

monocilia at the homologous structure to the murine PNC prior to the asymmetric shift of the *Nodal* expression renders it likely.

Amphibians

With knowledge of leftward flow in *X. laevis*, it was investigated if further amphibian species also develop a GRP and generate a cilia-driven leftward flow. During the course 'cell & developmental biology of *Xenopus*' (2007, Cold Spring Harbor Laboratories, NY, USA), neurula stage embryos of another urodele – *X. tropicalis* – and the caudate *Ambystoma mexicanum* (Axolotl) were collected. From SEM pictures (Tina Beyer) it was obvious, that *X. tropicalis* (n = 3) and *A. mexicanum* (n = 4) exhibited a GRP. Although, these structures bore monocilia, morphology analyzed in the central GRP regions (cf II.1.2) differed from *X. laevis*. In *X. tropicalis,* the GRP consists of ~150 cells (Blum et al. 2009b). Of these (n = 3), 92.15 ± 6.97% were ciliated with 80.39% of posterior polarization, thus being not significantly different from *X. laevis* ($p = 1.0$, $p = 0.241$, respectively). Mean cilia length amounted to 3.72 ± 0.83µm, and mean GRP cell surface area was 131.46 ± 65.54 which both were also not significantly different from *X. laevis.* Addition of fluorescent latex beads to the extracellular medium of dorsal explants cut from stage 16/17 *X. tropicalis* embryos revealed strong leftward flow (see below).

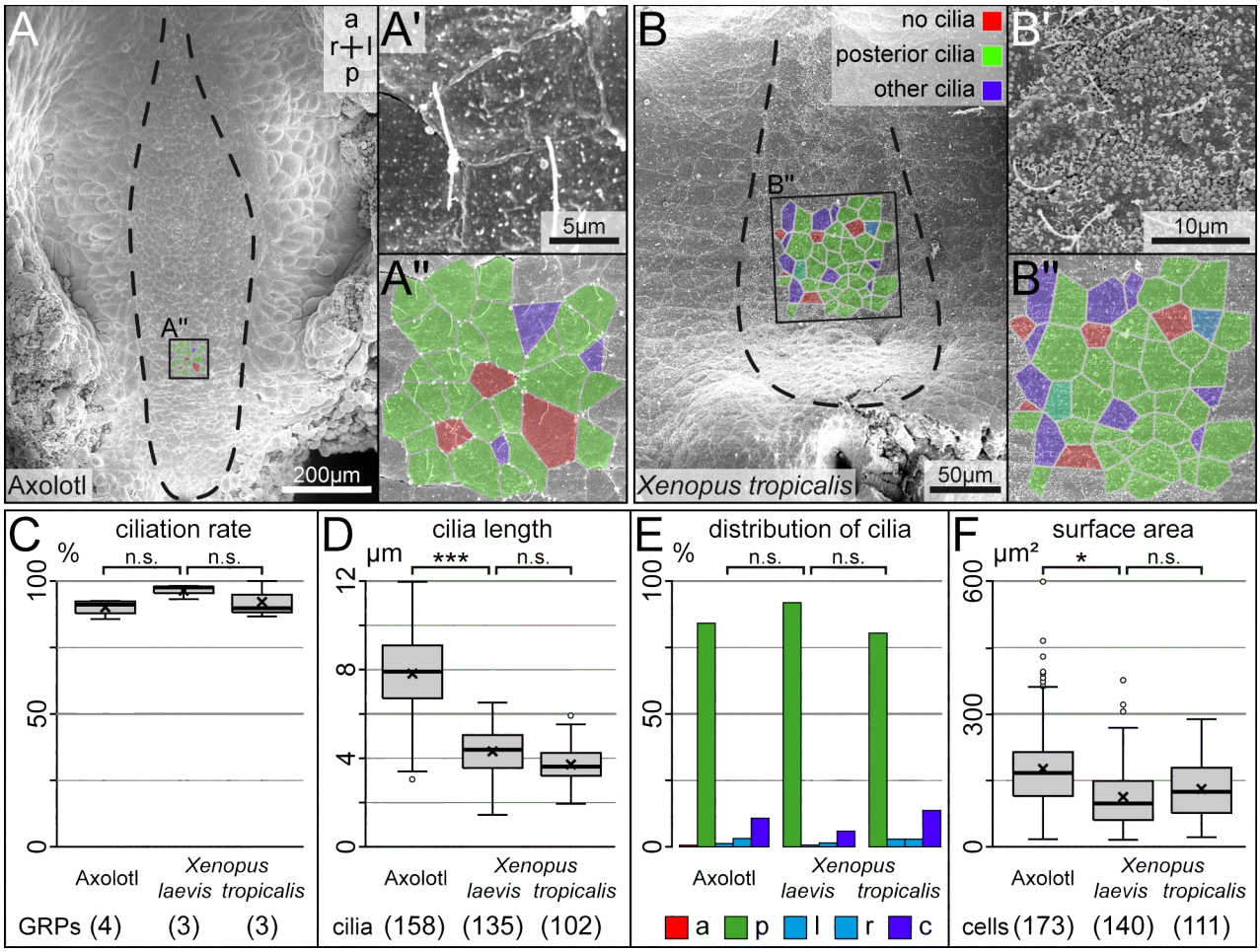

Fig. 24 Axolotl and *X.tropicalis* develop a GRP homologous to the GRP of *X. laevis*
(A-B) Ventral SEM photographs of dorsal explants cut from neurulating *A. mexicanum* **(A)** and *X. tropicalis* embryos **(A, B)** dorsal explants revealed monociliated GRPs (dashed lines). **(A', B')** Higher magnification of ciliated cells revealed mostly posteriorly polarization of GRP cilia **(A", B")**. **(C-F)** Statistical analysis of flow-relevant areas (A", B") revealed comparable ciliation rates, distributions of cilia and surface area of GRP cells to *X. laevis*. Note: cilia length was doubled in *A. mexicanum* **(D)**.
a, anterior; c, central; l, left; p, posterior; r, right; 'x' in boxplots represents mean value, whiskers extend to max 1.5×IQR

The GRPs of *A. mexicanum* stage 16-18 embryos were composed of ~1000 cells (Blum et al. 2009b). Mean length of cilia was very highly significantly increased to 7.82 ± 1.72µm compared to *X. laevis* ($p<0.001$) and mean GRP cell size was significantly larger (175.97 ± 94.56µm²; $p = 0.008$). However, ciliation rate (90.12 ± 3.16%) and distribution of cilia (84.18% posterior polarization) were not significantly different from *X. laevis*. The availability of only few neurula stage Axolotl embryos did not allow to acquire time-lapse movies of the quality sufficient to analyze flow statistically. However, it was clearly visible that the extra-cellular fluid was transported to the left side regarding the movement of particles (not shown).

The mutation in the mixed up mutant is downstream of leftward flow

During a gynogenetic screen by the group of Robert Grainger (University of Virginia, Charlottesville, VA, USA), *X. tropicalis* mutants which displayed heterotaxic organ situs were found (Noramly et al. 2005). Gynogenesis is utilized to quickly screen for naturally occurring mutations which are normally masked by the contribution of the DNA of both parents. In gynogenesis, the embryonic genome is derived entirely from the mother, therefore recessive mutant alleles can yield phenotypes. Gynogenetic haploid embryos are produced by fertilizing eggs with UV-irradiated sperm. The DNA of such treated sperm is damaged and does not contribute to the genome of the offspring, however, it is still able to activate the development of the embryo (Nace et al. 1970). Yet, haploidy is lethal to the embryo around mid-tadpole stage. Diploidy is therefore restored by exposing such zygotes early to high pressure by which the second meiotic division is blocked (Beattie et al. 1999). From the offspring of 160 females in this screen, 8 exhibited left-right asymmetry defects with three of which were genetically heritable ('*mixed up*', '*switched*', '*directionless*' cf. (Noramly et al. 2005).

Mixed up (*mip*) mutant *X. tropicalis* are viable and are characterized by developing heterotaxy of the visceral organs. In addition, a small portion of adult frogs showed subcutical edema (Fig. 25A), the fluid of which could be removed by using a syringe. However, the edema randomly reappeared (personal communication, Takuya Nakayama, UVA Charlottesville, USA). During embryogenesis, *Nodal* and *Pitx2c* are misexpressed displaying the failure of LR axis formation during embryogenesis (Fig. 25B and not shown). In a collaboration with the Grainger group, the *mip* mutant was investigated for hypothetical alterations of leftward flow. The batches that were analyzed comprised *+/mip* and mip/mip offspring. Leftward flow was comparable in both groups, reaching a mean velocity of 5.13 ± 1.21µm/s and a directionality of ρ = 0.53 ± 0.17 in *+/mip* embryos (n=24), and 5.27 ± 2.11µm/s and ρ = 0.55 ± 0.19 in homozygous (n=38) *mixed up* mutants (Fig. 25C-E). The mutated gene should hence be necessary downstream of leftward flow at the level of perception or transfer to the left LPM. Also it remains to be proven if the Coco/Xnr1 system is affected by the *mip* mutation.

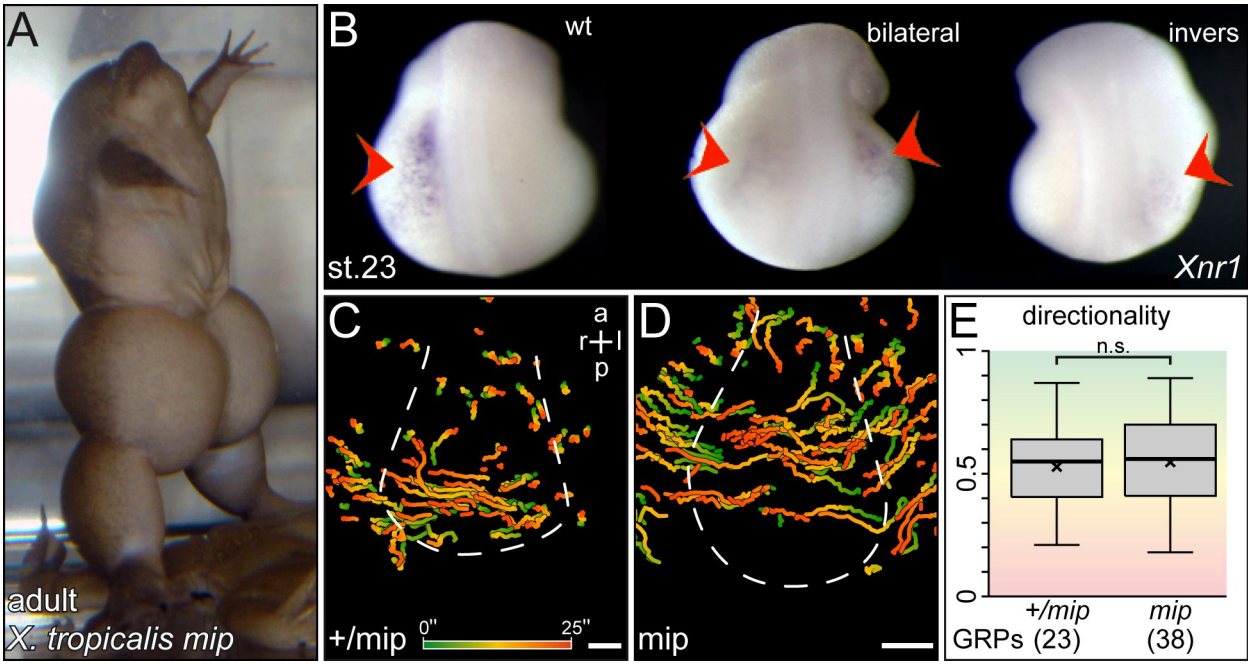

Fig. 25 The mixed-up mutation does not impact on leftward flow
(A) *Mixed-up* mutant *X.* tropicalis adults display enrichment of subcutical fluids. **(B)** During embryogenesis, the Nodal-cascade is mis-activated. GTT-projections of leftward flow of *+/mip* **(C)** and *mip* **(D)** specimens demonstrate normal leftward flow with comparable directionalities **(E)**. A and B are by courtesy of Takuya Nakayama (UVA Charlottesville, VA, USA).
a, anterior; l, left; p, posterior; r, right; 'x' in boxplots represents mean value, whiskers extend to max 1.5×IQR

Nevertheless, *mip* could be mapped to chromosome 1 but the very gene that harbors the mutation is not identified, yet (personal communication, Takuya Nakayama; Khokha et al. 2009).

Mammals

In mammals, leftward flow could be verified for the rodent *Mus musculus* being 4.3 ± 1.1µm/s fast by reaching the directionality of ρ = 0.67 at the posterior notochord (PNC) of 7.5dpf (n = 4) wildtype specimens (Fig. 26A, C; movies were analyzed collaboratively with Philipp Andre; Andre 2009). In the lagomorph *Oryctolagus cuniculus*, leftward flow was present from stages 5 to 8 at the PNC amounting to 2.4 ± 1.3µm/s by displaying a directionality of ρ = 0.59 in wildtype embryos (n = 4; Fig. 26D, F; time-lapse movies were acquired and analyzed collaboratively with Eva Duschek, Bitzer 2008).

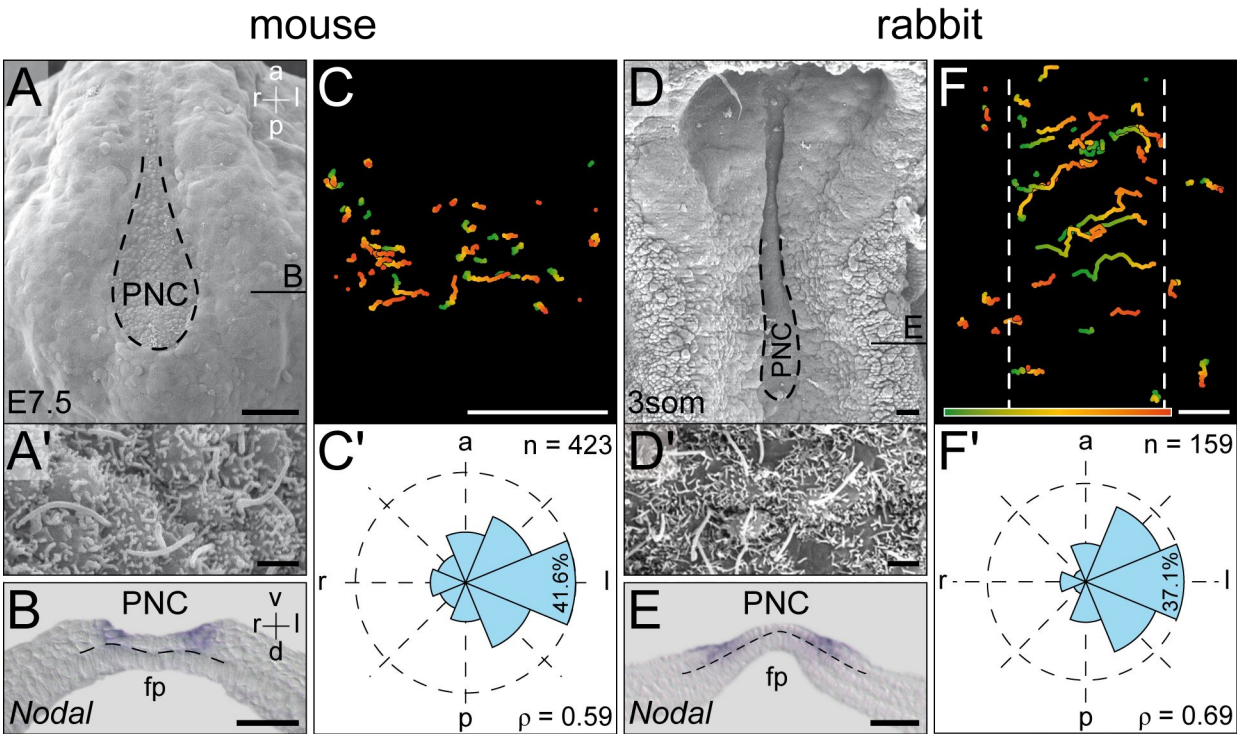

Fig. 26 The monociliated PNC of mouse and rabbit embryos drives leftward flow
The ciliated PNCs of mouse **(A-A')** and rabbit **(D-D')** embryos drive leftward flow **(C, F)**.
Mouse (A-C'; 7.5dpf) and rabbit (D-F'; 3 somite stage) embryos reveal monociliated cells at the posterior notochord (PNC) in SEM analysis (A, A', D, D'; ventral views). Transverse sections (levels indicated in A, D) of embryos with WMISH for *Nodal* which flanks the PNC (B, E). Exemplary still frame from leftward flow driven by the PNC cilia (GTT projections; C, F) with comparable directionality (C', F'). Figure adapted from (Blum et al. 2009a).
a, anterior; d, dorsal; fp, floorplate; l, left; p, posterior; r, right; v, ventral; scale bars represent 50µm; gradient bar represents 0-4.3” in C and 0-25” in F

II.4 Relation of early asymmetric LR determinants and leftward flow

The above experiments and analyses demonstrated necessity and conservation of the cilia driven leftward fluid flow at the epithelium of the PNC/GRP for breaking the initial symmetry of amphibian and mammalian embryos during neurula stages. However, especially in *Xenopus*, there is still an ongoing debate on symmetry breakage with models and hypotheses in favor of an earlier asymmetry establishing event, the most prominent of which is the 'Ion-flux' hypothesis (cf I.3.7). Here, an electrophoretic mechanism should lead to an asymmetric accumulation of a morphogen already during cleavage stages. Indeed, the neurotransmitter serotonin (5-hydroxytryptamine, 5-HT) was described to be asymmetrically distributed already at the 32-64 cell stage and might account for such morphogen (Fukumoto et al. 2005). In addition, when inhibited during a pharmacological screen, serotonin signaling was revealed to be crucial for LR axis formation (Fukumoto et al. 2005). The question arose if there was a connection of serotonin signaling and leftward flow and if and how the early asymmetry of 5-HT impacted thereon. In a joint project of our group and Michael Danilchik (OHSU, Portland, OR, USA; for detailed list of contributed work cf IV.1), the role of serotonin signaling was re-investigated in LR axis specification with attention to the symmetry breaking event of the leftward flow. In contrast to pharmacological inhibition experiments by incubation, serotonin signaling should be genetically inhibited by specifically impairing serotonin signaling via certain receptors.

II.4.1 Loss of serotonin signaling led to LR axis defects

When blocking receptor mediated signaling, there are two possibilities:

1. inhibition of the ligand – by direct quenching or by blocking its synthesis
2. inhibition of the receptor – pharmacological allosteric inhibition or knockdown of the gene encoding the receptor (or subunit)

The last step in the synthesis of serotonin is marked by the activity of the enzyme tryptophan hydroxylase (*tph1*). Blockage thereof should hence lead to loss of synthesized serotonin. Deducing from the time point of *tph1* expression, synthesis of 5-HT was analyzed during *Xenopus* development. Interestingly, *tph1* was not expressed until after neurulation (Axel Schweickert, personal communication). This is in good agreement with pharmacological inhibition experiments of this enzyme from cleavage to gastrulation which also did not affect laterality (Fukumoto et al. 2005). Therefore, inhibition of the serotonin synthesis was no option to manipulate serotonin signaling in early development as all provided 5-HT should be of maternal origin.

Hence, we focused on the serotonin receptors to interfere with 5-HT signaling. From a pharmacological screen where *Xenopus* serotonin receptors have been blocked, class 3 (5-HT_3) revealed 10-22% heterotaxic embryos (Fukumoto et al. 2005). To investigate serotonin signaling at the GRP, pharmacological inhibitors were not used because of their low efficiency and potential unclear cross reaction, knockdown experiments of the *Xenopus* serotonin receptor were be performed instead. As the 5-HT_3 receptor displays a pentameric structure, a subunit thereof was cloned in *Xenopus* (*xHtr3*) which showed 58% homology to the human gene encoding the subunit A (*hHTR3A)* of 5-HT_3. The human subunit h5-HT3A is well characterized by being composed of a signal peptide and the ligand binding domain (LBD) in the large N-terminal region, as well as four transmembrane (TM) regions with a large intracellular loop between TM3 and TM4 in the C-terminus (Fig. 27A). The LBD also exhibits essential loops for serotonin binding (loops A-F). Alterations to the arrangement of these loops cause inefficiency for binding serotonin as demonstrated by the human splice variant *hHTR3AT* (*hsv*, for simplicity) which lacks loops F and C by erroneous read-through into intronic sequences (Fig. 27A; Brüss et al. 2000; Niesler 2011). Told by

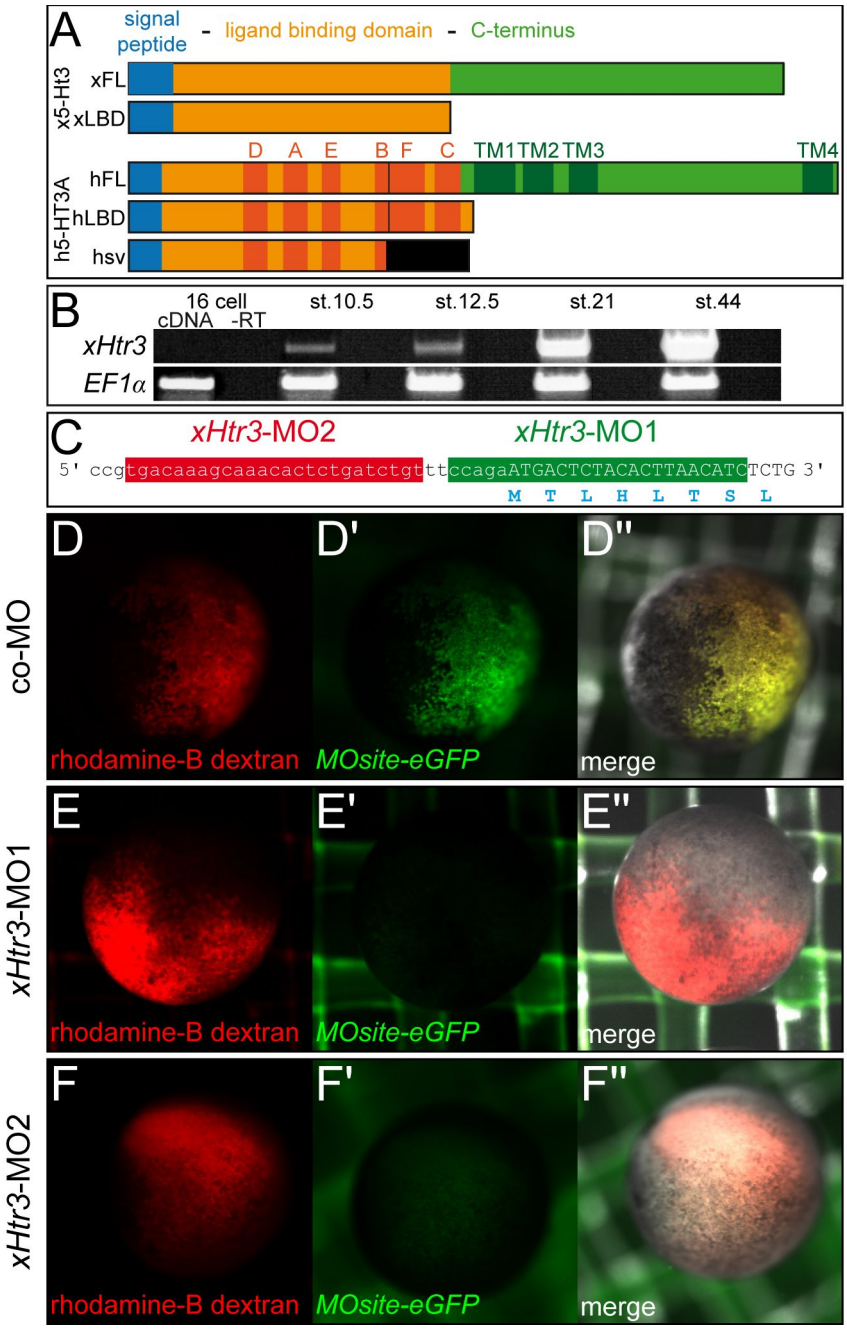

Fig. 27 Serotonin receptor class 3, cloning and specificity of MOs
(A) Serotonin receptor class 3 (5-HT_3). Schematic representation of domainstructure of full-length frog (xFL) and human (hFL) receptor subunits (x5-HT3, h5-HT3A), consisting of signal peptide (blue), ligand binding domain (LBD; orange) with six loops essential for 5-HT binding (A-F; red) and C-terminal region (green) with four transmembrane regions (TM; dark green) are characteristics of 5-HT3A. A human splice variant (hsv, 5-HT3AT) lacks binding-essential loops F and C but contains additional amino acids (black) due to read-through into intronic sequences (Niesler 2011). truncated constructs xLBD and hLBD lack C-terminus. **(B)** RT-PCR analysis demonstrated absence of maternal transcripts (16-cell) and onset of zygotic *xHtr3* transcription during gastrulation (stage 10.5). **(C)** 5'UTR and translational start sequence of *xHtr3.* Binding sites for MOs are indicated. **(D-F)** Fluorescence of *MOsite-eGFP* over-expression was blocked by co-injection of *xHt3*-MOs but not co-MO, demonstrating specificity of the former.

RT-PCR, *xHtr3* was first expressed from stage 10.5 onwards (Fig. 27B). Cloning of the full length frog *xHtr3* (*xFL*) allowed to interfere with serotonin signaling in *Xenopus* via two approaches.

In a first approach, two morpholinos against the *xHtr3 subunit* were designed in non-overlapping regions: one covering the start codon (*xHtr3*-MO1) and a second one against the 5' UTR region (*xHtr3*-MO2; Fig. 27C). To prove the specificity of the *xHtr3*-MOs, a 60bp fragment covering the part of the 5' UTR and start-codon region of *xHtr3* the MOs were designed against was cloned and fused to eGFP (MOsite-eGFP). In embryos of stage 9 which were injected animally at the 4-cell stage, fluorescence upon over-expression of 100ng/µl *MOsite-eGFP* mRNA was significantly reduced by co-injection of 2pmol *xHtr3*-MOs (Fig. 27D-F). This demonstrated specificity of *xHtr3*-MOs as translation of the reporter construct was inhibited. Therefore, serotonin signaling via receptor class 3 should be blocked specifically.

Second, a more broad approach for squelching serotonin off the embryo irrespective of the receptor class was introduced. This was achieved by over-expression of just the N-terminus (signal peptide + LBD) of *Xenopus Htr3* or human *HTR3A*. The well characterized *HTR3A* served as reference to deduce the sequence of the ligand binding domain of the frog *xHtr3* and both ligand binding domains (*xLBD*, *hLBD*) were subcloned into expression vectors.

II.4.2 Loss of serotonin signaling impaired cilia beat frequency in epidermis cilia bundles

In contrast to the sensitive RT-PCR (Fig. 27B), a WMISH with a specific probe for *xHtr3* could not verify location of this transcript until early tadpole stages. At stage 31 the punctate pattern in the epidermis (Fig. 28A) could be overlayed by an IHC against α-tubulin, demonstrating *xHtr3* expression in multiciliated cells (Fig. 28B). An additional IHC against serotonin revealed localization of 5-HT in two types of epidermal cells: multiciliated (Fig. 28C-C') cells and secretory cells (Fig. 28C''). Here 5-HT was found in vesicular structures inside of what supposedly were secretory cells (Fig. 28E) or being attached to some axonemes of the cilia bundles (Fig. 28D, D'). From rat brain

ependymal cilia and sea urchins it is known that 5-HT signaling can modulate ciliar beat frequency (CBF, Wada et al. 1997; Nguyen et al. 2001). The attachment of presumable 5-HT vesicles to epidermis cilia hinted for 5-HT signaling being involved in beating of these cilia. In *Xenopus*, the epidermal cilia bundles can be stained *in vivo* with membrane-RFP (*mRFP*) and their beat pattern can be acquired by time-lapse videography (Fig. 28F). When 5-HT signaling was inhibited in the epidermis by animal ventral injection of 1.3pmol *xHtr3*-MO1 or -MO2 at the 4-cell stage, the regular beat pattern of the the epidermis cilia was reduced or absent (Fig. 28G). When the full-length rescue construct of *x5Htr3* which was mutated in such that the MOs could not bind was co-injected (5ng mRNA + 0.25ng DNA), the impaired mostly motility could be rescued. This indicated an involvement of serotonin signaling for positively regulating CBF in the epidermis of *X. laevis*. Therefore, it was imaginable that loss of serotonin signaling could inhibit CBF of GRP cilia and therefore hinder leftward flow. Therefore, dorsal loss of serotonin signaling experiments should yield laterality defects.

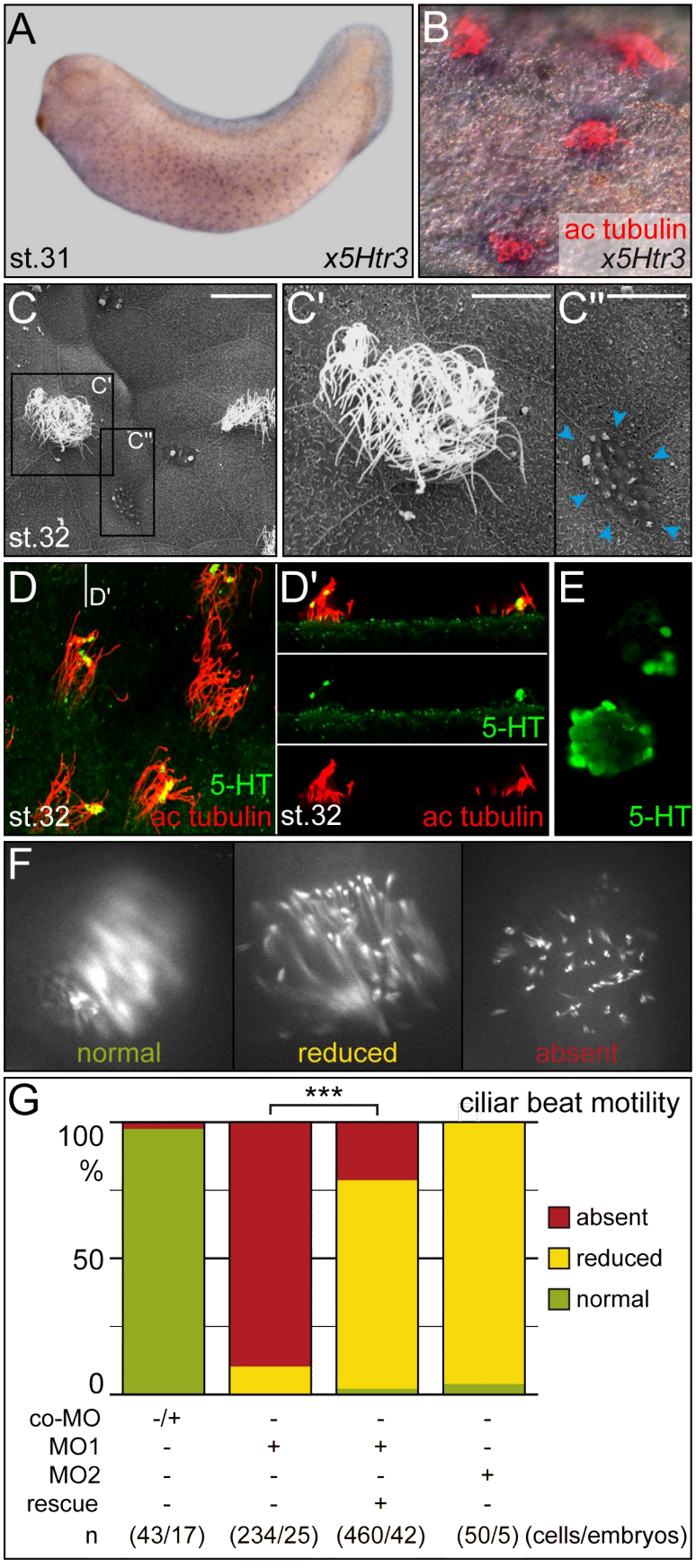

Fig. 28 Serotonin signaling drives beating of epidermal cilia bundles

(A) WMISH for *x5Htr3* revealed epidermal punctate pattern in tadpole stages. **(B)** Co-staining with α-tubulin revealed localization of *x5Htr3* in multi-ciliated epidermis cells.

(C) SEM pictures of epidermis cells. **(C')** Multiciliated cell, **(C")** secretory cell.

(D-D') IHC against serotonin (green) and acetylated tubulin (red) revealed vesicular localization of 5-HT in the epidermis. Larger 5-HT positive vesicles randomly attached to cilia bundles and membrane.

(E) Enrichment of 5-HT in vesicle-like structures of secretory cells.

(F) Beat patterns of wildtype (left) and *x5Htr3*-MO injected cells (middle, right). Fluorescence upon 100ng/µl *mRFP* injection. Maximum intensity projections of 5 sec time-lapse movies.

(G) Quantification of beat pattern distribution in control, *x5Htr3* impaired and *x5Htr3*-rescue-construct mRNA injected specimens.

Scale bars: 20µm (C), 10µm (C', C")

When targeted to the DMZ in 4-8 cell stage embryos, *xHtr3*-MOs and *LBDs* caused a variety of dose dependent phenotypes. High amounts of *xHtr3*-MOs and *LBDs* led to delay of blastopore closure, neural tube closure defects (NTD), dorsal curvature and small heads (Fig. 29A, concentrations indicated). Lower doses yielded embryos with a normal DAI of 5 (proper axis formation) which exhibited no phenotypes except laterality defects (Fig. 29B). When injected at the DMZ of 4-cell stage embryos, 2×1-1.5pmol *xHtr3*-MO1 or -MO2, as well as 2×40-60ng/µl *xLBD* or 1×40-60ng/µl *hLBD* mRNA in contrast to 2×1pmol co-MO led to laterality defects evaluated by the expression pattern of *Pitx2c* and *Nodal* following a WMISH (Fig. 29C, E). Over-expression of *hsv* (2×35ng/µl mRNA) that lacks essential loops for binding of serotonin (see above) served as control and revealed wildtype *Pitx2c* transcription (Fig. 29C), arguing that the

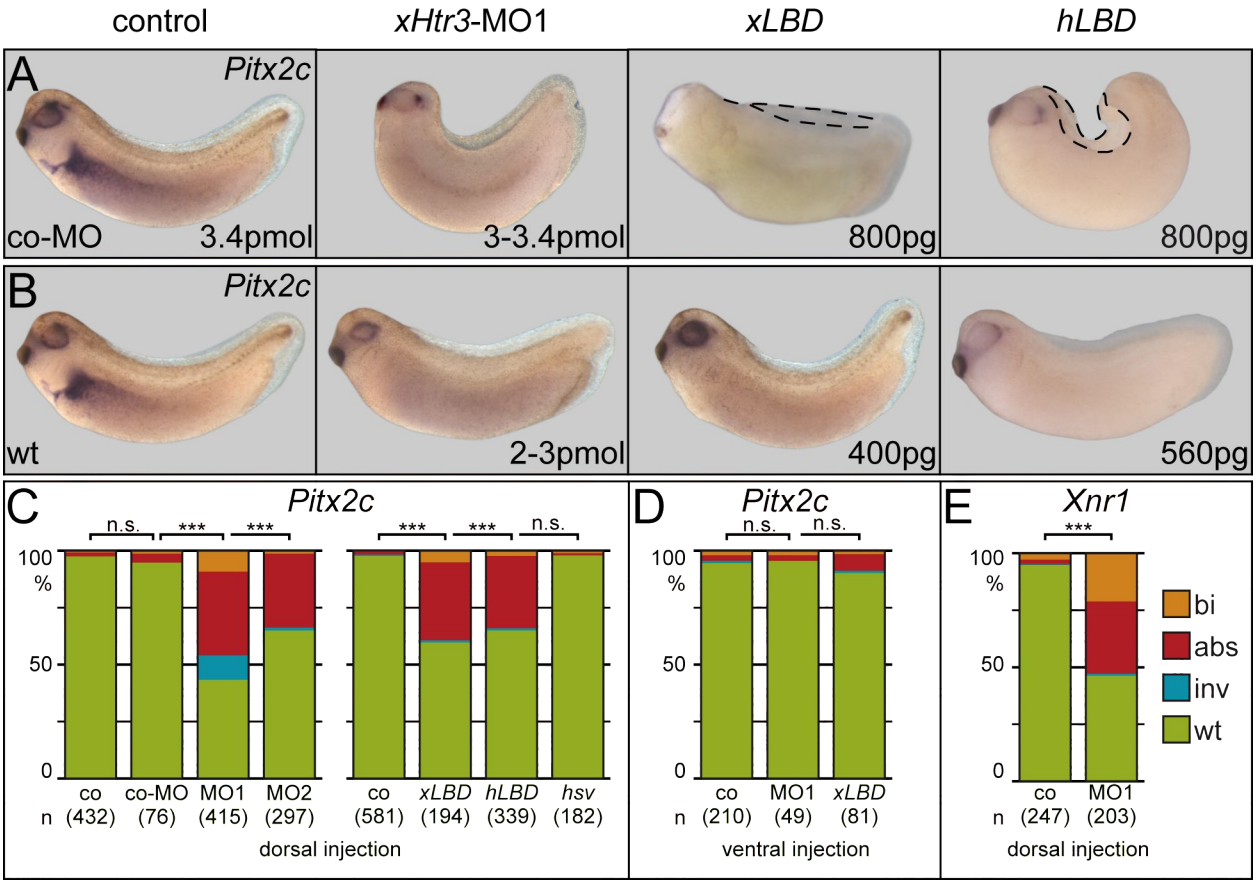

Fig. 29 Loss of serotonin signaling at the dorsal side led to severe phenotypes and laterality defects in a concentration dependent manner
(A) High doses of *xHtr3*-MO1, *xLBD* or *hLBD* led to neural tube closure defects, dorsal curvature and small heads. (B) Lower doses yielded embryos with a DAI of 5 that exhibited laterality defects. (C-E) WMISH for *Pitx2c* or *Nodal* revealed laterality defects. Dorsal (C, E) but not ventral injections (D) led to misexpression of left-sided marker-genes *Pitx2c* (C, D) and *Nodal* (E).
abs, absent; bi, bilateral; inv, dextral expression; wt, sinistral expression; numbers in brackets represent number of embryos analyzed

effect seen by the *LBDs* depended on proper 5-HT binding. Ventral injections of 2×1-1.5pmol *xHtr3*-MO1 and 2×40-60ng/µl *xLBD* mRNA at the 4-8 cell stage had no impact on laterality (Fig. 29D). As impairment of serotonin signaling reduced CBF in epidermis cells and dorsal knockdown revealed laterality defects, it was analyzed if consequently leftward flow is inhibited in serotonin signaling impaired specimens.

II.4.3 Loss of serotonin signaling led to absence of leftward flow caused by defects in GRP morphogenesis

To investigate if leftward flow is absent in serotonin signaling impaired specimens, embryos were injected at the 4-cell stage with 2×1-1.5pmol *xHtr3*-MO1 or -MO2, 40-60ng/µl *xLBD* or *hLBD* mRNA. Dorsal explants were prepared (cf IV.3.1)and leftward flow was acquired and analyzed as described (cf IV.3.2). Among injected embryos, leftward flow directionality dropped very highly significantly (Mann-Whitney-U test, statistical R) to mean qualities of $\rho = 0.37 \pm 0.18$ (MO1), $\rho = 0.50 \pm 0.11$ (MO2), $\rho = 0.40 \pm 0.22$ (*xLBD*), $\rho = 0.52 \pm 0.15$ (*hLBD*) compared to the mean directionality of wildtype flows ($\rho = 0.76 \pm 0.07$; Fig. 30A). In GTT projections this was obvious by bead trajectories traveling in all possible directions upon loss of serotonin signaling (Fig. 30D-E) compared to wildtype leftward moving beads (Fig. 30B).

As the lack of leftward flow can be caused by immotile cilia, ciliogenesis defects or lack of cilia due to improper formation of the GRP, dorsal explants of likewise injected specimens were investigated under the SEM and analyzed for morphology and ciliation (Fig. 31). The flow relevant central proportion of the GRP was analyzed (Fig. 31A-F) to circumvent masking of the differently ciliated somitic GRP cells (cf II.1.2). The mean characteristics of such subsets of wildtype GRPs were as follows: the wildtype GRP-center regions (Fig. 31A) exhibited cells that were $150.64 \pm 127.10 \mu m^2$ in mean size and displayed a ciliation rate of 90 ± 7%. Cilia thereof were 4.60 ± 1.54µm in length and of these 80.00% were polarized to the posterior pole (Fig. 31D-G). In serotonin impaired specimens, however, these parameters differed significantly compared to the wildtype condition. GRP-centers of *xHtr3*-MO1 morphants (Fig. 31B) were composed of cells that were $165.36 \pm 101.13 \mu m^2$ in size and 45 ± 21% of which were ciliated. Cilia thereof were 2.47 ± 1.08µm in length and 35.37% were posteriorly polarized (Fig.

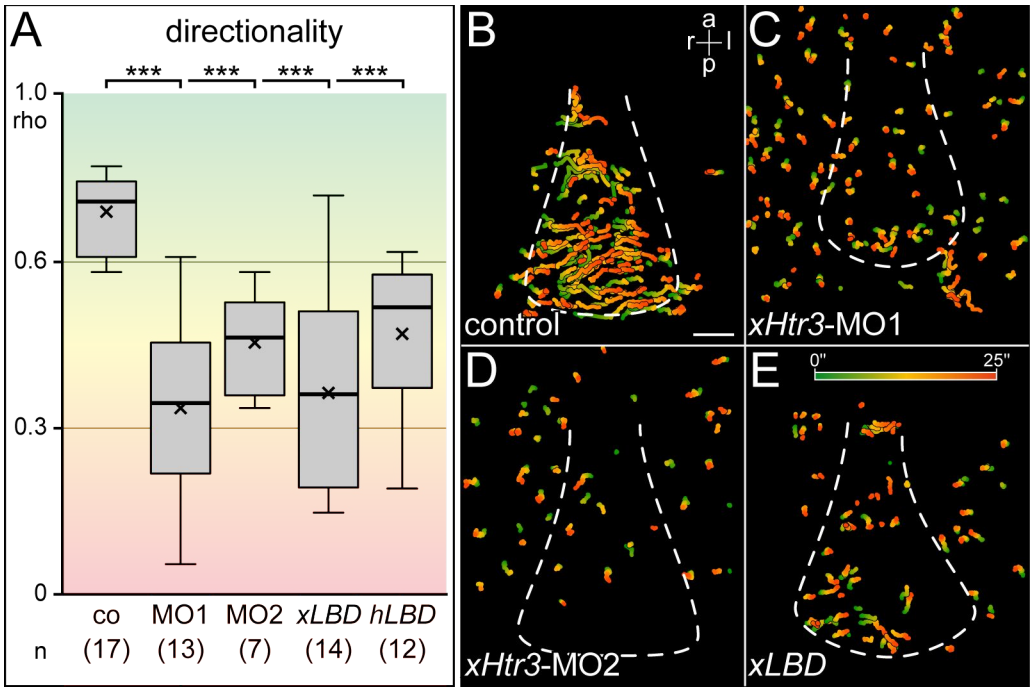

Fig. 30 Absence of leftward flow in serotonin signaling impaired specimens
(A) Quantification of leftward flow directionality (ρ) revealed very highly significant absence of wt leftward flow in controls. (B-E) GTT projections of leftward flow at the GRP in control **(B)**, *xHtr3*-MO1 **(C)**, *xHtr3*-MO2 **(D)**, *xLBD* mRNA **(E)** injected specimens.
a, anterior; l, left; p, posterior; r, right; scale bar represents 50µm, color gradient represents 25”; 'x' in boxplots represents mean value, whiskers extend to max 1.5×IQR

31D-G). In *xHtr3*-MO2 morphants, GRP-centers were made up of cells with a mean cell surface area of 142.95 ± 88.94µm². These displayed a ciliation rate of 66 ± 23% and cilia thereof were 3.07 ± 0.98µm long of which 45.24% were polarized to the posterior pole (Fig. 31D-G). GRP-centers of *xLBD* mRNA injected specimens (Fig. 31C) contained cells that were 221.53 ± 169.16µm² large in average and 71 ± 25% were ciliated. Cilia were 4.00 ± 1.37µm in length and 65.22% were posteriorly polarized (Fig. 31D-G). Injection of *hLBD* mRNA, led to GRP-center cells with mean surface area of 205.53 ± 178.05µm² by exhibiting a ciliation rate of 62 ± 29%. Cilia thereof were 4.21 ± 1.45µm long of which 64.10% were polarized to the posterior pole (Fig. 31D-G). Mean ciliation rate and mean cilia length dropped (very highly) significantly compared to wildtype GRP conditions and the mean surface area of GRP-center cells was increased very highly significantly in contrast to wildtype cells except for *xHtr3*-MO2 injected specimens. These findings did not meet the expected inhibition of CBF upon impairment of serotonin signaling, but revealed morphological defects of the GRP.

Therefore, the question arose when and how serotonin signaling impacted on the specification of the GRP.

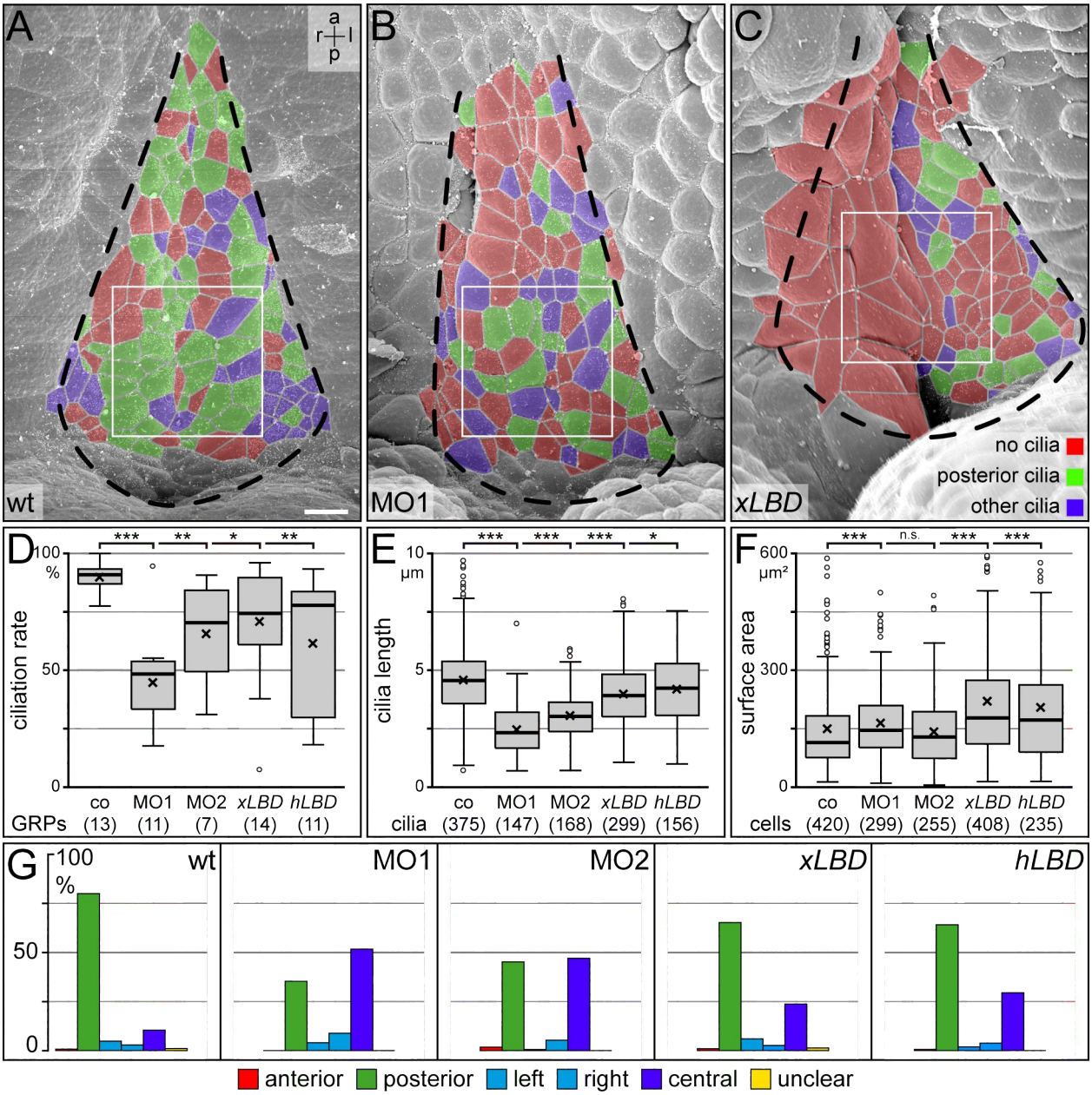

Fig. 31 Serotonin signaling is required for GRP morphology and ciliogenesis
(A-C) SEM photographs of wt (A), *xHtr3*-MO1 injected (B) and *xLBD* mRNA injected (C) stage 17 GRPs. Cells are colored for flow relevant cilia in posterior positions (green), cilia in other positions (blue) or absence of cilia (red). **(D-F)** Quantification of ciliation rate (D), cilia length (E) and surface area of GRP cells (F) in 86µm wide standard squares at GRP-centers (indicated by white squares in A-C) upon *xHtr3*-MO1, -MO2, *xLBD* or *hLBD* injections. **(G)** histograms of cilia distribution. Note significant reduction of posteriorly polarized cilia in serotonin signaling impaired specimens.
a, anterior; l, left; p, posterior; r, right; scale bar represents 25µm, 'x' in boxplots represents mean value, whiskers extend to max 1.5×IQR

II.4.4 Serotonin signaling is required for SM specification

The precursor of the GRP is the SM, i.e. the epithelial layer of the dorsal organizer (Shook et al. 2004). As the 5-HT signaling impaired GRP cells displayed mostly unciliated and larger cells, two possibilities were imaginable to cause this change. First, it was investigated if these altered GRP cells were still derived from the SM. To prove if the SM cells gastrulated normally and contributed to the GRP upon loss of serotonin signaling, embryos were unilaterally injected with *xHtr*-MO1 in combination with mRNA coding for the *lacZ* gene into the left DMZ of 4-cell stage embryos. Embryos were fixed at stage 17 and stained with the β-galactosidase substrate Rose-Gal. LacZ catalyzes Rose-Gal to yield a color change in cells that contain this enzyme, enabling following of descendants of the targeted blastomere(s). At neurulation, targeted cells were found contributing to the GRP (not shown and Vick 2009) which strongly indicated that serotonin signaling impaired cells were intact, gastrulated properly and reached their destination.

Second, it was investigated if the SM was not specified correctly. Because SM cells will give rise to the ciliated GRP, they already express *Foxj1*, a master control gene for motile cilia prior to gastrulation (Pohl & Knöchel 2004; Stubbs et al. 2008). At stage 9.5, *Foxj1* transcription could be demonstrated by WMISH in a crescent above the future dorsal lip (Fig. 32A), exclusively staining the superficial mesoderm (Fig. 32A'). During gastrulation, this tissue tightened medio-laterally, simultaneously crawling towards the dorsal lip at stage 10.5 (Fig. 32B). From stage 12 onwards, *Foxj1* positive cells followed involution movements into the embryo forming the GRP (not shown). To investigate, if impaired serotonin signaling impacted on SM specification, the level of *Foxj1* transcription was used as readout. Indeed, in embryos injected with 2×1.6pmol *xHtr3*-MO1 or -MO2, 2×40ng/µl *xLBD* or *hLBD* mRNA at the DMZ of the 4-cell stage, *Foxj1* expression was very highly significantly reduced or absent at gastrula stages (Fig. 32E, G, L). When 2×0.3ng/µl DNA + 2×5ng mRNA of the full length *Xenopus Htr3* subunit rescue construct was co-injected, *Foxj1* expression was reconstituted (Fig. 32F).

Downregulation of transcription upon loss of serotonin signaling could also be verified for another SM-marker: the TGF-β growth factor *Xnr3* whose expression is also

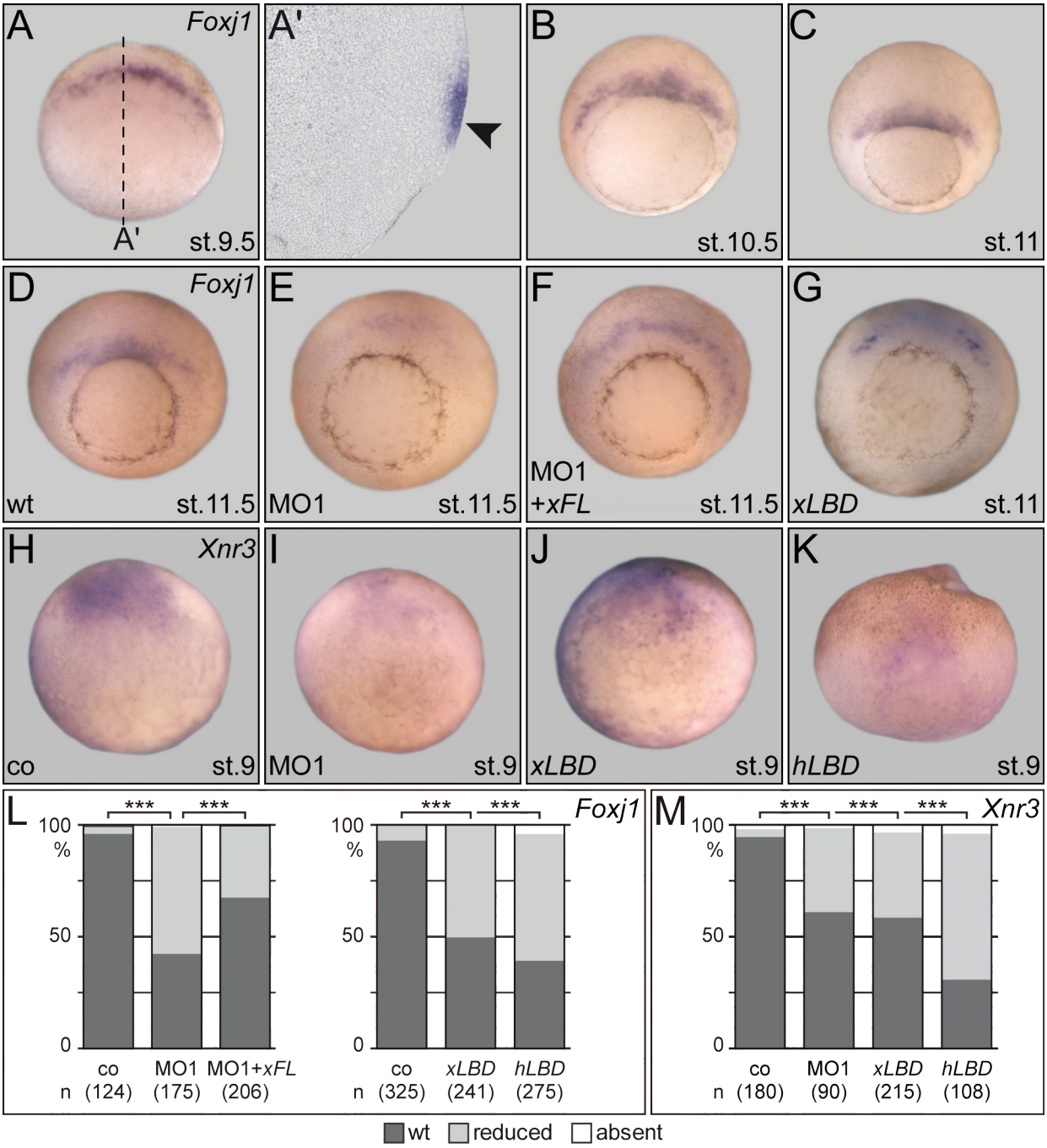

Fig. 32 Serotonin signaling is required for SM specification
(A-C) *Foxj1* transcription during gastrulation is restricted to the SM. **(D-G)** wt *Foxj1* mRNA expression (D) is reduced in *xHtr3*-MO1 (E) and *xLBD* mRNA (G) injected specimens but was rescued by co-injection of mutated *xFL* mRNA (F). **(H-K)** *Xnr3* transcription in the SM (H) was also diminished by loss of serotonin signaling upon injections with *xHtr3*-MO1 (I), *xLBD* (J) or *hLBD* mRNA (K). **(L, M)** Quantification of expression levels of *Foxj1* (L) or *Xnr3* (M). Note very highly significant reduction of SM-markers upon loss of serotonin signaling.
vegetal views, dorsal side up (A-J); dorsal view, animal side up (K)

restricted to the superficial layer of the early organizer (Fig. 32H; Smith et al. 1995). Again, injection of 2×1.6pmol *xHtr3*-MO1, 2×40ng/µl *xLBD* or *hLBD* mRNA into the DMZ of 4-cell stage embryos led to diminished or absent expression of *Xnr3* in the SM (Fig. 32I-K, M). As *Xnr3* is a direct target of the Wnt-pathway (Glinka et al. 1996; Smith et al. 1995), the question arose if there is an interplay of serotonin and Wnt-signaling and if both pathways acted on LR axis formation in combination. The high dose *xHtr3*-MO and LBD phenotypes also hinted to this possibility, as the AP and DV axes of such embryos were malformed (Fig. 29A). To test the hypothetical interplay, the best established embryological assay in the frog, namely the induction of secondary axis formation by ectopic ventral activation of the Wnt pathway was utilized (cf II.2.1.2; Moon & Kimelman 1998).

II.4.5 Serotonin signaling mediated competence for canonical Wnt signaling

If serotonin signaling would interfere with Wnt signaling, alterations in the formation of secondary axes are to be expected upon impairment of 5-HT signaling. *XWnt8* mRNA injections into single ventral blastomeres of 4-8 cell stage embryos induced double axes in 80% of cases (Fig. 33B). Secondary axes were rated 'complete' for developing a full second axis including the head and 'partial' for axis lacking cranial structures (Fig. 33A). Interestingly, when serotonin signaling was impaired by co-injection of either *xHtr3*-MO1, *xHtr3*-MO2, *xLBD* or *hLBD* mRNA, the rate of secondary axis formation was very highly significantly reduced to about 50% in all cases (Fig. 33B). However, when double axes were induced with more downstream factors of the Wnt-pathway, i.e. *Xdsh* (Fig. 33C) or *XSia* mRNA (Fig. 33D), no significant inhibition of secondary axis formation was achieved by co-injection of *xHtr3*-MO1 or *xLBD* mRNA. The reduced amount of *xHtr3*-MO1 injected conjoined twins could be recapitulated by co-injection of mRNA of the full length *x5Htr3* rescue construct (Fig. 33E). The reduction of DAs upon injection of *hLBD* mRNA which is meant to quench endogenous 5-HT, could be rescued by co-injection of 50pMol 5-HT HCl (Fig. 33F). These epistatic experiments demonstrated that the axis induction potential was not *per se* abolished in serotonin signaling depleted embryos.

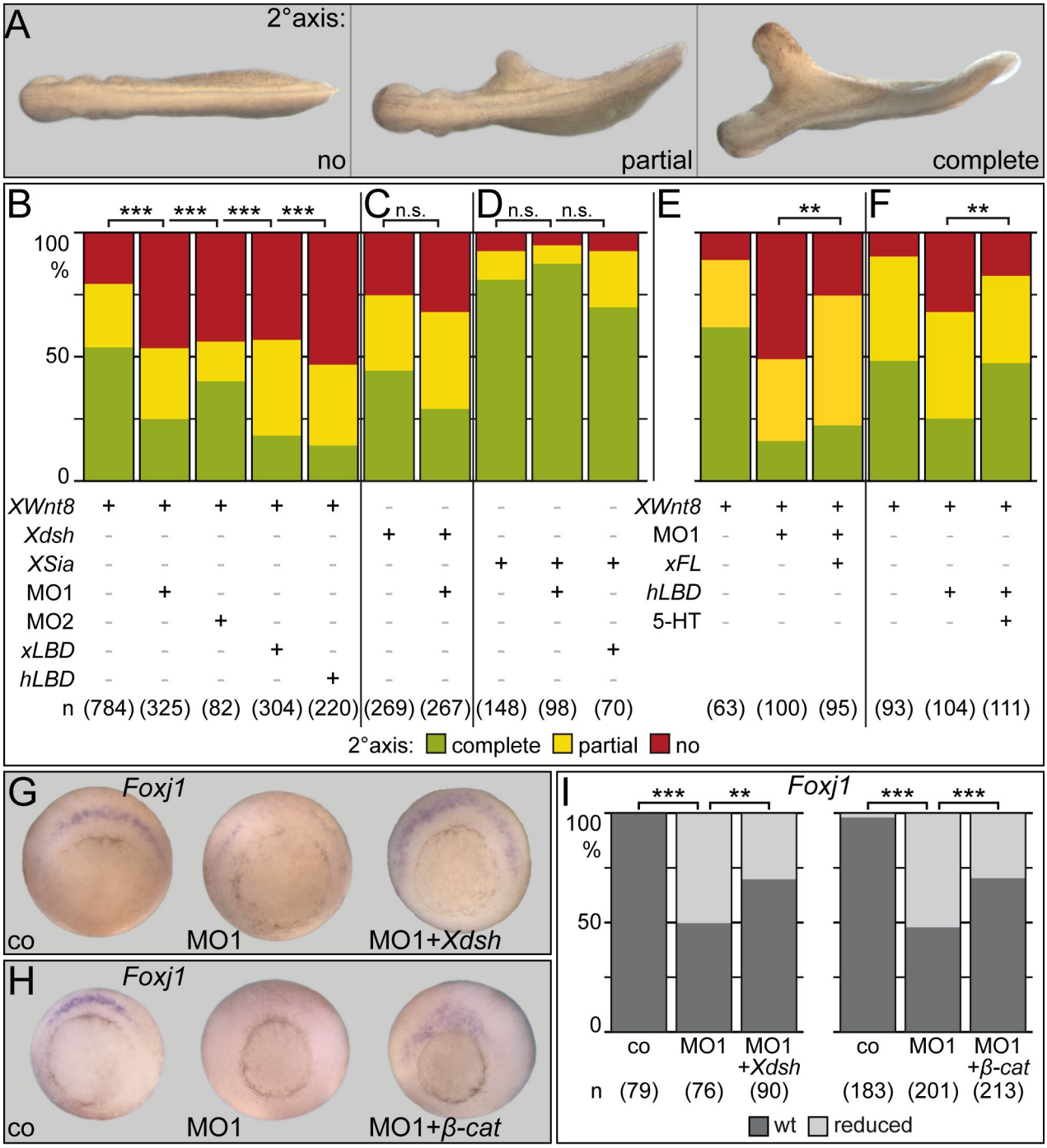

Fig. 33 Interplay of serotonin and Wnt signaling

(A) Categorization in complete, partial or absent secondary (2°) axes of embryos injected with *XWnt8* mRNA at the 4-8 cell stage. (C-D) Co-injection of *xHtr3*-MO1, -MO2, *xLBD* or *hLBD* mRNA inhibited formation of secondary axes induced with *XWnt8* **(B)** but not *Xdsh* **(C)** or *XSia* mRNA **(D)**. MO1 reduction of 2° axes was rescued upon *xFL* mRNA/DNA co-injection **(E)**. *hLBD* mRNA mediated reduction of 2° axes was rescued upon exogenous supply of 5-HT **(F)**. (G-I) *Foxj1* expression was rescued with downstream Wnt factors upon loss of serotonin signaling. WMISH for *Foxj1* revealed reduction upon *xHtr3*-MO1 injection which could be rescued by *Xdsh* **(G)** or *β-cat* mRNA **(H)**. **(I)** Quantification of *Foxj1* WMISH readout.

Numbers in brackets represent numbers of embryos analyzed. (A) Dorsal views, anterior to the left; (G-H) ventral views, dorsal side up

Therefore, it was analyzed if the SM specification defects observed in serotonin signaling impaired embryos could also be rescued with downstream factors of the Wnt pathway, i.e. if *Foxj1* expression was maintained by both, serotonin and Wnt signaling. Indeed, the reduction of *Foxj1* expression upon *x5Htr3*-MO1 injection into the DMZ of 4-cell stage embryos was (very) highly significantly rescued by co-injection of either *Xdsh* (Fig. 33G, I) or *β-catenin* (Fig. 33H-I) mRNA.

II.4.6 No asymmetric localization of 5-HT during early cleavage stages

The above experiments demonstrated that axis induction was depending on serotonin as well as Wnt signaling. Ventral or dorsal depletion of serotonin signaling inhibited secondary or primary axis formation, respectively, including the specification of the SM. This hinted for a non-asymmetric function of 5-HT in contrast to a previous report in which 5-HT was shown to be asymmetrically localized already at the 32-64 cell stage.

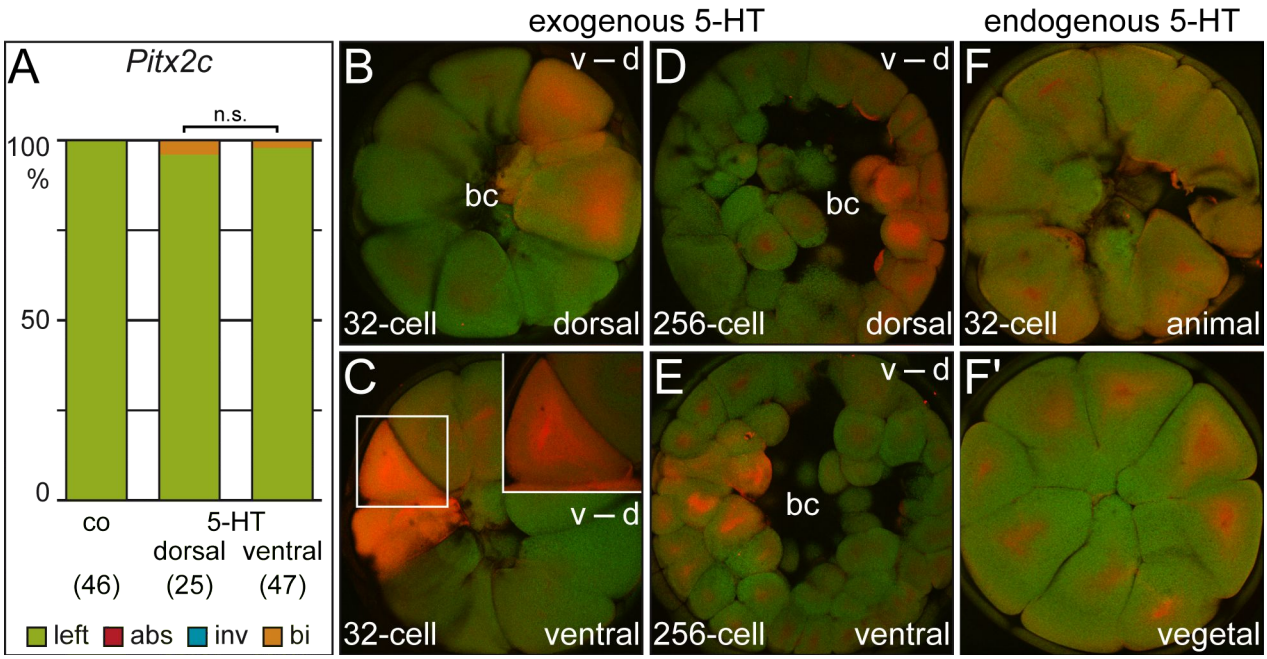

Fig. 34 Ectopic 5-HT has no impact on LR axis formation and stays in cell lineage, endogenous 5-HT is not asymmetrically distributed
(A) Quantification of WMISH for *Pitx2c* of embryos injected with 20ng 5-HT at the 4-cell stage in either dorsal or ventral blastomeres. **(B-F')** IHC against 5-HT (red). Note: ectopic injection of 20ng 5-HT stayed in cell-lineage and did not spread to adjacent cells **(B-E)**. endogenous 5-HT was not asymmetrically localized (exemplary 32-cell stage; animal half **F**, vegetal half **F'**). Green channel represents auto-fluorescence of yolk.
abs, absent; bc, blastocoel; bi, bilateral; d, dorsal; inv, inverse; v, ventral; numbers in brackets represents numbers of embryos analyzed

This asymmetry was also thought to be dependent for LR axis formation (Fukumoto et al. 2005). To analyze if asymmetric 5-HT accumulation impacted on LR axis formation, 20ng serotonin was injected into single dorsal or ventral blastomeres. This amount is approximately a 16-fold molar excess compared to the endogenous 5-HT content (Fukumoto et al. 2005). However, regardless of the site of injection, ectopic 5-HT did not alter neither asymmetric *Pitx2c* expression (Fig. 34A) nor organ situs (not shown).

This unexpected effect could possibly be caused by degradation of the injectate as it is known that serotonin metabolizing enzymes like the monoaminoxidase-1 are maternally provided (Fukumoto et al. 2005). To investigate the distribution of ectopic 5-HT and its hypothetical degradation, an immunhistological method was developed by Michael Danilchik (OHSU Portland, OR, USA) which was capable of detecting subcellular serotonin localization in entire embryos as well as in high resolution. Interestingly, 5-HT injected into single blastomeres at the 4-cell stage could be found in 32- and 256-cell stage embryos, arguing against a degradation (Fig. 34B-E). 5-HT also stayed in the lineage of the injected blastomeres, i.e. descendants of such blastomeres contained high amount of 5-HT in contrast to the adjacent cells (Fig. 34B-E). In addition, the reported asymmetric localization of 5-HT could not be verified. Careful re-investigation at the cleavage stages were conducted, i.e. 40 embryos were evaluated at four time points between 32- and 64-cell stage. In all embryos investigated, neither DV nor LR asymmetries were recorded (Fig. 34F-F'). However, some characteristics of serotonin distribution can be summarized from cleavage up to early gastrula stages: (1) 5-HT was present in all blastomeres with the cells of the animal hemisphere exhibiting a higher amount than the vegetal cells. (2) 5-HT localized to apical and baso-lateral membranes of all blastomeres with no cell exhibiting particular enrichment. (3) Most 5-HT localized around the perinuclear region of blastomeres in a punctate pattern. This pattern persisted up to blastula stages.

II.4.7 5-HT localized to the superficial layer of early gastrula stages

During early gastrula stages, 5-HT was enriched in the whole superficial layer of the animal hemisphere in which the SM is situated at the dorsal side (Fig. 35A,B). Again, 5-HT signal was lower in the vegetal than animal hemisphere with a sharp boundary obvious at the forming dorsal lip whose bottle cells belong to the animal hemisphere and contained more serotonin than the adjacent vegetal cells (Fig. 35C). Compared to the localization patter of 5-HT during cleavage stages, serotonin was also found at the perinuclear region as well as in the apicolateral membranes of each cell.

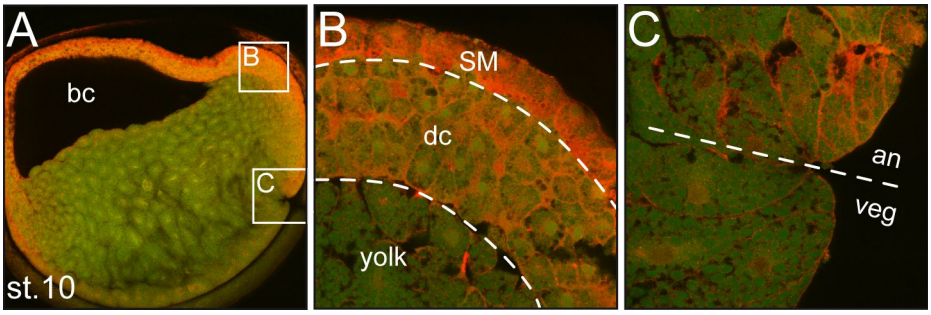

Fig. 35 5-HT accumulates in the superficial layer of early gastrula stages
IHC against serotonin (red) at stage 10.
(A) overview of sagittal section. **(B)** In the animal hemisphere, 5-HT accumulated in the superficial layer and consequently in the prospective SM at the dorsal side. Deep cells (dc) contained lower amounts of 5-HT and the yolk only miniscule 5-HT. **(C)** Bottle cells of the forming dorsal lip contained more 5-HT than vegetal adjacent cells. Note: perinuclear as well as apical and basolateral membrane localization of 5-HT was also obvious in this stage.
an, animal; veg, vegetal; green channel represents auto-fluorescence of yolk

In summary, serotonin signaling could be shown to be essential for LR axis formation by specifying the SM in an interplay with the Wnt pathway. Therefore serotonin signaling indirectly impacted on leftward flow as it provided proper morphology to the GRP where flow is generated. Further, the localization analysis falsified the previously reported early asymmetry of serotonin during early cleavage (Fukumoto et al. 2005).

III Discussion

The present work was conducted to analyze characteristics and requirements for the cilia-driven leftward flow to establish the LR axis in *X. laevis*. A hierarchy of factors impacting on the setup, conduction and perception of leftward flow and thus on laterality could be revealed. In *Xenopus*, an alternative mechanism for symmetry breakage was postulated (the 'ion-flux' hypothesis) which precedes leftward-flow. As leftward flow is necessary for symmetry breakage, it was therefore analyzed if and how the core-factor of the 'ion-flux', namely serotonin signaling, would impact thereon. With the help of the established hierarchy, serotonin signaling was shown to be necessary for the specification of the epithelium that drives leftward flow. Thus the necessity of 5-HT signaling was verified, however, function and time of action differed from published data. Further, in a theoretical approach it was addressed if a mechanism preceding leftward flow is at all plausible for symmetry breakage in *X. laevis*.

III.1 LR axis in *Xenopus*: early determinants vs. leftward flow

Regarding the timepoints of postulated symmetry breakages in *X. laevis*, three possibilities arise. (1) As the AP axis is oriented with the first cleavage furrow (Klein 1987), it is imaginable that this first cell division could possibly be asymmetrical by which a morphogen or determinant could accumulate only in one blastomere. (2) The 'ion-flux' hypothesis postulates a symmetry breakage during early cleavage stages by an asymmetrical accumulation process of morphogens relevant for LR axis formation (Fukumoto et al. 2005). (3) In this work, the cilia-driven leftward flow generated at the GRP during neurula stages was demonstrated to be necessary for LR axis formation (Schweickert et al. 2007). In the following it is discussed if early asymmetries are even plausible to specify the LR axis, if leftward flow acts as amplifier for the hypothetical early asymmetries or if leftward flow might be the sole event to specify the LR axis in *X. laevis*.

III.1.1 Is an early LR symmetry breakage in *X. laevis* even plausible?

In the theoretical approach on how hypothetical early asymmetries might act on laterality in *X. laevis*, it was suggested that (1) an early dorsal asymmetric determinant might asymmetrically act in terms of providing structure or function on the setup, conduction, perception or transfer of the left cue generated by leftward flow; (2) early ventral asymmetries were found rather unlikely to directly signal or specify the LR axis (cf I.4.1).

III.1.1.1 asymmetric leftward flow is based on a symmetrical fundament

The claim that an early dorsal asymmetric determinant (cf I.4.1) could unilaterally impede or modulate the setup, execution or read-out of the cilia-driven leftward flow is not supported by the results of this work. It was shown that SM specification, GRP formation, ciliogenesis, polarization of the GRP cilia and expression of the leftward flow target, namely the interplay of Coco and Xnr1, rely on symmetrical signaling and display a symmetrical setup with an underlying symmetrical morphology in reference to the posterior midline (cf II.2). Sole the leftward flow that is generated by the intrinsic chirality of the cilia rotation acted asymmetrically on the reduction of *Coco* (cf II.2.4). In addition, the possibility of activation or inhibition of the Nodal-cascade in the LPMs in a predictive manner by modulation of *Coco* expression at the GRP (Schweickert et al. 2010), further excluded a role of the hypothetical early dorsal asymmetric determinant in transfer of the flow-generated signal towards the left LPM. These experiments render hypothetical early dorsal asymmetric determinants unlikely to impact on LR axis formation besides or by cilia-driven leftward flow in *X. laevis*.

In the theoretical approach (cf I.4.1) involvement of early ventral asymmetric determinants for LR axis formation appeared rather unlikely. This queastioned the ventral function of 5-HT. Indeed, inhibition of 5-HT signaling on the ventral side did not cause aberrant laterality. In contrast, dorsal impairment of 5-HT signaling impacted on the LR axis (see below). As this is in contrast to a published ventral right accumulation

and early function of serotonin (Fukumoto et al. 2005), 5-HT distribution was re-investigated.

III.1.1.2 The reported early asymmetric ventral right accumulation of serotonin could probably depict a methodological artifact

The whole-mount immunocytochemical approach for 5-HT detection via confocal fluorescence microscopy could not verify the reported early asymmetric localization of 5-HT by Fukumoto et al. 2005. This could either be caused by (1) lack of specificity of the AB, (2) cross-reaction of the AB with degradation products of 5-HT which probably could have masked the proposed asymmetric localization or (3) equal distribution of endogenous 5-HT.

First, specificity of AB-reaction and the method utilized could be demonstrated as exogenous 5-HT was detected inside the injected blastomeres and descendants thereof. In addition, endogenous as well as exogenous 5-HT was found to be incorporated in vesicle like structures accumulating at the apico-lateral membranes and the perinuclear region of each blastomere with no particular asymmetry throughout. Interesting in this context was the absence of the postulated gap junction (GJ) related transfer of 5-HT as exogenous serotonin stayed in lineage of the injected blastomere.

Second, cross-reaction of the utilized AB with degradation products of 5-HT that in theory could mask an asymmetric appearance is also unlikely. If serotonin would be asymmetrically localized, degradation products thereof should likewise be accumulated and would add to the fluorescence signal.

Third, the conclusion can be drawn that serotonin and/or its degradation products are equally distributed among blastomeres of early cleavage stages. 5-HT enrichment at the perinuclear region was already depicted but not further mentioned by Fukumoto et al. 2005 (cf Figure 3G-I, K in Fukumoto et al. 2005). When single optical sections of the acquired z-stacks were examined in which the plane of section grazed the 5-HT rich membrane of a blastomere by chance, staining could give the false impression of 5-HT being asymmetrically enriched (Mike Danilchik, personal communication). Therefore, it

is likely that the hypothesized asymmetrical localization of 5-HT is based upon an unfortunate selection of 5-HT stained sections by Fukumoto et al. 2005.

These findings render it unlikely that an early dorsal or ventral asymmetric localization of a determinant should impact on LR axis formation. However, a cytoplasmic mechanism like asymmetric cell division is well established among the animal kingdom. Although being phylogenetically distant, snails clearly demonstrate that the LR axis can already be specified during the first cleavage stages (Grande & Patel 2009; Kuroda et al. 2009). In addition in *Caenorhabditis elegans*, PAR proteins accomplish asymmetric localization of factors which results in two daughter cells of different molecular composition and cell fates (Nance 2005). But also in vertebrates, asymmetric cell division is detectable. In human embryonic stem cells and mammalian cell culture, proteins that were targeted for degradation were demonstrated to be asymmetrically distributed in the arising daughter cells during somatic mitosis (Fuentealba et al. 2008).

In this respect, the observation that in *Xenopus* sperm-entry driven orientation of the first cleavage furrow coincides with the DV axis (Klein 1987) and the two emerging blastomeres give rise to left and right cell-lineage, may suggest an asymmetrical distribution model. Indeed, it was speculated that the cortex of the oocyte has an intrinsic chirality that might act via actin fibers to asymmetrically pattern the pre-cleaved zygote right after fertilization (Danilchik et al. 2006). An asymmetrical first cell division or imprinting of hypothetical oocyte chirality could theoretically determine the future LR axis. Imaginable in this context could be that leftward flow depicts the amplifier of an hypothetical earlier distributed effector of laterality.

III.1.1.3 It is not early determination but the position of the organizer that defines the LR axis

If such a hypothetical early predetermination of the future left and right sides of the embryo would exist with the first cleavage, the LR axis should inseparably be connected with the first cleavage plane. For investigation of the relevance of a hypothetical predefined LR axis, the orientation of the AP axis needs to be uncoupled

experimentally from the first cleavage furrow. If the LR axis is inseparably connected with the plane of the first cleavage, predictable laterality defects should occur in such specimens.

Sperm entry triggers cortical rotation by which vegetally deposited dorsalizing factors are shifted to the opposite side inducing the dorsal organizer (Moon & Kimelman 1998). By this mechanism, the DV axis is defined. This MT-dependent shifting can be blocked by irradiation with UV-light which depolymerizes MTs (Holowacz & Elinson 1993). Thus, the intrinsic factors that specify the organizer are retained vegetally incapable of signaling. Hence, no axial coordinate system is introduced. However, segregation of pigment in the animal hemisphere still allows to distinguish between the former fates of the blastomeres at the 4-cell stage. Ectopic activation of the canonical Wnt-pathway rescues organizer formation in UV-irradiated specimens with activation of zygotic transcription around stage 9 (Kessler 1997; Bae et al. 2011). This treatment results in wildtype embryos. As the location of the rescue-organizer can be defined by targeted injection, the future orientation of the DV axis can be uncoupled from the orientation of the first cleavage furrow.

Alterations to laterality in *Xenopus* can easily be detected by scoring the organ situs. Three organs are recorded for specific asymmetry (outflow-tract of the heart, gall bladder, gut coiling) with each having 50% chance of being normal or inverted in fully randomized specimens. A random orientation of all three organs therefore leads only up to 12.5% (50% × 50% × 50% = 12.5%) of specimens displaying *situs solitus* by chance. The same percentage is expected for *situs inversus* (concurrent inversion of all three organs), leaving 75% of expected heterotaxia.

If the LR axis would be predefined, four scenarios are imaginable: (1) The organizer can be rescued in its former position (Fig. 36A). An early defined LR axis would therefore be expected to exhibit a Nodal-cascade in the left LPMs and therefore should yield ~100% of wildtype embryos. (2) If the organizer is induced at the former ventral side (Fig. 36B), the pre-defined LR axis would be inverted which should drive the Nodal-cascade in the newly right side, giving rise to nearly 100% of embryos displaying *situs inversus*. (3) If the organizer is rescued in former left blastomeres (Fig. 36C), the right-identity of the former right blastomere descendants would give rise to both LPMs. Hence, the LPMs should lack laterality information, the Nodal-cascade should be

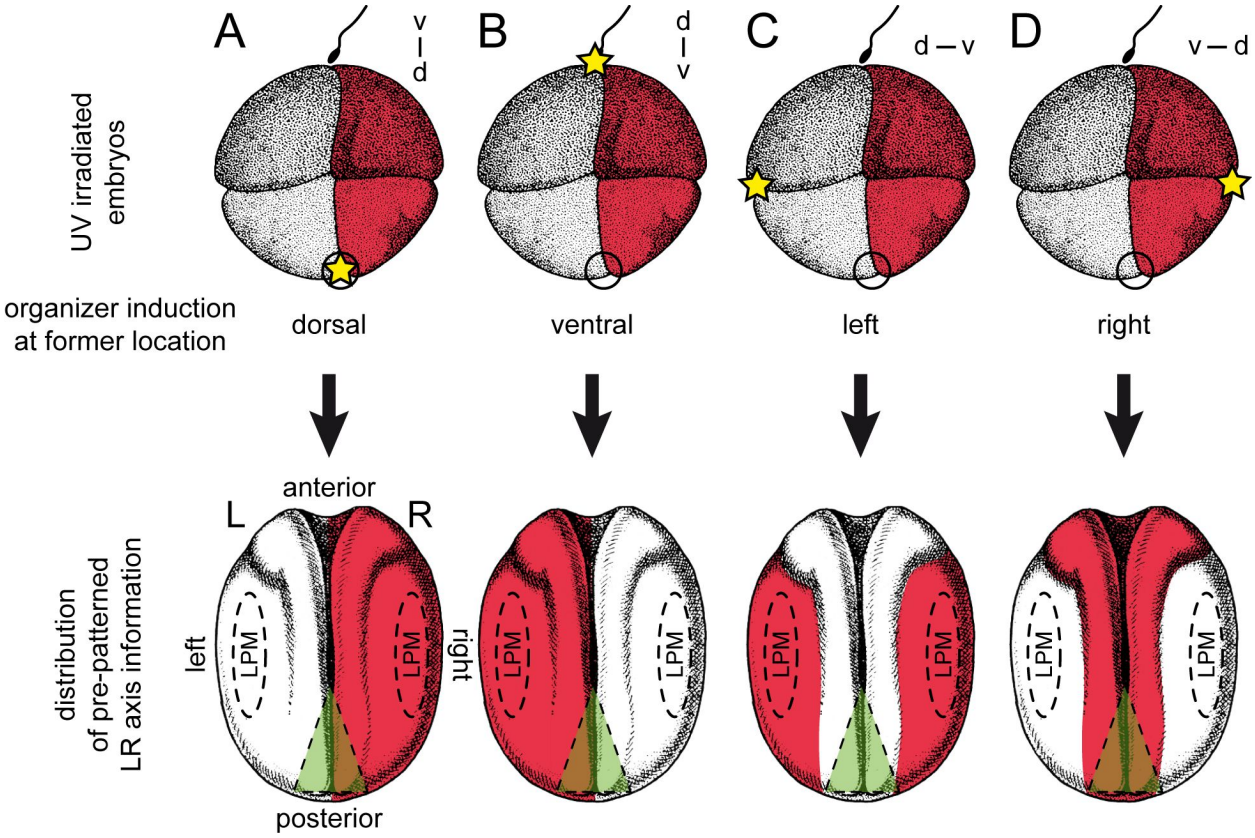

	Nodal cascade	left	right	absent	bilateral
expected	organ situs	*situs solitus*	*situs inversus*	heterotaxia	heterotaxia
	% *situs solitus*	100	0	12.5	12.5
reported*	% *situs solitus*	74	73	75	
	(n)	(102)	(168)	(81)	

**Siamois* mRNA induced axis formation in UV irradiated embryos; Vandenberg and Levin, 2010

Fig. 36 Theoretical expectation of laterality if LR axis would be defined with first cleavage.
(A-D) Schematic targeting of LR tissue upon different sites of organizer rescue. (Top row) 4-cell stage embryos with hypothetical predetermined LR axis are shown (red, right; uncolored, left). Initial ventral and dorsal blastomeres are indicated by sperm symbols (entry site) and circle (former organizer), respectively. Organizer rescue in UV-irradiated embryos could be targeted to four distinct positions (yellow star) relative to the initial dorso-ventral (DV) and hypothetical pre-determined LR axes. Organizer rescues can be performed at former dorsal **(A)** or ventral (**B**; sperm entry) side or at former left **(C)** or right **(D)** blastomeres. Newly induced dorso-ventral axis is indicated (d-v). (Middle row) Cell fates of hypothetically predetermined left and right blastomeres are superimposed on neurula specimens (red, initial right side). Note: the GRP (green triangle) is always induced at the site of organizer formation (dorsal). (Bottom row) Expected appearance of Nodal-cascade and resulting asymmetric organ placements which range from *situs solitus*, *situs inversus* to randomization of single organs (heterotaxia). Note the differences in the frequency of expected *situs solitus* and the published experimental data by Vandenberg & Levin 2010. 4-cell and neurula stage drawing altered from Nieuwkoop & Faber (1967).

absent resulting in randomization of organ situs (12.5% *situs solitus* by chance). (4) Induction of the organizer at the former right side (Fig. 36D) would dictate the former left side which contains the laterality information to contribute to both LPMs. This suggests bilateral Nodal-cascade activity which also would result in randomization of organ situs, i.e. only 12.5% *situs solitus* by chance.

In contrast, if the LR axis is defined by the organizer dependent leftward flow at the GRP (green triangles in Fig. 36), the new left side should always express the Nodal-cascade and *situs solitus* should be evident in nearly 100% of cases.

In an original publication of the Levin group, exactly such experiments have been performed (Vandenberg & Levin 2010). After UV-irradiation, the organizer was rescued via mRNA injection of *Siamois* differentially targeted to the former dorsal, ventral or lateral blastomeres of early cleavage stages. In all cases ~75% *situs solitus* was reported (74% former dorsal, 73% former ventral, 75% former lateral; Fig. 38; cf table 1 in Vandenberg & Levin 2010). In a second approach, the method called 'tipping' was used to rescue the organizer. By tipping, the UV-irradiated one cell stage embryos are tilted 30-90° toward one side. Subsequently, gravity mimics cortical rotation by displacing the maternally deposited dorsalizing factors towards the lowest position (Scharf & Gerhart 1980). Thus the side pointing downwards becomes dorsal. Via this method, however, the rescue cannot be specifically targeted to a distinct former side of the embryos. Hence, this method randomly places the new organizer in respect of the former axis coordination. Theoretically, if LR axis would be predetermined, only 1/4 of tipped embryos would by chance have the new organizer rescued at the former dorsal position. Therefore only about 1/4 (mathematically correct 31.25%) of all tipped embryos would be expected to display *situs solitu*s. Interestingly, up to 97% of tilted UV-irradiated embryos exhibited *situs solitus* (Vandenberg & Levin 2010). This allows three conclusions: (1) regardless of the position of the newly induced organizer a proper LR axis is established de-novo; (2) the quality of rescue is higher with the endogenous amount and composition of dorsalizing factors than with ectopical activation of the Wnt-pathway, but (3) ectopical activation of the Wnt-pathway post-MBT suffices to rescue all three body axes.

The above experiments and hypotheses render it most unlikely that any early asymmetric mechanism exists which could impact on LR axis formation in *X. laevis*. Sole the presence and location of the (induced) organizer dictates LR axis formation. Two assumptions can be drawn thereof: (1) the organizer could somehow be an asymmetrical organ by itself or (2) the organizer generates a functional GRP and leftward flow to establish the LR axis de-novo. The latter assumption is most likely the case as investigation of the secondary organizer during the generation of conjoined twins revealed a second GRP that drove leftward flow. However, it is unknown but also unlikely that the existence of the primary organizer might impact on GRP formation of the induced organizer. Therefore it needs to be investigated if a induced organizer in rescued UV-irradiated embryos instructs a functional GRP and leftward flow. If this is the case, blockage of leftward flow by knockdown of cilia motility (*dnah9-SB*-MO) or methylcellulose treatment should again abolish orientation of the LR axis. This would ultimately demonstrate that the orientation of the LR axis is caused by the cilia-driven leftward flow de-novo.

III.1.2 The cilia-driven leftward flow is conserved and breaks the initial symmetry in *X. laevis*

The processes that culminate in establishment of the leftward flow investigated in this work are causative for the leftward flow and precede the asymmetric Nodal-cascade in the left LPM. Inhibition of ciliogenesis and mis-polarization of cilia abolishes LR axis

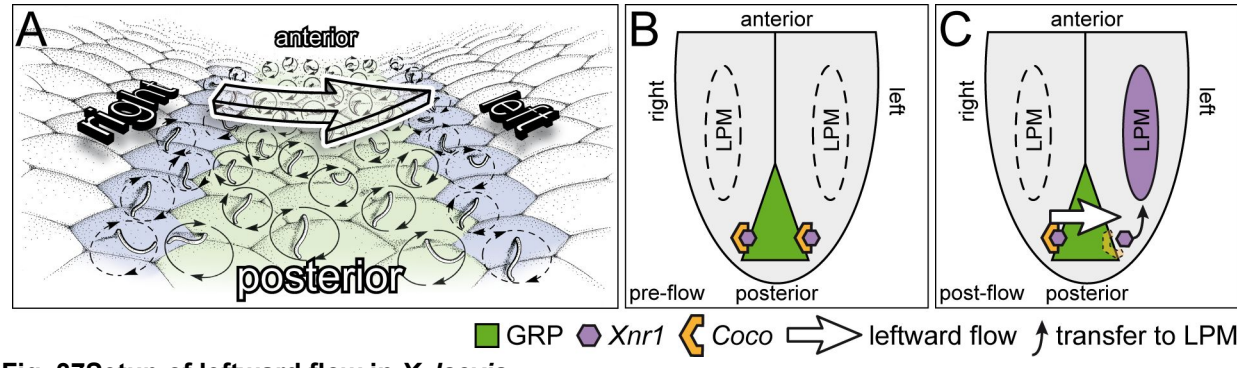

Fig. 37 Setup of leftward flow in *X. laevis*
(A) Schematic drawing of stage 17 GRP with polarized hy/nGRP cilia (green). Note: unpolarized sGRP cilia are assumed immotile and sGRP cells exhibit *Coco*/*Xnr1* expression. **(B)** In pre-flow stages Coco represses Xnr1; no expression of the Nodal-cascade in the LPMs. **(C)** In post-flow stages, Xnr1 is released from Coco repression in the left sGRP cells, subsequently *Xnr1* is expressed in left LPM triggering the Nodal-cascade.

formation in all cases. The results of this work further demonstrates that read-out of leftward flow occurs in the left somitic GRP (sGRP) cells by flow-mediated down regulation of *Coco* expression. Further, the sGRP cells and cilia are unique and could account for the signaling-center of leftward flow (Fig. 37).

III.1.2.1 Somitic GRP cilia might not contribute to leftward flow

In mouse, the so-called crown-cells which are the most lateral cells of the PNC express *cerl-2* and *Xnr1* (Marques et al. 2004). Cilia of these cells are assumed to be immotile and get mechanically bent by leftward flow. Subsequently, an asymmetric calcium wave propagates at the left PNC margin which is thought to be necessary for further activation of the Nodal-cascade in the left LPM (McGrath et al. 2003). In *Xenopus*, it was shown that the lateral sGRP cells also express the homologs of the same genes: *Coco* and *Xnr1* (Fig. 21). In addition, sGRP cilia are shorter than the remainder cilia and further project centrally (Fig. 6). Therefore two questions arose: (1) Do sGRP cilia contribute to leftward flow and (2) is polarization of GRP cilia dependent on length or motility?

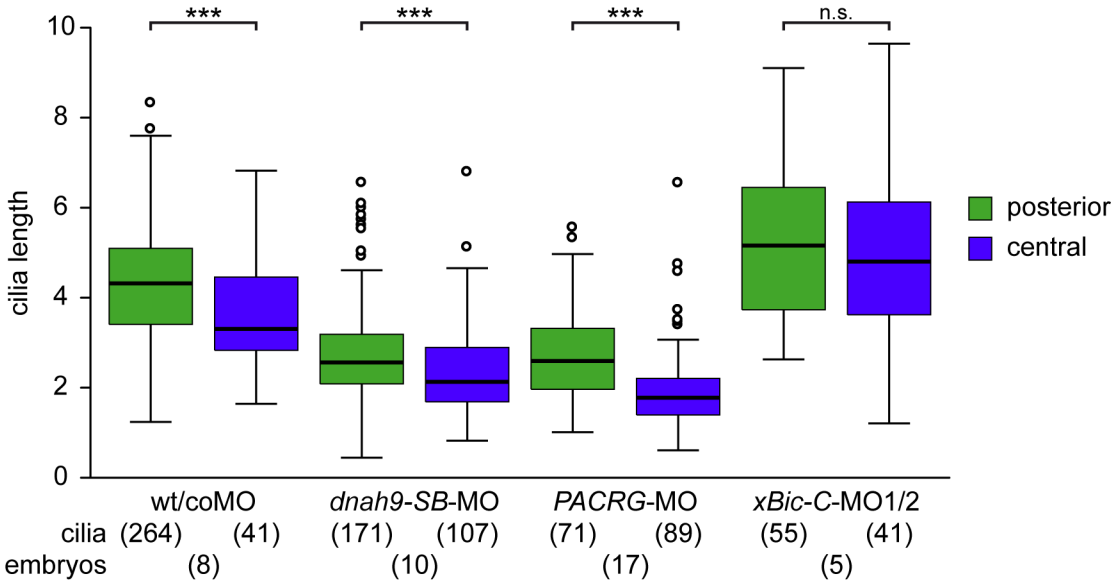

Fig. 38 Comparison of hy/nGRP cilia alignment and length
Comparison of cilia length of posterior (green) and central (blue) cilia from GRP centers (hy/nGRP; merged data of II.2.2 and II.2.3). Except for *xBic-C* impaired GRP centers, central cilia were very highly significantly shorter in wildtype or co-, *dnah9-SB* and *xlPACRG* morphant specimens.

First, central cilia are regularly seen in cells of developing GRPs at stages 15/16 (Schweickert et al. 2007). At these stages, particles are often trapped by centrally projecting cilia that generate local vortices. During development, cilia get progressively polarized towards the posterior pole (Schweickert et al. 2007) and particle entrapment by cilia is no longer recorded. In *xBic-C* impaired specimens however, elongated cilia mis-polarized and local vortices were visible again (Fig. 20D; Maisonneuve et al. 2009). Follwing this reasoning, it can be assumed that the lateral sGRP cilia are immotile. Else, such vortical entrapments would be expected above sGRP cells, i.e. at the lateral margins of the GRP, which is not the case (Fig. 5A', B'; Fig. 16A; Fig. 22A,B).

Second, as sGRP cilia are assumed immotile and are in addition shorter than the remaining GRP cilia, the question arose if length or motility of GRP cilia account for polarization. In the *Xenopus* epidermis, cilia re-align their basal bodies in a flow-mediated self-organizing fashion (Mitchell et al. 2009). In the skin, this re-alignment happens in the direction of the current. If such a mechanism would account for alignment of GRP cilia, however, this would require the basal bodies to be aligned orthogonally with leftward flow. In addition, the basal bodies of the immotile PNC cilia in the *iv/iv* mouse are properly aligned (Hashimoto & Hamada 2010). This suggests that motility is not necessary for posterior polarization. If motility would account for posterior localization in the GRP, cilia in *dnah9-SB*-MO injected specimens that display arrested or severely impaired motility (Fig. 16F-F'', Vick et al. 2009) should not be aligned posteriorly. Unexpectedly, *dnah9* knockdown also reduced cilia length (cf II.2.2). However, comparison of polarization and length of hy/nGRP cilia among all cilia-affecting treatments of this work revealed that the length of unpolarized cilia was very highly significantly shorter than that of posteriorly polarized cilia (Fig. 38). In the meantime, it was demonstrated that the PNC and GRP cilia are aligned by the PCP pathway (Antic et al. 2010; Borovina et al. 2010; Song et al. 2010). Thus elongation might give feedback on the mechanism shifting the cilium posterior-wards.

As the cilium is a structure under constant turnover (Marshall & Rosenbaum 2001), it is doubtful that there is a possibility to molecularly inhibit cilia motility without affecting cilia length or the cytoskeleton. Interesting in this notion would be to investigate the positioning of cilia that were exposed to methylcellulose treatment which does not affect the intracellular cytoskeleton. Under this increased viscosity conditions, leftward flow is

inhibited, however, cilia beating is not fully arrested but appears to be affected (Schweickert et al. 2007). Investigation of cilia length in correlation to polarization of these cilia might contribute to understand if and how length, motility and polarization interact.

The assumed immotility of sGRP cilia in combination with *Coco*/*Xnr1* expression in the sGRP cells could render this entity the leftward flow perceiving signaling-center. As leftward flow releases Xnr1 from Coco repression, the sGRP cells and cilia might play a major role in perception of leftward flow. In mice and zebrafish it was demonstrated that an asymmetric calcium wave (McGrath et al. 2003; Sarmah et al. 2005) is necessary for further downstream signaling. This calcium wave could as well take place in *X. laevis* to trigger the asymmetrical repression of *Coco*. Injection of an *in vivo* calcium reported into the GRP cells might reveal such functionality. How calcium might acquire down regulation of *Coco* expression remains elusive.

In summary, the logical approach on early asymmetries, published data and the present work demonstrate that it is most likely that leftward flow is the symmetry breaking event in *X. laevis*. Further, the organizer suffices to align the LR axis de-novo. However, the contradicting reports on the necessity of early ventral asymmetric serotonin signaling for LR axis formation was not supported by this work. In contrast, serotonin signaling was found to be a dorsal determinant in providing competence for the setup of leftward flow.

III.1.3 Serotonin signaling in *X. laevis* is necessary for leftward flow

The early asymmetric localization of serotonin could not be verified, thus the reported impact of serotonin signaling in general and especially via receptor class 3 was re-investigated on LR axis formation in the light of cilia-driven leftward flow. To narrow down the critical timepoint of serotonin signaling function for LR axis formation, pharmacological inhibition was not utilized. Instead, *x5Htr3* was knocked down to specifically lose signaling via 5-HT receptor class 3. In addition, 5-HT should be quenched by overexpression of just the ligand binding domain of *x5Htr3*. As

overexpression of the LBD mimicked the phenotypes of the *x5Htr3*-MOs, both treatments should specifically inhibit 5-HT signaling. In contrast, over-expression of the human splice variant (hsv) that lacks the LBD yielded no phenotype. Therefore it is highly likely that the LBD specifically inhibited serotonin signaling. The nature of this inhibition is not known but it is imaginable that the LBDs could act by either quenching 5-HT or blocking receptor function in a dominant-negative manner. However, both approaches led to down regulation of *Foxj1* and *Xnr3* expression in the SM.

In this way, the necessity of serotonin signaling for LR axis formation could be verified by the present work. However, 5-HT signaling was found to impact on LR axis formation at the dorsal side and during gastrulation instead of the proposed asymmetric ventral activity during early cleavage. In addition, serotonin signaling was demonstrated to provide competence for canonical Wnt-signaling. This further suggests canonical Wnt to act on LR axis formation in *Xenopus*.

III.1.3.1 Serotonin signaling provides competence for Wnt-signaling

As the classical Wnt target gene *Xnr3* was down regulated upon loss of serotonin signaling and SM identity was rescued by downstream Wnt-effectors, an implication of 5-HT signaling and canonical Wnt could be envisaged. This hint was supported by the DA assay as impairment of 5-HT signaling via receptor class 3 abolished secondary axis formation in *xWnt8* but not *Dsh* or *Siamois* induced axes. Two conclusions can be drawn thereof: (1) impairment of 5-HT signaling via receptor class 3 interferes upstream of *Dsh* with the canonical Wnt-pathway. (2) There is no dorsal bias of 5-HT function as the DA assay was performed on the ventral side. The latter conclusion confirms the observed equal enrichment of 5-HT in the whole superficial layer of the animal hemisphere during blastula/gastrula stages. It is therefore tempting to speculate that 5-HT signaling provides competence for the canonical Wnt-pathway. In support of this, a genome wide siRNA screen for canonical Wnt regulators has identified the serotonin receptor class 3 (Christof Niehrs, personal communication).

How this competence might be mediated molecularly remains elusive but two possibilities for serotonin signaling on the canonical Wnt-pathway are imaginable: (1)

5-HT_3 can serve as co-receptor for Wnt-signaling or (2) 5-HT signaling can impact on Wnt signalosomes.

Signalosomes are vesicle-like structures that emerge from internalization of the frizzled-LRP6 complex after binding of a Wnt ligand (Bilic et al. 2007). In neurosynaptic vesicles, the lumen is acidified by the vacuolar H^+-ATPase (vATPase). This high proton concentration is used to sequester serotonin by the vesicular monoamine transporter (vMAT) into the synaptic vesicles (Morel 2003). As Wnt-signalosomes are also acidified via the vATPase (Bilic et al. 2007), a hypothetical shuttling mechanism of 5-HT into these signalosomes is imaginable. This assumption further requests vMAT to be present in Wnt-signalosomes, also. However, intracellular free serotonin seems to be rapidly degraded by the monoamine-oxidase which renders an uptake mechanism of free 5-HT from the cytosol unlikely (Gaspar et al. 2003). As 5-HT is preserved from degradation by being enclosed in vesicles, two other possibilities emerge: (1) the serotonin vesicles could fuse with signalosomes to provide competence for Wnt-signaling. (2) The apicobasal localization of serotonin vesicles could also allow to spill their contents into the extracellular space after fusion with the apical cellular membrane. Subsequent internalization by the signalosomes could thereby include extra-cellular 5-HT. As the nature of the 5-HT vesicles is rather unknown, no suggestion can be favored. However, loss of serotonin signaling by overexpression of the LBD is thinkable to block 5-HT in any case. As the *LBD* mRNA is transcribed and processed in the endoplasmic reticulum and the golgi apparatus, the protein is shuttled in vesicles towards the membrane. As the LBD lack transmembrane domains, it is thought to be released in the extracellular medium to quench 5-HT. If intracellular intervesicular fusion exists, 5-HT could also be quenched inside of the vesicles.

However the mechanism will be for serotonin signaling, 5-HT is undoubtedly involved in the Wnt-pathway as exogenous supply thereof could rescue secondary axis impairment via *LBD* over-expression.

III.1.3.2 *Foxj1* expression in the SM might rely on calcium channel activity of the Serotonin receptor class 3

The present work demonstrates that serotonin signaling is involved in the induction of *Foxj1* in the SM. How 5-HT signaling accomplishes the expression of *Foxj1* is unclear. However, as the class 3 receptor is a ligand gated cation channel, involvement of calcium is likely as in DMZ but not VMZ explants, calcium waves propagate (Wallingford et al. 2001). Ca^{2+} activity is envisaged to accomplish two distinct functions. First, intercellular Ca^{2+} is necessary for convergent extension as Ca^{2+} depletion with Thapsigargin in *X. laevis* (Wallingford et al. 2001) and zebrafish (Creton 2004) led to shortened AP axes. However, Thapsigargin treatment did not change mesodermal fate of DMZ cells in the frog (Wallingford et al. 2001). Second, intracellular Ca^{2+} signaling is required for KV formation in zebrafish (Kreiling et al. 2008; Schneider et al. 2008) and ciliogenesis of the GRP (Hatayama et al. 2011). In preliminary experiments, *Foxj1* expression in the SM of *Xenpous* was reduced upon brief treatment of Thapsigargin (Axel Schweickert, unpublished). General competence for SM specification was not impaired in *xHtr3* depleted embryos as *Dsh* and *β-catenin* could rescue the *Foxj1* expression and thus SM identity. These findings support serotonin receptor class 3 mediated Ca^{2+} signaling to specify ciliogenesis of the GRP as a result of inducing *Foxj1*.

To investigate this assumed interaction, two experiments are imaginable. First, injection of *in vivo* calcium reporters like calcium-green-dextran into the DMZ should reveal hypothesized absence of calcium waves in 5-HT signaling impaired specimens. Second, artificial increase of calcium levels due to application of Ca^{2+}-ionophores or caged calcium at the DMZ in Serotonin signaling impaired specimens should rescue *Foxj1* expression. Because of the broad functional role of calcium in embryonic development, especially on gastrulation processes, rescue of Foxj1 expression by exogenous Ca^{2+} could be challenging and would require fine tuned titration to identify the adequate amount of calcium. To circumvent side effects like influence of deeper mesodermal tissue, such rescue experiments could be performed in explants of the dorsal superficial layer.

III.1.3.3 5-HT signaling might acquire ciliogenesis and cilia motility

Besides specification of the SM, serotonin signaling could adopt a second role in *X. laevis*. From studies of cilia in sea urchins (Wada et al. 1997) and rat brain ependymal cells (Nguyen et al. 2001), it is known that serotonin can positively influence the cilia beat frequency (CBF). Similarly, inhibition of 5-HT signaling via receptor class 3 reduced or abolished CBF in multiciliated cells in the epidermis of tailbud stage *Xenopus* embryos. In addition, cells with arrested cilia bundles seemed to contain a lower amount of cilia than unaffected ciliated cells.

It needs to be investigated if serotonin signaling is also dependent for *Foxj1* expression in ciliated epidermis cells.

5-HT signaling dependent calcium could provide cilia motility

Regulation of rat brain ependymal CBF by serotonin signaling was proposed to most-likely act via the 5-HT_2 receptor family which raise intracellular IP_3 levels when activated (Nguyen et al. 2001). This triggers release of Ca^{2+} from the endoplasmic reticulum which in turn opens Ca^{2+}-release-activated-Ca^{2+} channels. The subsequent influx of extracellular Ca^{2+} might directly alter CBF. A likewise activity of 5-HT signaling in *Xenopus* could be argued for as *5Htr*$_3$ morphant epidermis cilia bundles demonstrated decreased CBF. This phenotype could likely be caused by the Ca^{2+} channeling activity of 5-HT_3. Ca^{2+} could either directly impact on CBF like it is demonstrated from *C. reinhardtii* where Ca^{2+} can directly modulate movement of certain dynein arms. Also imaginable is binding of Ca^{2+} to calcium-calmodulin (CaM) which associates with the radial spokes and central MTs of the axoneme and drives CBF. However, CaM activity in vertebrates seems to have no direct influence on CBF, instead the second messengers cAMP or cGMP are CaM depending regulators of CBF by mediating phosphorylation of dynein arms via PKA or PKG, respectively (reviewed in Schmid & Salathe 2011).

Ciliogenesis likely depends on serotonin signaling mediated calcium

In the protozoa *Tetrahymena thermophila*, biogenic amines like serotonin were also shown to regulate CBF and in addition, positively influence ciliogenesis by increasing

the number of cilia per cell (Castrodad et al. 1988). In *T. pyriformes*, the Ca^{2+} chelator EGTA negatively regulated cilia regeneration (Rodríguez & Renaud 1980). Therefore, calcium signaling might be involved in proper ciliogenesis of *x5Htr3* morphant multiciliated epidermis cells. However, as 5-HT signaling is necessary for *Foxj1* expression in the SM, a likewise function is imaginable for the ciliated epidermis cells. Ciliogenesis and CBF regulation both depend on calcium, however it seems that accurate concentration and probably timing of intracellular Ca^{2+} levels and use of specific second calcium-related messengers distinguishes between both processes.

Interesting in this context would be to analyze if serotonin signaling also provides motility for GRP cilia or influences ciliogenesis and thus drives leftward flow. However, the altered SM/GRP morphology of 5-HT signaling impaired specimens did not allow for investigating this questioning. Though, as downstream effectors of the canonical-Wnt pathway rescued *Foxj1* expression in 5-HT signaling affected embryos, this condition should in theory also give rise to a ciliated GRP in absence of 5-HT signaling. In such specimens, the influence of 5-HT on GRP cilia could be investigated. However, preliminary results of such rescued embryos displayed absence of the Nodal-cascade from the left LPM (Tina Beyer, personal communication). In the light of 5-HT signaling providing CBF and probably ciliogenesis, this could hint for the leftward flow not to take place correctly. Further, it is unknown if all other prerequisites for leftward-flow are present in 5-HT signaling impaired and downstream Wnt-effectors rescued specimens: ciliogenesis, polarization of cilia and most important, expression of *Xnr1* and *Coco* in the sGRP cells.

In summary, serotonin signaling might display a dual role in *Xenopus* embryogenesis. The present work revealed 5-HT signaling as a dorsal factor by providing competence for Wnt-signaling and SM specification. Therefore serotonin signaling is necessary for LR axis formation in a different way than originally postulated in the 'ion-flux' hypothesis.

III.1.4 Further assumed factors of the 'ion-flux' hypothesis also feed into the setup of cilia-driven leftward flow

In the meantime, other components involved in the 'ion-flux' hypothesis could also be connected with cilia-driven leftward flow. The ion-pump H^+/K^+-ATPase was postulated to act asymmetrically by setting up a voltage gradient across early cleavage stage embryos (Aw et al. 2007). Subsequently it was hypothesized that a morphogen could be asymmetrically transferred through GJ according to the pH gradient (Levin 2003). However, knockdown of *H^+/K^+-ATPase* in the DMZ revealed impairment of leftward flow (Peter Walentek, personal communication). In addition, GJ implicated distribution of factors during cleavage stages was also argued to be unlikely (Landesman et al. 2000). In support of this, GJ communication could be shown to impact on laterality as the paraxial *Xnr1* domain was absent from sGRP cells after knockdown of connexin 26 (Beyer 2011). Also another ion-pump assumed of early asymmetric localization in *Xenopus*, the vATPase led to ciliogenesis defects in KV of zebrafish, when impaired (Adams et al. 2006). Taken together, these findings question the 'ion-flux' hypothesis for symmetry breakage in general.

III.2 The organ situs phenomenon of Siamese twins is caused by leftward flow

The formation of conjoined or Siamese twins has always attracted attention of embryologists. Conjoined twinning occurs throughout the animal kingdom with the most prominent cases in vertebrates and humans. Since more than a century ago, a curious situs phenomenon in Siamese twins is known: the left twin consistently exhibits *situs solitus* whereas the situs of the right twin is randomized or inverted (cf II.2.1.2, Fig. 13B). This observation was further specified in human and chick embryos. As these develop over a blastodisc, it was obvious that laterality of the right twin was only affected when the axes developed parallel to one-another (thoracopagus, parapagus, cephalopagus). In contrast, AP axes of conjoined twins that are arranged in-line, i.e. head-to-head (craniopagus) or tail-to-tail (ischiopagus) do not exhibit LR defects (Levin et al. 1996). In the former conjoined twins, the identified laterality phenomenon was

verified and explained as a result of the midline-barriere established by Antivin. In this respect, the Nodal-cascade of the left twin is thought to activate Antivin which in turn should block Nodal-signaling from all other LPMs of the conjoined embryos (Levin et al. 1996). However, a mechanism how the Nodal-cascade should be activated only in the left LPM of the left twin was not provided.

In amphibian embryos, besides ventral transplantation of an organizer, ectopical activation of the canonical Wnt-pathway in the VMZ triggers formation of a secondary axis (Lemaire & Kodjabachian 1996; Nascone & Mercola 1997). As *Xenopus* embryos develop spherically and hence Siamese twins only have the possibility to gastrulate over the same blastopore, head-to-head orientation of both axes is impossible by the mode of amphibian gastrulation. Therefore, all conjoined twins in *X. laevis* state thoracopagi, parapagi or dicephali dependent on the distance of both developing axes. The situs phenomenon of conjoined twins that were ectopically induced with canonical Wnt-pathway effectors in principle resembles the well known observation (Nascone & Mercola 1997). As the induced axis is traceable upon which side of the endogenous axis it will come to lie, a further conclusion could be drawn: it is not induction but left position that causes wildtype heart formation in DAs. That means regardless of which is the induced axis, only the twin on the left exhibits wildtype heart orientation, which is randomized in the right twin (Nascone & Mercola 1997). The most recent publication on situs organization in *Xenopus* Siamese twins again employs the 'ion-flux' hypothesis as mechanism to acquire this phenomenon (Vandenberg & Levin 2010). Besides being highly unlikely to exist, it is not conclusive how this hypothetical early acting mechanism could provide LR axis information to the induced organizer that forms after MBT. It is further suggested that the primary organizer somehow pattern the early zygote in such that a secondary organizer could align LR in respect to its own AP and DV axes. It is not conclusive how this organization could be acquired via an early asymmetry defining mechanism.

If one again assumes that the LR axis would be somehow predefined in conjoined twins, the prediction of the organ situs would vary from the observed situs phenomenon. Because the second organizer opposes the primary one, a predefined laterality condition would be mirrored for the second twin (Fig. 39). As long as this twin would be aligned to the right, the expected organ arrangement would match the reported organization of the DAs with displaying *situs solitus* for the left and laterality defects for the right twin – although one would expect a constant appearance of situs inversion for the induced twin which was not reported. If the induced axis would come to lie on the left of the endogenous axis, the situation would be mirrored. In this case, the left twin should display laterality defects (*situs inverus*) but the right one should be

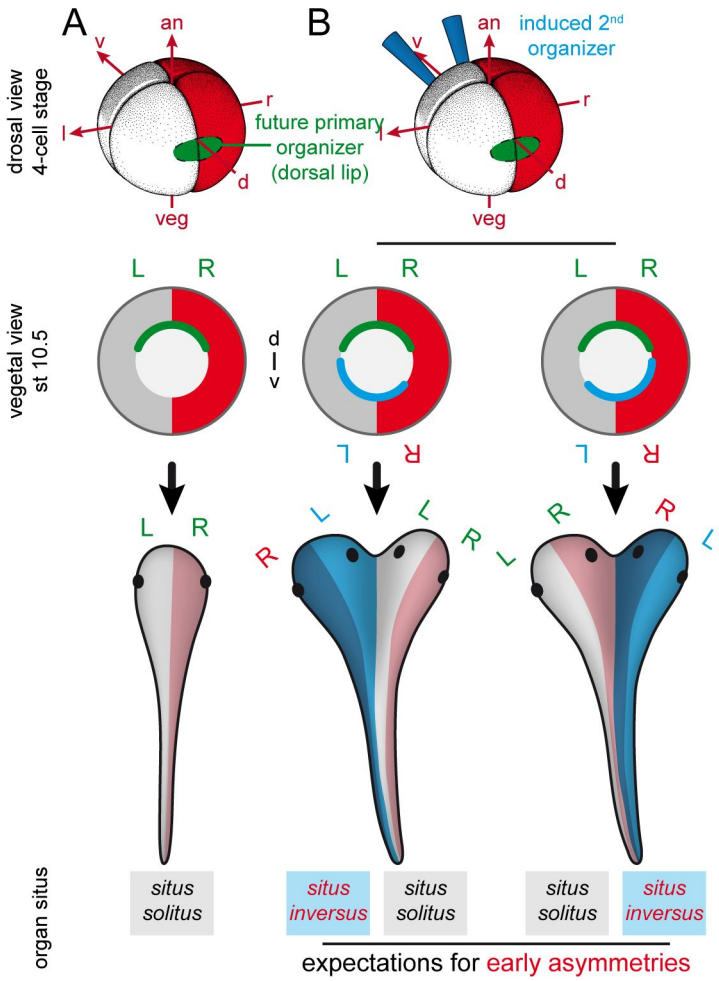

Fig. 39 Expected organ situs in conjoined twins with hypothetical early specification of LR axis
(A) If early asymmetric determinants would define the LR axis, left (blank) and right (red) sides were already defined at onset of gastrulation and would split the dorsal lip (green) into a left and right identity. **(B)** Induction of a second organizer (blue) would result in dorsalizing the ventral lip with mirrored LR orientation. Note: always the induced twin (blue) would display heterotaxia (or more precisely: *situs inversus*) regardless of side of induction
an, animal; d, dorsal; l, L, left; r, R, right; v, ventral; veg, vegetal

normal. By this consideration, it is obvious that if the LR axis would be predefined, always the induced embryo would display laterality defects (in particular *situs inversus*) regardless of the side on which it develops. If in addition the suggested Antivin-mediated midline barriere mechanism would take place because of crosstalk of the axes, it is still not comprehensible how induced left twins would acquire wildtype situs only.

A hypothesis for symmetry breakage can only be regarded valid if it could also explain the situs phenomenon of Siamese twins without flaws. Hence if leftward flow would account for laterality in Siamese twins, the situation would be as follows: for 'parallel' developing conjoined twins which display a fused GRP, the leftward flow of the right twin was in continuity with the leftward flow of the left twin (Fig. 14A). Any asymmetric cue, if transported or generated could thereby only signal on the far left side of this fused GRP(Fig. 40A). In this setup it is unimportant which axis is the induced as leftward flow always acts throughout the whole fused GRP. With this it is imaginable that only the left side of the left GRP, presumable the sGRP cells, obtain the asymmetrical cue. Therefore, it needs to be investigated, if *Coco* is repressed on the far left side, inducing the Nodal-cascade in the left LPM of the left embryo. In terms of *Pitx2c* transcription, one would expect left sided expression in the left conjoined twin and absent expression in the right twin which indeed was the most prominent case in 'parallel' developing axes (Fig. 14, Fig. 13A, C).

Leftward flow as mechanism for symmetry breakage was further supported by the finding of 'separated' conjoined twins that exhibited more often left-sided Nodal-cascades (Fig. 13) which is likely caused by both GRPs driving individual leftward flows and could signal independently from one-another (Fig. 40B). In addition, only in 'separated' twins it was found that both axes could exhibit wildtype left *Pitx2c* expressions (Fig. 14, Fig. 21C).

Taken together, the observed expression patterns of *Pitx2c* resembled the reported orientation of organ situs in conjoined twins (Fig. 13B, Fig. 40C). This demonstrates that the phenomenon of organ situs in conjoined twins is only dependent on the distance of the developing axes.

Wildtype *Pitx2c* expression and thus wildtype orientation of organs can only surface if

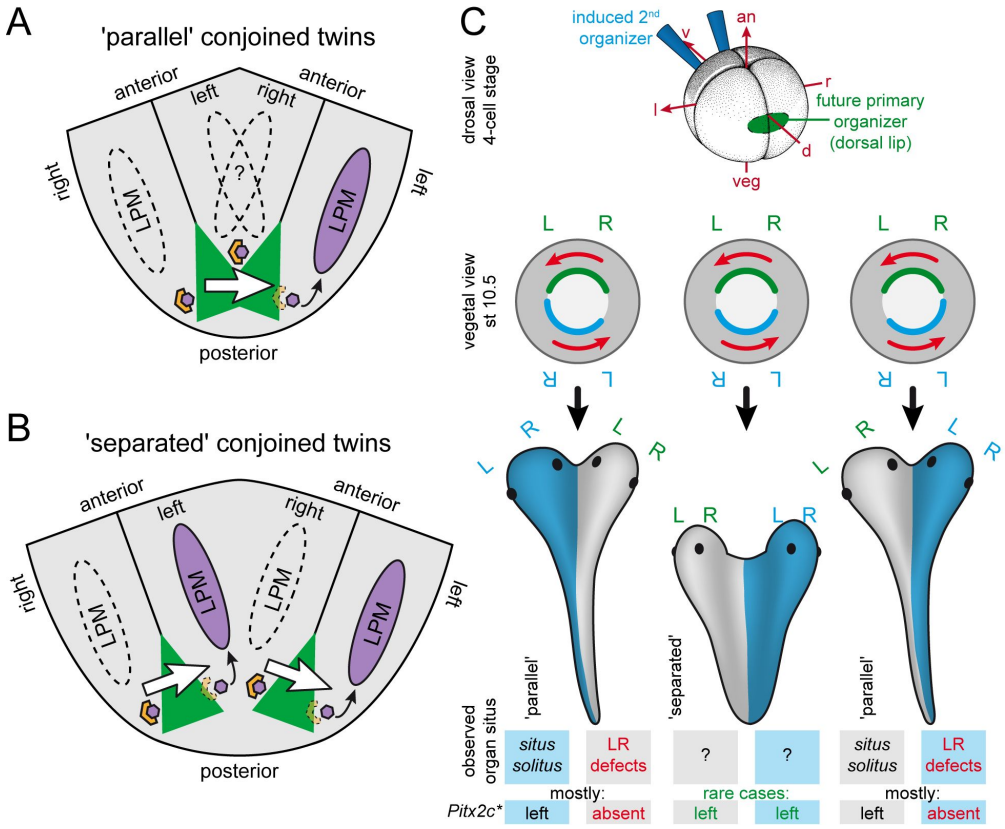

Fig. 40 Two leftward flow scenarios in conjoined twins explain observed organ situs.
(A, B) Schematic ventral view of dorsal explants of 'parallel' (A) and 'separated' (B) conjoined twins. **(A)** In 'parallel' DAs, endogenous and induced GRPs (green) are fused, driving a major flow (white arrow) from the right side of the right twin to the left side of the left twin. Only on the far left, *Coco* should be downregulated, releasing repression of Xnr1 to activate the Nodal-cascade in the left LPM. **(B)** In 'separated' DAs, both GRPs drive individual leftward flows each downregulating its left *Coco* domain. Xnr1 would be free to activate the Nodal-cascade in both individual respectively left LPMs. **(C)** Setup and observation of organ situs dependent on leftward flow in conjoined twins. Ventral induction of second organizer (blue) due to injections of Wnt-pathway components at early cleavage leads to secondary dorsal lip formation (blue) opposing the initial dorsal lip (green) at stage 10.5. Note: red arrows display orientation of later occurring direction of leftward flows on each future GRP. Regardless of side of induction, the left twin mostly displayed wildtype *Pitx2c* expression whereas the right twin exhibited altered *Pitx2c* information which matched the observed organ situs. Only in 'separated' DAs, double wildtype conditions of *Pitx2c* were found. *Summary of *Pitx2c* expression patterns of Fig. 14 and Tisler 2011.
an, animal; l, L, left; d, dorsal; r, R, right; v, ventral; veg, vegetal

the left LPM is properly formed. In 'parallel' developing embryos, it is unclear if LPM tissue is specified in between both axes. This tissue demarcates the left side of the right twin. Therefore, if this tissue is absent, it is obvious that the Nodal-cascade could not take place there and the right twin has no chance to develop wildtype organ situs. In addition, leftward flow can only be sensed and further processed if the sGRP cells are present. sGRP cells normally flank the GRP laterally, therefore in a fused GRP they should be detectable in the center. However, it is unclear if these cells exist and if so, if

the leftward flow that overrides these cells would signal. Further as in 'parallel' developing embryos also the presomites are shared in between both axes, it is unknown if a transfer to the LPM would be achievable at all. In contrast, from the rare but possible expression pattern of left *Pitx2c* transcripts in both axes of 'separated' twins, four conclusions can be drawn: (1) both axes have a left LPM (2) both GRPs should drive a functional flow (3) both GRPs should be flanked by sGRP cells whose *Coco* expression should be down regulated post-flow on either left side, (4) a secondary organizer suffices to induce a proper LR axis.

To verify that leftward flow accounts for the laterality phenomenon in conjoined twins, inhibition of this current in the left twins should rescue the Nodal-cascade in the right twin. However, this is only possible if a LPM is induced in between both axes and sGRP cells are present and functional inside the fused GRPs. Therefore, it can be suggested that the farther the distance of both axes is, the more LPM should be induced in between and the easier the induction of the Nodal-cascade / organ situs of the right twin should be. The observation that tail-to-tail human and chick embryos do not display situs aberrations supports this assumption. Because the designated 'separate' conjoined twins emerge from the optimal distance of both axes (180°) which represents a tail-to-tail orientation.

In conclusion, leftward flow as the mechanism to establish the LR axis is also responsible for the organ situs phenomenon in Siamese twins. The present work strongly supports this event to be the symmetry breaking mechanism in *X. laevis* as it could for the first time explain and predict laterality in conjoined twins and singelton embryos.

III.3 Conservation and limitation of the leftward flow for laterality

The present work supports the cilia driven leftward flow to specify the LR axis like it was found in zebrafish, medaka, mouse and rabbits. In addition, a functional GRP that drives a leftward flow was also verified for *X. tropicalis* and *A. mexicanum.* In all cases leftward flow is present in remnants of the archenteron. To assume that leftward flow is highly conserved, basal species of the deuterostomian phylogeny should also display

leftward flow to specify the LR axis. Indeed, besides the Nodal-cascade, archenteral cilia could be found in the echinodermate *P. lividus*. Although cilia motility or leftward flow was not demonstrated their sole existence suggests such functionality.

However, in chick embryos a cilia-driven fluid flow was not found to date. Chick embryos develop as a flat blastodisc with the primitive streak growing out of a cellular thickening, the so-called Koller's sickle. Before the notochord starts to grow out of the node, i.e. even before the Nodal-cascade is activated, an asymmetric cell migration is reported that deforms the node itself to be morphologically asymmetrical (Gros et al. 2009). As a result, the bilateral midline Nodal domain known from the other vertebrates already initiates left-asymmetrically, hence Nodal is only activated in the left LPM (Dathe et al. 2002). How the asymmetric cell-migration is triggered to affect the morphology of the node remains elusive. If a cilia driven leftward flow takes place in chick, this event should precede the morphological asymmetry of the node. However, with the axonemal marker PACRG, no patch of cilia was found in early chick development (Fig. 10), arguing against this assumption. In further support of this, the talpid mutant that lacks pirmary cilia was not reported to exhibit laterality defects (Yin et al. 2009), rendering it unlike that chick laterality is caused by a cilia dependent mechanism. In addition, the difference of chick embryos compared to the other vertebrates that develop leftward flow is the apparent lack of a superficial mesoderm of which the ciliated epithelium derives (Shook et al. 2004). It is further thinkable that the birds as an branching outgroup of the vertebrates lost leftward flow mediated asymmetry by establishing an alternative mechanism. Very interesting in this regard would be to investigate laterality in basal reptiles, the ancestors of birds.

Nevertheless, leftward flow, ciliogenesis at the archenteral epithelium, nature of the perception of leftward flow and the downstream transfer of the asymmetric signal towards the LPM are under constant investigation among all model-organisms strengthening the conservation of this event for non-avian vertebrate symmetry breakage.

IV Materials & Methods

IV.1 contribution to the joint projects

If not stated differently, all data presented were acquired by myself. All SEM pictures in the present work were acquired by Tina Beyer. Below are the detailed contributions to the collaborative projects performed during this work:

dnah9/*PACRG*

The work presented in chapter II.2.2 was performed collaboratively with Philipp Vick (Vick 2009; Vick et al. 2009)

- Philipp Vick: cloning and WMISH of *dnah5*, *dnah9*, MO mediated knockdown
- Tina Beyer: acquisition of SEM pictures
- Thomas Thumberger: MO mediated knockdown, SEM analysis, all PACRG experiments, leftward flow analysis, SEM analysis

Bicaudal C

The work presented in chapter II.2.3 was performed collaboratively with our group and the group of Daniel Constam (ISREC, Lausanne; Maisonneuve et al. 2009)

- *Charlotte Maisonneuve* & *Isabelle Guilleret*: all mouse embryology and part of publication, knockout, time-lapse acquisition of leftward flow raw-data
- *Philipp Andre*: time-lapse acquisition of leftward flow raw-data in mouse
- *Tina Beyer*: SEM acquisition/analysis
- *Thomas Thumberger*: SEM analysis, leftward flow analysis (*X. laevis*/mouse), injections, statistics
- *Philipp Vick*: WMISH of xBic-C, MO mediated knockdown (injections), see also (Vick 2009)

Nodal & *Coco*

The work presented in chapter II.2.4 was performed in a collaboration of our group (Schweickert et al. 2010):

- *Axel Schweickert*: epistasis experiments, MO mediated knockdown
- *Philipp Vick, Maike Getwan & Melanie Eberhardt*: *Xnr1*/*Coco* WMISH and vibratome sections, epistasis experiments of *Xnr1*/*Coco*/leftward flow (MO-, MC-injections), see also (Vick 2009)
- *Tina Beyer*: SEM pictures
- *Isabelle Schneider*: *MyoD* WMISH and vibratome sections
- *Thomas Thumberger*: inhibition of leftward flow, leftward flow analysis (*dnah9*/MC/*Xnr1*/*Coco*), statistics

Serotonin

The work presented in the chapter on serotonin signaling (II.4) was conducted collaboratively in a joint project of our lab and Mike Danilchik (OHSU, see below).
The following collaborators (in alphabetical order) contributed equally:

- *Tina Beyer*: SEM acquisition and analysis, injections, DA assay, WMISH

- *Mike Danilchik* (OHSU, Portland, Oregon, USA): serotonin IHC, re-investigation of 5-HT localization
- *Thomas Thumberger*: leftward flow analysis, microsurgery, injections, DA assay, MO rescue, LBD rescue, WMISH, IHC, SEM analysis, statistics, coding of computer based analysis-tools, monitoring of epidermal cilia motility
- *Philipp Vick*: cloning, injections, *β-gal* staining, microsurgery, DA assay, WMISH

further collaborators:

- *Axel Schweickert* & *Susanne Bogusch*: cloning of constructs (*MOsite-eGFP, LBDs, xFL, hsv*), injections, DA assay, MO rescue, LBD rescue, monitoring of epidermal cilia motility, WMISH, RT-PCRs
- *Matthias Tisler*: DA assay, MO rescue, LBD rescue
- *Beate Niesler* (UKH Heidelberg, Germany): guidance with serotonin receptors and advice on cloning subunit fragments
- *Peter Walentek*: contribution of *Foxj1* probe

IV.2 Obtaining of embryos

IV.2.1 Xenopus laevis

Obtaining of *Xenopus* embryos

For embryonic experiments, *Xenopus laevis* females were stimulated for ovulation by subcutaneous injection with 50µl of human chorionic gonadotropin (hcg) one week prior to oviposition. About 10-12h before desired oviposition, females were injected subcutaneously with 450-700µl of hcg. The following day the spawning was supported by manual massage (Sive et al. 2000).

In vitro fertilization

In vitro fertilization was done with sperm extracted from *Xenopus* testes isolated from adult males and kept in 1×MBSH at 4°C. For fertilization about 1-2mm^3 of the testis was placed in 1ml 1×MBSH, macerated and subsequently added to the eggs. After 1-5min double destilled water (DDW) was added and fertilization began. About 40min later eggs were incubated for max. 7min in 2% cystein (pH 7.99) to be dejellied. Cystein solution was removed by several washing steps in 0.1×MBSH. For injection, eggs were washed and further kept in 1×MBSH in Petri dishes. Embryos were staged acoording to (Nieuwkoop & Faber 1967)

Microinjections

For injection, embryos were transferred to 2% Ficoll solution in a Petri dish coated with agarose. Embryos were injected at the 4-8 cell stage using a Harvard Apparatus setup with a thin glass-needle (5-10µm diameter). Drop size was calibrated to about 7-8nl per injection. In all experiments only 4-8 cell embryos with a clear dorso-ventral segregation of pigment were used for injections (Klein 1987; Danilchik & Black 1988) and only correctly targeted specimens (controlled by co-injected lineage tracer rhodamine-B dextran (~70000mmol weight): 0.5-1.0µg/µl) were processed for further analysis.

Fixation of embryos

for WMISH:
Embryos were cultivated in 0.1×MBSH + Penstrep to stage of interest and transferred into 4ml of freshly prepared 1×MEMFA for fixation. After incubation for 1-2h at room temperature (RT) or overnight at 4°C, embryos were washed 2× with EtOH (incubation 20min) stored in EtOH at -20°C.
for WMIHC:
Embryos were cultivated in 0.1×MBSH + Penstrep to stage of interest and transferred into 4ml of freshly prepared 4% PFA solution for fixation. After incubation for 1h at RT, embryos were washed several times in PBS^-.

IV.2.2 Mouse

All mouse embryos used in this work were derived from timed matings of C57Bl/6j. All steps involving isolation and culture of embryos were conducted under sterile conditions using sterile buffers, media, lab-ware and instruments. Fixation in a solution of 4% paraformaldehyde in PBS^- (4% PFA) was conducted for 1h at RT or overnight at 4°C. Animals were sacrificed by cervical dislocation. After the abdominal cavity of the dead animal had been opened, the uterus was removed as a whole and transferred to PBS^+. Uteri were transferred to fresh PBS+, separated into individual deciduas and subsequently removed under a stereomicroscope using watchmaker's forceps. The deciduas were transferred to another culture dish with fresh PBS^+ carefully dissected in half and the embryos were isolated. Staging of the embryos was performed according to (Downs & Davies 1993). For the analysis of leftward flow, embryos were transferred to a culture dish containing F10 culture medium at RT above a thin layer of agarose.

IV.2.3 Rabbit

Embryos were obtained from timed matings of NZW rabbits. All steps involving isolation and culture of embryos were carried out under sterile conditions using sterile buffers, media, labware and instruments. After the abdominal cavity of the dead animal had been opened, the uterus was removed in whole and transferred to PBS^+ in a 50ml Falcon Tube. If the embryos were to be used for leftward flow observation, the uterus was processed natively. Uteri from both were transferred into fresh PBS+ in a large Petri dish (10cm in diameter) where excess fat and mesenteria were removed and the uterus was separated into pieces between the embryo implantation sites. Single parts of the uterus were again transferred into fresh PBS^+ and dissected further under a stereomicroscope using fine tweezers and iridectomy scissors. The bulging uterine tissue opposite of the implantation site was carefully cut and removed until the embryo covering the mucosa became accessible. The embryo together with as much surrounding extra-embryonic tissue as possible was cautiously detached from the mucosa and transferred into another dish with fresh PBS^+ ready for time-lapse acquisition. Embryos were staged according to (Hamburger & Hamilton 1992).

IV.2.4 Chicken

Embryos were obtained from timed incubations of fertilized hen eggs. After incubation for the desired length of time eggs were taken out of the incubator making sure that the embryo stayed on top by not rotating them. Then, eggs were cracked into a 10cm Petri dish using the rim of the dish. If the vitelline membrane stayed intact and the blastoderm was roughly centered on the yolk, the preparation proceeded with removing the thick albumen covering the blastoderm with a folded tissue or a plastic pipette. Once an area of vitelline membrane large enough was cleared, the filter paper ring was placed onto the yolk framing the embryo. The vitelline membrane was then cut around the filter paper ring using fine scissors. The ring including the embryo attached to the vitelline membrane was gently lifted with tweezers and any remaining yolk was removed by stroking the vitelline membrane in a centrifugal fashion with blunt tweezers. The embryo was then transferred into a small Petri dish containing either simple saline or PBS^{+} to remove as much yolk as possible by gently flushing the saline over the blastoderm. Embryos were fixed in 4% PFA for 1h at RT and afterwards rinsed in EtOH for storage. Embryos were staged according to (Hamburger & Hamilton 1992).

IV.2.5 Sea urchins

Adult sea urchins of *P. lividus* were collected from the Mediterranean Sea at the Croatian Adriatic Coast and kept in an aerated seawater tank. Gametes were obtained by intracelomic injection of 0.5M KCl in filtered sea water. Eggs were washed with filtered sea water and fertilized by adding drops of diluted sperm. Embryos were cultured at room temperature under gentle agitated by bubbling of culture medium (sea water) with a motor-driven pump. Gastrula stage embryos were used *in vivo* for time-lapse acquisition or fixed in 4% PFA in filtered seawater for IHC staining. Embryos were staged according to http://www.stanford.edu/group/Urchin/dev.htm

IV.3 *in vivo* approaches

IV.3.1 Preparation of dorsal explants

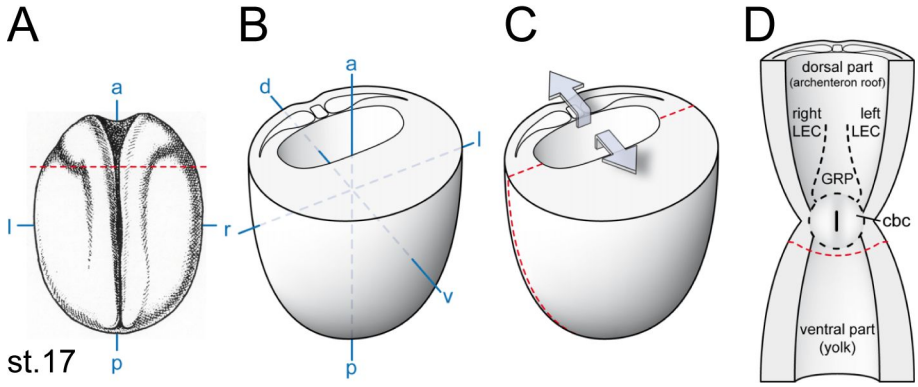

Fig. 41 Preparation of dorsal explants
Head region is removed (red line in A) to open archenteron (B). Dissection of the dorsal posterior part along red dashed lines (C), ventral and dorsal parts are pulled apart (arrows in C). Dorsal explant is completed by removal of the yolk ventral of the circumblastoporal collar (D; red dashed line).
a, anterior; cbc, circumblastoporal collar; d, dorsal; l, left; LEC, lateral endodermal crest; p, posterior; r, right; v, ventral

Embryos are placed in 1×MBSH in a agarose coated Petri dish. Dorsal explants are prepared *in vivo* by removing of cranial structures, slicing left and right sides and pulling dorsal from ventral side apart. Final section ventral of the cbc provides dorsal explant (Fig. 41). Debris of explants is removed by gently pipetting explants in medium.

IV.3.2 Acquisition and analysis of leftward flow

For leftward flow analysis, objective slides were prepared with a square of vaseline. The square was filled with 1×MBSH together with 500nm fluorescent beads at a dilution of 1/2500. Dorsal explants were dissected and subsequently transferred into the medium within the square of vaseline and covered by a cover slip. The slide was then investigated under a microscope. For leftward flow, 2fps and 500 pictures were acquired during a time-lapse videography (AxioVision 4.6). Movies were further processed as described in II.1.1.

IV.3.3 Acquisition of CBF

CBF of multiciliated epidermis cilia was investigated after injection of 100ng/µl *mRFP* mRNA in animal ventral blastomeres of 4-cell stage embryos. Movies were taken via the 'digital high speed recorder' (AxioVision 4.6) on Axioplan2 equipped with AxioCam Hsm. CBF was empirically scored. For demonstrative purposes, maximum-Z-projection was performed in ImageJ.
CBF of GRP cilia was investigated after injection of 100ng/µl *PACRG-eGFP* mRNA into the prospective DMZ at the 4-cell stage. Timelapse movies were acquired (10fps) and maximum-Z-projection was performed.

IV.4 Scanning electron microscopy (SEM)

All SEM photography in this thesis was performed by Tina Beyer (Beyer 2011). Dorsal explants were freshly dissected in 0.1×MBSH and fixed in a mixture of 2% paraformaldehyde (PFA) and 2.5% glutaraldehyde (GA) for 1hr at RT or overnight at 4°C. Specimens were washed 3×10min in 0.1M phosphate buffer (PB, pH7.5) and were postfixed for 1-2hrs in 1% OsO4/0.1M PB at 4°C. After extensive washing embryos were gradually dehydrated in an ethanol series and stored in 100% EtOH at -20°C until submitted to the drying procedure. Critical point drying was performed using CO_2 as drying agent. Embryos were sputtered with gold and viewed under a LEO DSM 940A. Evaluation of GRP characteristics were performed as described in II.1.2.

IV.5 Morpholino-oligonucleotide mediated knockdown

Morpholinos are gene-specific, synthetic, stable, single-stranded antisense-oligonucleotides that bind the complementary mRNA of the gene of desire to prevent translation or splicing thereof (Gene Tools, LLC, Philomath, USA). After injection into the cell, MOs bind to the mRNA and specifically inhibit translation of the mRNA. As knockdown efficiency and endogenous gene activities differ, concentration for every MO was determined individually. MOs were used at 0.25-8 pmol/embryo (i.e. injected at a concentration between ~30 and ~500µM) as indicated.
Specific morpholinos used in this work are:

dnah5-SB-MO:	5′ TGTACAGACCTGATTACCCTCTAGA 3′
dnah9-SB-MO:	5′ CATAGGAATCAACTCACTTTTTCTC 3′
dnah9-AUG-MO:	5′ GGTCACGTTTTGGAGGTGCAGTGGC 3′
xBic-C-MO1:	5′ TAGACTCGCACTGAGCCGCCATTCT 3′
xBic-C-MO2:	5′ CCATTGTGCTACTGCCGCCGCTAAC 3′
xHtr3-MO1:	5′ GATGTTAAGTGTAGAGTCATTCTGG 3′
xHtr3-MO2:	5′ ACAGATCAGAGTGTTTGCTTTGTCA 3′
Coco-MO:	5′ CTGGTGGCCTGGAACAACAGCATGT 3′
Xnr1-MO:	5′ GCTGTCAGAAATGCCATGCTTGCAC 3′
xIPACRG-MO:	5′ TGCTTGTCTCAAACACCATATTCAC 3′

For control-injections to exclude injection artifacts either the standard control- or the random control-morpholino were used.

IV.6 Reverse Transcriptase Polymerase chain reaction (RT-PCR)

Isolation of RNA

Total RNA of desired stages was extracted by phenol-chloroform extraction and EtOH precipitation with Peqlab peqGold Trifast solution following the peqGold Trifast protocol. 1ml of the solution was used for the isolation of RNA of about 3 embryos. RNA was eluted in 25µl sterile DDW, measured photometrically and stored at -80°C.

First strand cDNA synthesis

cDNA was synthesized from total RNA preparations by reverse transcription using MMLV Reverse Transcriptase. A standard protocol started with 1µg of total RNA to which 0.5µl of random hexamers wese added and filled up with sterile water to a total volume of 14µl. The solution was heated to 70°C for 5min melting secondary structures within the template. Further snap cooling on ice prevented these structures from reforming. The reagents were then supplemented with 5µl 5×M-MLV Reaction Buffer, 1.25µl 10mM dNTPs, 1µl (200units) of M-MLV RT and filled up to a volume of 25µl. After an initial incubation for 10min at RT, the reaction was put to 50°C for another 50min to complete first strand synthesis. The reaction was stopped by heating to 60°C. The cDNA was stored at -20°C.

Standard PCR protocol

For a 25µl PCR reaction 1µl of prepared template cDNA was mixed with 2mM dNTPs, 1U of Taq DNA polymerase, 5µl 5×Buffer, 1µl of each forward and reverse primer at a concentration of 10µM and filled up to 25µl with sterile DDW. A standard PCR cycling program comprises (1) 1min at 95°C, (2) 30sec at 95°C, (3) 30sec-1min at a primer pair specific annealing temperature and (4) 1min/1000bp of amplifiable nucleotide sequence at 72°C. Steps (2) to (4) were repeated for 35 times before the reaction was (5) stopped and kept in the cycler at 8°C. Step (1) and (2) yield a denaturation of the double-stranded template DNA, step (3) allows for hybridization of primers to the single-stranded DNA. Step (4): the Taq polymerase elongates the sequences at the primer's 3' end. For the detection of gene expression using RT-PCR, steps (2) to (4) were repeated between 28 and 33 times. If the product was intended to be further amplified in bacteria (for cloning), an extra 10min step at 72°C were added after 35-40 cycles to make use of the Taq Polymerase's Terminal Transferase activity, that adds an extra deoxyadenosine onto each 3' end of already existing double-stranded PCR products. This creates a single 3'-A overhang that can be utilized for ligation into a cloning vector.

IV.7 Oligonucleotides for PCR

For the design of primers, sequences were obtained either from NCBI EST database or by BLAST search of the *Xenopus tropicalis* genome (http://www.jgi.doe.gov) with a corresponding published mouse sequence. The following primer combinations (forward, fwd; reverse, rev) and PCR conditions were used:

gene		primer (5'-3' orientation)	
xlPACRG	fwd	TGGATCCATGGTGTTTGAGACAAGCAAAGCAACA	
	rev	ATGAATCCTGCTTGCTGAACTGACTCGAGATAT	
	rev*	ATGAATCCTGCTTGCTGAACCTCGAGATAT	*for in-frame fusion
	fwd*	TGGATCCATGGTCTTCGAAACTAGTAAGGCAACA	* for rescue
mmPACRG	fwd	CCCTCTCCTCCCCTAAACTC	with eGFP
	rev	CGTGCTTGCTGAACTGACCG	
ocPACRG	fwd	ATGCCGAAGAGGACTAAACTGCTG	
	rev	ACCTACGAGTCTTGCTTGCT	
ggPACRG	fwd	GCTGCGGGGAGATGGTAGTG	
	rev	GAACGCTACGGTGGAGAAACTG	
dnah5	fwd	CTTTGGTGTCATTGGAATAGGGC	
	rev	AGTATCCCAGCCATGTGAGG	
dnah9	fwd	TGCAAACACTGTTGCCATGGC	
	rev	TGGGGTTTTTTCCTTGCAGAAG	
***xHtr3* (*xFL*)**	fwd	CATTGGAATGGACCAATGAATA	
	rev	GTCAGGCCGGTTATTTGTGTT	
xHtr3rescue	fwd	ATATCGATATGACCTTGCATCTCACGAGCCTGCTGCTC	MO-site mismatch
	rev	ATCTCGAGTTATGTTGCCCAAACAATAATAAGAAT	
xLBD	fwd	ATGAATTCATGACTCTACACTTAACATCTCTGC	
	rev	CAATAAAACGGGCCCCTGTTGTTTAGCTCGAG	
hLBD	fwd	ATGAATTCATGCTTGGAAAGCTCGCTATGCTGCTG	
	rev	ATCTCGAGTCAGCTGACCACATAGAAGAGGGGCCGC	

IV.8 Cloning & selection

Ligation of PCR products into cloning vectors

PCR-products were ligated into the linearized pGEM-T Easy (Promega) vector with the T4 ligase. In a standard reaction, 2.5µl of ligation buffer, 0.5µl of vector and 0.5µl of T4 ligase were combined with 1.5µl of fresh PCR amplificate. The reaction was incubated for 1h at RT or overnight at 4°C and then transformed into bacteria.

Bacterial transformation and clonal selection

The ligated vectors were transformed into chemically competent XL1-blue cells using the heat shock method. Different volumes (typically 100, 150) of bacteria-solution were plated on LB-agar selective plates (100µg/ml ampicillin / 0.5mM IPTG / 80µg/ml X-Gal) and incubated overnight at 37°C. The missing blue color of the clones indicated insertion of a PCR product into the multiple cloning site of the incorporated vector. Such clones were selected for amplification and analysis using a mini-prep procedure.

Cloning of the *xlPACRG-eGFP* fusion-construct

For to generate the fusion-construct, the full-length coding sequence covering primers of *xlPACRG* were modified in such that the stop-codon of the reverse primer was removed. Furthermore, distinct restriction recognition sites were introduced to the primers. Primers designed for *eGFP* were operated the same way. Enzymatic restriction was performed on each purified amplificate. The fusion-construct was generated by inserting both fragments into a prepared pCS2+ expression vector, simultaneously. The specific arrangement of restriction sites allowed the incorporation of *xlPACRG* into the vector only when *eGFP* was ligated to its 3' end

IV.9 Amplification of gene sequences

Preparation of small amounts of plasmid DNA (mini-prep)

Plasmid DNA from *E. coli* cultures was isolated using a modified alkaline lysis protocol. All centrifugation steps were performed at RT. 3ml of selective LB medium (100µg/ml Ampicillin) were inoculated with a single white bacteria colony from a selective plate and grown overnight with at 37°C by constant shaking. 1.5ml of the culture was poured into a micro centrifuge tube and bacteria were pelleted in a micro centrifuge at 5000rpm for 5min. Supernatant was discarded and the pellet was resuspended by vigorous vortexing in 100µl P1 buffer. When the bacteria suspension appeared uniform, 200µl of P2 buffer were added for alkaline lysis and the tube was inverted several times to thoroughly mix the reagents. After 5min reaction was stopped by neutralizing with 150µl of P3, again inverting the tube several times. After 20min of incubation on ice, the lysate was cleared from precipitate containing genomic DNA, cell debris, proteins and potassium dodecyl sulphate by centrifugation in a micro centrifuge at 13000 rpm for 10min. Supernatant was transferred to a fresh tube and mixed well with 1ml of 100% EtOH. After precipitation for 30min at -20°C the plasmid DNA was pelleted by centrifuging at 13000 rpm for 10min. The pellet was dried and resuspended in 50µl sterile DDW.

Preparation of medium amounts of plasmid DNA (midi-prep)

100ml of selective LB medium (100µg/ml ampicillin) were inoculated with 1ml of a solution of a positively tested bacteria clone and grown overnight in a 1000ml conical flask with vigorous shaking at 37°C. Bacteria were harvested by centrifugation, lysed and DNA was purified following the Promega “PureYield Plasmid Midiprep System” using the vacuum method.

Measuring the concentration of nucleic acids

The concentration of nucleic acids in aqueous solutions was determined via spectrophotometry. The ratio of absorption (A) at 260nm and 280nm wavelength indicated the purity of the solution (pure nucleic acid solution: 1.8 for DNA, 2.0 for RNA). The content of either DNA or RNA was inferred from the A260 value with 1 unit corresponding to 50µg/µl DNA and 40µg/µl RNA.

Restriction enzyme digests of DNA

To check for insertion of the correct PCR product after mini-prep, inserts were released from the plasmids by digestion with a restriction enzyme cutting on both sides of the multiple cloning site. Typically to 5µl of plasmid-DNA, 2µl 10x buffer, 0.2 µl BSA and 0.5µl enzyme were added, the mixture was filled up with 12.3µl sterile DDW to a final volume of 20µl and incubated at 37°C for 2hrs. After digestion the whole volume of the reaction was analyzed on an agarose gel. For linearization digests typically 20µg of plasmid-DNA was used in a 100µl reaction. 4µl of restriction enzyme were used and the digestion was incubated overnight at 37°C. Approximately 600ng of the digestion were controlled on a 1% agarose gel.

Agarose gel analysis

The products of each reaction were checked on a standard 1.0-1.5% agarose gel with a concentration of 0.4µl/ml ethidium bromide solution.

Synthesis of capped RNA

For capped RNA synthesis the Ambion kit mMESSAGE mMACHINE (High yield capped RNA Transcription kit) was used. For the reaction 4µl nuclease free H_2O, 10µl 2×NTP/CAP (ATP, 10mM; CTP, 10mM; UTP, 10mM; GTP, 2mM, cap analog, 8mM), 2µl 10×buffer, 2µl linearized CS^{2+} (~2 µg) and 2µl enzyme mixture (containing SP6 RNA polymerase) were mixed. After incubation for 2h at 37°C, 1µl DNase was added with a subsequent incubation of 15min. Then mRNA was twice phenol-chloroform extracted and precipitated in isopropyl alcohol. Concentration of the mRNA was then determined by spectrophotometry and the quality by running on an agarose gel.

IV.10 Whole mount *in situ* hybridization

In vitro transcription of RNA probes

200ng linearized plasmid with the insert of interest was used as a template. 20u of either Sp6 or T7 polymerase were added to a mixture of template, 4µl Transcription Buffer, 0.5µl (= 20units) RNasin, 2µl DTT and 2µl 10x Dig-Mix. After adding sterile DDW to a final volume of 20µl the mixture was incubated at 37°C for 2hrs. After gel check with 2µl in 10µl DDW on a 1% agarose gel, 115µl 100% EtOH and 3.75µl 4M LiCl were added to the mixture and RNA was precipitated at -20°C for at least 30min. After centrifuging 13 000rpm at 4°C for 20min; the resulting pellet was rinsed in 70% EtOH and centrifuged again for 5min. The pellet was air-dried and resuspended in 50µl of a 1:1 mixture of sterile DDW and formamide. The RNA was stored at -80°C.

In situ hybridization

Whole mount in situ hybridization used to detect the expression pattern of specific genes in *Xenopus* embryos. Protocol originally adapted from the De Robertis lab (Belo et al. 1997).

Day 1

All steps (except Proteinase K) until pre-hybridization were performed on ice. On the

first day of the procedure, tissue was prepared for taking up the antisense RNA probe, which hybridizes to the endogenous target RNA. Embryos were rehydrated from storage in 100% ethanol through a graded series of 75%, 50% and 25% ethanol in PBS$^-$. Embryos were washed three times for at least 5min in
PBS$^-$w and then the tissue was permeabilized for ~15-20min in 10µg/µl Proteinase K in PBS$^-$w at RT. Digestion was stopped in 2mg/ml glycine followed by three washing steps in PBS$^-$w for 5min each. The tissue was then refixed for 15min at RT in 4% PFA supplemented with 0.2% glutaraldehyde. After washing three times in PBS$^-$w for 5min the embryos were transferred into a 1:1 mixture of hybridization solution and PBS$^-$w. After equilibration in 100% hybridization solution, a pre-hybridization period in 900µl hybridization solution at 65°C for 2-3hrs eliminated endogenous phosphatases. Depending on the concentration of the RNA, about 1µl of antisense probe (~20ng) diluted in 100µl hybridization solution was added to the vial and the embryo was incubated with the probe overnight at 70°C.

Day 2

On the second day excess antisense probe was removed in high stringency washing steps and the tissue was prepared for incubation with the anti-digoxygenin antibody. In a first step, 1 to 3 washing steps (30min each) in 100% hybridization mix at 70°C were used to reduce background staining depending on the probe. Then the solution was again replaced with 800µl hybridization solution. In three steps (5 min each) each 400µl of 2xSSC (pH 4.5) were added and the embryo was washed twice in 2xSSC (pH 7) at 70°C afterwards. The washing steps in SSC were followed by four washing intervals in MABw, twice at RT for 10min and another two times at 70°C for 30min. Afterwards, embryos were washed three times in PBS$^-$w at RT for 10min each and were then pre-incubated in antibody-blocking buffer at 4°C for 2hrs. In a second tube, the anti-digoxygenin antibody coupled to alkaline phosphatase was diluted 1/10,000 and pre-blocked for the same time. After the 2hrs of pre-incubation, the blocking buffer was replaced with the antibody-solution and the embryos were incubated with the antibody overnight at 4°C on a laboratory shaker.

Day 3

On the third day, unbound antibody was removed in extensive washing steps and the staining reaction was started. Embryos were rinsed and then washed six times for 45min each in PBS$^-$w containing 0.1% BSA. The washing in BSA was followed by two washing steps with PBS$^-$w for 30min each and embryos were then transferred into AP1 buffer, which adjusts the pH of the tissue for the optimal reaction of the alkaline phosphatase. AP1 buffer was changed 1-4 times according to probe type and then replaced by a 1:1 mixture of AP1 buffer and BMPurple, the substrate for the alkaline phosphatase. The staining process was controlled and stopped by washing in PBS$^-$w, when the expected signal had reached a dark blue to violet color. A gradual methanol series intensified the signal and the embryos were afterwards stored in 100% methanol at -20°C.

Histological analysis of embryos after *in situ* hybridization

After rehydration embryos were equilibrated in a small volume of embedding medium (~1ml). 2ml of embedding medium were mixed shortly but vigorously with 142µl of glutaraldehyde and poured into a square mold formed of two glass brackets. The mixture was allowed to harden and the equilibrated embryo was transferred upon the surface of the block, excess embedding medium was carefully removed. Another 2ml of embedding medium mixed with glutaraldehyde were poured into the mold so that the embryo was now sandwiched between two layers of embedding mix. The hardened block was trimmed with a razor blade and glued onto a plate. The plate was mounted into the holder of the vibratome and 30µm thick sections were prepared. The sections were arranged onto glass slides, embedded with mowiol and protected with glass cover slips.

IV.11 Statistical analysis

Statistical calculations of marker gene expression patterns, cilia distribution, cilia length, cell size, ciliation rate and mean leftward flow velocities were performed using Pearson's chi-square test or Mann-Whitney-U test in statistical R (R Development Core Team 2011).

IV.12 Photo documentation

Documentation of living or fixed embryos was performed after stepwise rehydration in PBS^- with a Zeiss dissecting microscope STEREO Discovery.V12 or a LEICA MZFLIII with a digital camera (AxioCam HRc, Zeiss). Analyses of vibratome sections were performed with a Zeiss microscope Axioskop2 equipped with a digital camera (AxioCam HRc, Zeiss). For image processing (contrast, background, layout) Asobe Photoshop CS3 and Adobe Illustrator CS3 were used. All pencil drawings were created by Bernd Schmid and further processed with Photoshop.

IV.13 Buffers, Solutions and Media

For *in situ* hybridization:

Phosphate Buffered Saline 10× (PBS$^-$, 1l)
80g NaCl
2g KCl
14.4g Na_2HPO_4
2.4g KH_2PO_4
800ml DDW
adjust pH to 7.4, add DDW to 1l, autoclave.

PBSw (500ml)
500ml PBS^-
500µl Tween20.

Alkaline Phosphatase Buffer (AP1, 1l)
100ml 1M TRIS pH 9.5
20ml 5M NaCl
50ml 1M MgCl
add DDW to 1l.

Maleic Acid Buffer 5×(MAB, 1l)
58.05g (100mM) Maleic Acid
43.83g (150mM) NaCl
800ml DDW
adjust pH to 7.5 with 10N NaOH, add DDW to 1l, autoclave.

Sodium Citrate Buffer 20×(SSC, 1l)
175.3g NaCl
88.2g Sodium citrate
800ml DDW
adjust pH to 7.0, add DDW to 1l, autoclave.

Hybridization solution (1l)
10g Boehringer Block
500ml Formamide
250ml SSC 20×
Heat to 65°C for 1 hour
120ml DDW
100ml Torula RNA (10mg/ml in DDW; filtered)
2ml Heparin (50mg/ml in 1×SSC pH 7)
5ml 20% Tween-20
10ml 10% CHAPS
10ml 0.5M EDTA

Antibody Blocking Buffer
10% Heat Inactivated Goat Serum
1% Boehringer Block
0.1% Tween-20
dissolve in PBS at 70°C, vortexing frequently, then filter (0.45µm)

For frog experiments:

5×MBSH (1l)
25.7g NaCl
0.375g KCl
1g $NaHCO_3$
1g $MgSO_4/7H_2O$
0.39g $(CaNO_3)^2/4H_2O$
0.3g $CaCl_2/2H_2O$
11.9g Hepes
5 ml Penicillin/Streptomycin

10×MEMFA (500ml)
2M MOPS (pH 7.4)
200ml 100mM EGTA
10ml 1M $MgSO_4$
add DDW to 1l, autoclave.

1×MEMFA
10 % 10×MEMFA
10 % Formaldehyde 37%
80 % H_2O

Gurdon's buffer
88mM NaCl
15mM HEPES
1mM KCl
15mM Tris-HCl, pH 7.6

Ficoll
2% Ficoll diluted in 1×MBSH

Cystein
2% Cystein diluted in DDW. Adjust pH to 7.99.

For bacteria culture:

Super Optimal Catabolite repression medium (S.O.C.)
0.5% Yeast extract
2.0% Tryptone
10mM NaCl
2.5mM KCl
10mM $MgCl_2$
10mM $MgSO_4$
20mM Glucose
autoclave

Lysogeny Broth (LB) medium
1% Tryptone
1% NaCl
0.5% Yeast extract
adjust pH to 7.0, autoclave.

LB agar
1% Tryptone
1% NaCl
0.5% Yeast extract
adjust pH to 7.0, add 15g/l agar before autoclaving.

For other applications:

Embedding medium for vibratome sections
2.2g Gelatine
135g Bovine Serum Albumin
90g Sucrose
dissolve in 450ml PBS.

Mowiol (Mounting medium)
96g Mowiol 488
24g Glycerol
24ml DDW
stir for 2h, then add
48ml TRIS 0.2M pH 8.5
stir for 20min at 50°C
centrifuge for 15min at 5000rpm, keep supernatant
and store at -20°C.

Tris Acetate EDTA Buffer (TAE)
40mM Tris-acetate
2mM EDTA
adjust pH to 8.0.

For DNA preparation:

P1
50mM TRIS HCl
10mM EDTA pH 8
add RNaseA (DNase free) to a final concentration of 100µg/ml

P2
0,2M NaOH
1% SDS

P3
3M Potassium acetate, pH 5.5

IV.14 Sources of supply

IV.14.1 Chemicals and labware

2-Propanol	Roth, Karlsruhe
Acetic acid	AppliChem, Darmstadt
Agarose	Roth, Karlsruhe
Albumin fraction V	AppliChem, Darmstadt
Ampicillin	AppliChem, Darmstadt
Anti-Digoxigenin-AP	Roche, Mannheim
BM Purple	Roche, Mannheim
Boehringer Block	Roche, Mannheim
Bovine serum albumin	AppliChem, Darmstadty
BSA	AppliChem, Darmstadt
CAS-Block	Invitrogen, Karlsruhe
CHAPS	Sigma, Schnelldorf
Chloroform	Merck, Darmstadt
Cystein	Roth, Karlsruhe
Desoxynucleosidtriphosphate (dNTPs)	Promega, Mannheim
DIG RNA Labeling Mix	Roche, Mannheim
Dimethylsulfoxid (DMSO)	Roth, Karlsruhe
Disodium hydrogen phosphate	AppliChem, Darmstadt
Dithioreitol (DTT)	romega, Mannheim
DMSO	Roth, Karlsruhe
EDTA	Roth, Karlsruhe
Ethanol	Roth, Karlsruhe
Ethidium Bromide	Roth, Karlsruhe
Ethyl-p-Aminobenzoat (Benzocain)	Sigma, Schnelldorf
Ethylenediamine tetraacetic acid EDTA	Roth, Karlsruhe
Ethyleneglycol tetraacetic acid EGTA	Roth, Karlsruhe
Ficoll	AppliChem, Darmstadt
FluoSphere 500nm	Molecular Probes (Invitrogen), Karlsruhe
Forceps (#3, #5)	Fine Science Tools, Heidelberg
Formaldehyd	AppliChem, Darmstadt
Formamide	Roth, Karlsruhe
Gelatine	Roth, Karlsruhe
Glass coverslips	Roth, Karlsruhe
Glass slides	Roth, Karlsruhe
Glucose	AppliChem, Darmstadt
Glutaraldehyde	AppliChem, Darmstadt
Glycerol	Roth, Karlsruhe
Glycin	AppliChem, Darmstadt
Goat serum	Sigma, Schnelldorf
HCG (human chorionic gonadotropin)	Sigma, Schnelldorf
HCl (37%)	Merck, Darmstadt
Heparin	Sigma, Schnelldorf
Hepes	AppliChem, Darmstadt
Heptanol	Roth, Karlsruhe
Injection syringe F1, 1ml	B. Braun, Melsungen
Injection-needle Sterican (0,4x20 mm)	B. Braun, Melsungen
Lambda-DNA	Promega, Mannheim
Ligase (T4-Ligase)	Promega, Mannheim

Lithium chloride	Serva, Heidelberg
Loading Buffer	AppliChem, Darmstadt
Magnesium chloride	Roth, Karlsruhe
Magnesium sulfate	AppliChem, Darmstadt
Maleic acid	Roth, Karlsruhe
Methanol	Roth, Karlsruhe
Micro centrifuge tubes	Sarstedt, Nümbrecht
Objective slides	Roth, Karlsruhe
Oligonucleotides	Operon, Cologne
Osmium tetroxide	Plano, Wetzlar
Parafilm	Roth, Karlsruhe
Paraformaldehyde	AppliChem, Darmstadt
PBS+ (10x)	Gibco (Invitrogen) Karlsruhe
Penicillin/Streptomycin	Gibco (Invitrogen) Karlsruhe
pGEM-T-Easy-Vektor	Promega, Mannheim
Phenol/chloroform (Rotiphenol)	Roth, Karlsruhe
Plastic pipettes	Sarstedt, Nümbrecht
Proteinase K	Roth, Karlsruhe
Rhodamine-B-dextran	Molecular Probes (Invitrogen), Karlsruhe
RNAse A	Roth, Karlsruhe
RNAsin	Promega, Mannheim
Rose-Gal	Roth, Karlsruhe
Saccharose	Applichem, Darmstadt
Sodium acetate	Roth, Karlsruhe
Sodium chloride	Roth, Karlsruhe
Sodium citrate	Roth, Karlsruhe
Sodium dihydrogen phosphate	AppliChem, Darmstadt
Sodium hydroxide	AppliChem, Darmstadt
Sp6-RNA-Polymerase	Promega, Mannheim
Sucrose	AppliChem, Darmstadt
Syringe filters	Whatman, Dassel
T7-RNA-Polymerase	Promega, Mannheim
Taq-DNA-Polymerase (Go-Taq)	Promega, Mannheim
Torula RNA	Sigma, Schnelldorf
TRIS base	AppliChem, Darmstadt
TRIS HCl	AppliChem, Darmstadt
Triton-X100	Serva, Heidelberg
Tryptone	AppliChem, Darmstadt
Tween-20	AppliChem, Darmstadt
X-Gal	Roth, Karlsruhe

IV.14.2kits

DNA-Purification-Kit (Easy-Pure)	Biozym, Hessisch Oldendorf
mMESSAGE mMACHINE SP6	Ambion, Darmstadt
pGEM-T Easy Vector System	Promega, Mannheim
PureYield Plasmid Midiprep System	Promega, Mannheim
PeqGOLD TriFast	Peqlab, Erlangen

IV.14.3Proteins and Antibodies

Restriction enzymes and buffers	Promega, Mannheim
Modifying enzymes and buffers	Promega, Mannheim
Mouse anti-acetylated α-tubulin	Sigma, Schnelldorf
Rabbit anti-serotonin	Millipore (Chemicon), Billerica, MA, USA
Anti-digoxigenin-AP	Roche, Mannheim
Cy3 Anti-Mouse IgG F(ab')2 fragment	Sigma, Schnelldorf
Cy2 Anti-Mouse-conjugated Fab fragment IgG (H+L)	Jackson ImmunoResearch, Suffolk
Alexa Fluor 488 donkey Anti-Rabbit IgG (H+L)	Invitrogen, Karlsruhe
Rabbit anti-PACRG	Rockland Immunochemicals, Gilbertsville, PA, USA

IV.14.4Special Hardware

Peltier Thermal Cycler PTC-200	Biozym, Hessisch Oldendorf
Vibratome	Leica, Bensheim
Stereo microscope	Zeiss, Oberkochen
Zeiss DSM 940A	Zeiss, Oberkochen
LSM 5 Pascal	Zeiss, Oberkochen
Axioplan 2	Zeiss, Oberkochen
Critical point dryer CPD 030	Balzers, Austria
Sputter coater SCD 050	Balzers, Austria
LEO DSM 940A	Zeiss, Oberkochen

IV.15 Animals

Frogs

Adult African clawed frogs (*Xenopus laevis*) were obtained from Guy Pluck, Xenopus express, Ancienne Ecole de Vernassal, Le Bourg 43270, Vernassal, Haute-Loire, France. They were and kept species-appropriate at a 12h light-cycle in the animal facility of the Institute of Zoology, University of Hohenheim.

Some parts of the Materials and Methods sections have been adapted from (Bitzer 2008; Andre 2009; Vick 2009; Beyer 2011).

IV.16 Acknowledgement

I like to thank Janet Heasmen, John Wallingford, Chris Kintner and Matthias Gerberding for plasmids and Ray Keller and David Shook for help with time-lapse movies of blastopore closure. Special thanks to JW, RK and Axel Schweickert for experimental advice and lively scientific discussions.

V list of Abbreviations

5-HT	5-hydroxytryptamine, serotonin
5-HTR3A	5-HT_3 subunit A (protein)
5-HT_3	serotonin receptor class 3
AB	antibody
abs	absent
AC	apical constriction
AP	anterior-posterior
bi	bilateral
bp	basepair
cbc	circumblastoporal collar
CBF	cilia beat frequency
CE	convergent extension
cf	confer
cr	*Chlamydomonas reinhardtii*
DA	double-axes (also conjoined or Siamese twins)
DAI	dorso-anterior index
DMZ	dorsal marginal zone
DNA	deoxyribonucleic acid
dpf	days post fertilization
dr	*Danio rerio*
DV	dorso-ventral
E	embryonic day
e.g.	exempli gratia
eGFP	*enhanced green fluorescent protein*
Foxj1	*forkhead box J1*
fps	frames per second
gg	*Gallus gallus*
GJ	gap junctions
GJC	gap junctional communication
GRP	gastrocoel roof plate
GTT	gradient-time-trail
hFL	full length *hHTR3A*
hHTR3A	gene encoding human 5-HT_3 subunit A
hHTR3AT	gene encoding human splice variant of 5-HT_3 subunit A
hLBD	*hHTR3A* signal peptide + LBD
hs	*Homo sapiens*
hsv	*hHTR3AT*
hyGRP	hypochordal GRP cells
i.e.	id est
IFT	intraflagellar transport
IHC	immunohistochemistry
iv	*inversus viscerum*

KV	Kupffer's vesicle
LBD	ligand binding domain
LEC	Lateral endodermal crest
lefty	*left-right determination factor*
lof	loss-of-function
LPM	lateral plate mesoderm
LR	left-right
lrd	*left-right dynein*
MBT	midblastula-transition
MC	methyl-cellulose
mip	*mixed-up*
mm	*Mus musculus*
MO	morpholino-oligonucleotide
MOsite	morpholino-oligonucleotide binding site
mRFP	*membrane red fluorescent protein*
mRNA	messenger ribonucleic acid (RNA)
MT	microtubuli
nGRP	notochordal GRP cells
NTD	neural tube defects
NVP	nodal vesicular parcel
oc	*Oryctolagus cuniculus*
PACRG	*PARK2-co-regulated gene*
PARK2	*parkinson protein 2*, *E3 ubiquitin protein ligase* (*parkin*)
PCP	planar cell polarity
Pitx2c	*paired like homeodomain 2c*
PNC	posterior notochord
RNA	ribonucleic acid
SEM	scanning electron microscopy
sGRP	somitic GRP cells
SM	superficial mesoderm
st.	stage
tb	*Trypanosoma brucei*
TF	transcription factor
VMZ	ventral marginal zone
WMISH	whole mount *in situ* hybridization
Wnt	*wingless-type MMTV integration site family*
wt	wildtype
XCR2	*teratocarcinoma-derived growth factor 1 pseudogene 2*
xFL	full length *xHtr3*
xHtr3	gene encoding *Xenopus* 5-HT_3 subunit
xl	*Xenopus laevis*
xLBD	*xHtr3* signal peptide + LBD
Xnr1	*Xenopus nodal related 1*
Xnr3	*Xenopus nodal related 3*

VI Bibliography

Abràmoff, M.D., Magalhães, P.J. & Ram, S.J., 2004. Image Processing with ImageJ. *Biophotonics International*, 11(7), pp.36-42.

Adachi, H., Saijoh, Y., Mochida, K., Ohishi, S., Hashiguchi, H., Hirao, A. & Hamada, H., 1999. Determination of left/right asymmetric expression of nodal by a left side-specific enhancer with sequence similarity to a lefty-2 enhancer. *Genes & development*, 13(12), pp.1589-600.

Adams, D.S., Robinson, K.R., Fukumoto, T., Yuan, S., Albertson, R.C., Yelick, P., Kuo, L., McSweeney, M. & Levin, M., 2006. Early, H+-V-ATPase-dependent proton flux is necessary for consistent left-right patterning of non-mammalian vertebrates. *Development (Cambridge, England)*, 133(9), pp.1657-71.

Afzelius, B.A., 1976. A human syndrome caused by immotile cilia. *Science (New York, N.Y.)*, 193(4250), pp.317-9.

Andre, P., 2009. *Delimitation of the organizer from the posterior notochord : descriptive and functional studies in mouse and African clawed frog*. Universität Hohenheim.

Antic, D., Stubbs, J.L., Suyama, K., Kintner, C., Scott, M.P. & Axelrod, J.D., 2010. Planar cell polarity enables posterior localization of nodal cilia and left-right axis determination during mouse and Xenopus embryogenesis. *PloS one*, 5(2), p.e8999.

Aw, S., Adams, D.S., Qiu, D. & Levin, M., 2007. H,K-ATPase protein localization and Kir4.1 function reveal concordance of three axes during early determination of left-right asymmetry. *Mechanisms of development*, 125(3-4), pp.353-72.

Bae, S., Reid, C.D. & Kessler, D.S., 2011. Siamois and Twin are redundant and essential in formation of the Spemann organizer. *Developmental biology*, 352(2), pp.367-81.

Beattie, C.E., Raible, D.W., Henion, P.D. & Eisen, J.S., 1999. Early pressure screens. *Methods in cell biology*, 60, pp.71-86.

Beddington, R.S. & Robertson, E.J., 1999. Axis development and early asymmetry in mammals. *Cell*, 96(2), pp.195-209.

Belo, J.A., Bouwmeester, T., Leyns, L., Kertesz, N., Gallo, M., Follettie, M. & De Robertis, E.M., 1997. Cerberus-like is a secreted factor with neutralizing activity expressed in the anterior primitive endoderm of the mouse gastrula. *Mechanisms of development*, 68(1-2), pp.45-57.

Beyer, T., 2011. *The role of serotonin and gap junctions in left-right development of Xenopus laevis*. Universität Hohenheim.

Bilic, J., Huang, Y.-L., Davidson, G., Zimmermann, T., Cruciat, C.-M., Bienz, M. & Niehrs, C., 2007. Wnt induces LRP6 signalosomes and promotes dishevelled-dependent LRP6 phosphorylation. *Science (New York, N.Y.)*, 316(5831), pp.1619-22.

Bisgrove, B.W., Essner, J.J. & Yost, H.J., 1999. Regulation of midline development by antagonism of lefty and nodal signaling. *Development (Cambridge, England)*, 126(14), pp.3253-62.

Bitzer, E.S., 2008. *Establishment of a new in vitro Culture System and functional Analysis of Sonic Hedgehog and FGF8 in the Determination of Laterality in the Rabbit Embryo*. Universität Hohenheim.

Blum, M. et al., 2007. Ciliation and gene expression distinguish between node and posterior notochord in the mammalian embryo. *Differentiation; research in biological diversity*, 75(2), pp.133-46.

Blum, M., Beyer, T., Weber, T., Vick, P., Andre, P., Bitzer, E. & Schweickert, A., 2009a. Xenopus, an ideal model system to study vertebrate left-right asymmetry. *Developmental dynamics : an official publication of the American Association of Anatomists*, 238(6), pp.1215-25.

Blum, M., Weber, T., Beyer, T. & Vick, P., 2009b. Evolution of leftward flow. *Seminars in cell & developmental biology*, 20(4), pp.464-71.

Borovina, A., Superina, S., Voskas, D. & Ciruna, B., 2010. Vangl2 directs the posterior tilting and asymmetric localization of motile primary cilia. *Nature cell biology*, 12(4), pp.407-12.

Boterenbrood, E.C. & Nieuwkoop, P.D., 1973. The formation of the mesoderm in urodelean amphibians. *Wilhelm Roux' Archiv f r Entwicklungsmechanik der Organismen*, 173(4), pp.319-332.

Brennan, J., Norris, D.P. & Robertson, E.J., 2002. Nodal activity in the node governs left-right asymmetry. *Genes & development*,

16(18), pp.2339-44.

Brown, N.A. & Wolpert, L., 1990. The development of handedness in left/right asymmetry. *Development (Cambridge, England)*, 109(1), pp.1-9.

Brüss, M., Barann, M., Hayer-Zillgen, M., Eucker, T., Göthert, M. & Bönisch, H., 2000. Modified 5-HT3A receptor function by co-expression of alternatively spliced human 5-HT3A receptor isoforms. *Naunyn-Schmiedeberg's archives of pharmacology*, 362(4-5), pp.392-401.

Campione, M. et al., 1999. The homeobox gene Pitx2: mediator of asymmetric left-right signaling in vertebrate heart and gut looping. *Development (Cambridge, England)*, 126(6), pp.1225-34.

Cartwright, J.H.E., Piro, N., Piro, O. & Tuval, I., 2007. Embryonic nodal flow and the dynamics of nodal vesicular parcels. *Journal of the Royal Society, Interface / the Royal Society*, 4(12), pp.49-55.

Castrodad, F. a, Renaud, F.L., Ortiz, J. & Phillips, D.M., 1988. Biogenic amines stimulate regeneration of cilia in Tetrahymena thermophila. *The Journal of protozoology*, 35(2), pp.260-4.

Cheng, a M., Thisse, B., Thisse, C. & Wright, C.V., 2000. The lefty-related factor Xatv acts as a feedback inhibitor of nodal signaling in mesoderm induction and L-R axis development in xenopus. *Development (Cambridge, England)*, 127(5), pp.1049-61.

Clement, J.H., Fettes, P., Knöchel, S., Lef, J. & Knöchel, W., 1995. Bone morphogenetic protein 2 in the early development of Xenopus laevis. *Mechanisms of development*, 52(2-3), pp.357-70.

Colas, J.F., Launay, J.M., Vonesch, J.L., Hickel, P. & Maroteaux, L., 1999. Serotonin synchronises convergent extension of ectoderm with morphogenetic gastrulation movements in Drosophila. *Mechanisms of development*, 87(1-2), pp.77-91.

Cooke, J., 2004. Developmental mechanism and evolutionary origin of vertebrate left/right asymmetries. *Biological reviews of the Cambridge Philosophical Society*, 79(2), pp.377-407.

Creton, R., 2004. The calcium pump of the endoplasmic reticulum plays a role in midline signaling during early zebrafish development. *Brain research. Developmental brain research*, 151(1-2), pp.33-41.

Danilchik, M.V. & Black, S.D., 1988. The first cleavage plane and the embryonic axis are determined by separate mechanisms in Xenopus laevis. I. Independence in undisturbed embryos. *Developmental biology*, 128(1), pp.58-64.

Danilchik, M.V., Brown, E.E. & Riegert, K., 2006. Intrinsic chiral properties of the Xenopus egg cortex: an early indicator of left-right asymmetry? *Development (Cambridge, England)*, 133(22), pp.4517-26.

Dathe, V., Gamel, A., Männer, J., Brand-Saberi, B. & Christ, B., 2002. Morphological left-right asymmetry of Hensen's node precedes the asymmetric expression of Shh and Fgf8 in the chick embryo. *Anatomy and embryology*, 205(5-6), pp.343-54.

Davis, N.M., Kurpios, N.A., Sun, X., Gros, J., Martin, J.F. & Tabin, C.J., 2008. The chirality of gut rotation derives from left-right asymmetric changes in the architecture of the dorsal mesentery. *Developmental cell*, 15(1), pp.134–145.

Dawe, H.R., Farr, H., Portman, N., Shaw, M.K. & Gull, K., 2005. The Parkin co-regulated gene product, PACRG, is an evolutionarily conserved axonemal protein that functions in outer-doublet microtubule morphogenesis. *Journal of cell science*, 118(Pt 23), pp.5421-30.

Deblandre, G. a, Wettstein, D. a, Koyano-Nakagawa, N. & Kintner, C., 1999. A two-step mechanism generates the spacing pattern of the ciliated cells in the skin of Xenopus embryos. *Development (Cambridge, England)*, 126(21), pp.4715-28.

Downs, K.M. & Davies, T., 1993. Staging of gastrulating mouse embryos by morphological landmarks in the dissecting microscope. *Development (Cambridge, England)*, 118(4), pp.1255-66.

Duboc, V., Röttinger, E., Lapraz, F., Besnardeau, L. & Lepage, T., 2005. Left-right asymmetry in the sea urchin embryo is regulated by nodal signaling on the right side. *Developmental cell*, 9(1), pp.147-58.

Dubé, F. & Amireault, P., 2007. Local serotonergic signaling in mammalian follicles, oocytes and early embryos. *Life sciences*, 81(25-26), pp.1627-37.

Essner, J.J., Amack, J.D., Nyholm, M.K., Harris, E.B. & Yost, H.J., 2005. Kupffer's vesicle is a ciliated organ of asymmetry in the zebrafish embryo that initiates left-right development of the brain, heart and gut. *Development (Cambridge, England)*, 132(6),

pp.1247-60.

Feistel, K. & Blum, M., 2006. Three types of cilia including a novel 9+4 axoneme on the notochordal plate of the rabbit embryo. *Developmental dynamics ▪ : an official publication of the American Association of Anatomists*, 235(12), pp.3348-58.

Fitzpatrick, P.F., 1999. Tetrahydropterin-dependent amino acid hydroxylases. *Annual review of biochemistry*, 68, pp.355-81.

Fuentealba, L.C., Eivers, E., Geissert, D., Taelman, V. & De Robertis, E.M., 2008. Asymmetric mitosis: Unequal segregation of proteins destined for degradation. *Proceedings of the National Academy of Sciences of the United States of America*, 105(22), pp.7732-7.

Fukumoto, T., Kema, I.P. & Levin, M., 2005. Serotonin signaling is a very early step in patterning of the left-right axis in chick and frog embryos. *Current biology ▪ : CB*, 15(9), pp.794-803.

Gaspar, P., Cases, O. & Maroteaux, L., 2003. The developmental role of serotonin: news from mouse molecular genetics. *Nature reviews. Neuroscience*, 4(12), pp.1002-12.

Gerhart, J. & Keller, R., 1986. Region-specific cell activities in amphibian gastrulation. *Annual review of cell biology*, 2, pp.201-29.

Gilbert, S.F., 2006. *Developmental Biology* eighth edi.,

Glinka, A., Delius, H., Blumenstock, C. & Niehrs, C., 1996. Combinatorial signalling by Xwnt-11 and Xnr3 in the organizer ephithelium. *Mechanisms of development*, 60(2), pp.221–231.

Grande, C. & Patel, N.H., 2009. Nodal signalling is involved in left-right asymmetry in snails. *Nature*, 457(7232), pp.1007-11.

Gros, J., Feistel, K., Viebahn, C., Blum, M. & Tabin, C.J., 2009. Cell movements at Hensen's node establish left/right asymmetric gene expression in the chick. *Science (New York, N.Y.)*, 324(5929), pp.941-4.

Gurdon, J.B. & Hopwood, N., 2000. The introduction of Xenopus laevis into developmental biology: of empire, pregnancy testing and ribosomal genes. *The International journal of developmental biology*, 44(1), pp.43-50.

Hamburger, V. & Hamilton, H.L., 1992. A series of normal stages in the development of the chick embryo. 1951. *Developmental dynamics ▪ : an official publication of the American Association of Anatomists*, 195(4), pp.231-72.

Hannon, J. & Hoyer, D., 2008. Molecular biology of 5-HT receptors. *Behavioural brain research*, 195(1), pp.198-213.

Hashimoto, M. & Hamada, H., 2010. Translation of anterior-posterior polarity into left-right polarity in the mouse embryo. *Current opinion in genetics & development*, 20(4), pp.433-7.

Hashimoto, M. et al., 2010. Planar polarization of node cells determines the rotational axis of node cilia. *Nature cell biology*, 12(2), pp.170-6.

Hatayama, M., Mikoshiba, K. & Aruga, J., 2011. IP(3) signaling is required for cilia formation and left-right body axis determination in Xenopus embryos. *Biochemical and biophysical research communications*, (June), pp.1-5.

Heasman, J., 2006. Maternal determinants of embryonic cell fate. *Seminars in cell & developmental biology*, 17(1), pp.93-8.

Hojo, M. et al., 2007. Right-elevated expression of charon is regulated by fluid flow in medaka Kupffer's vesicle. *Development, growth & differentiation*, 49(5), pp.395-405.

Holowacz, T. & Elinson, R.P., 1993. Cortical cytoplasm, which induces dorsal axis formation in Xenopus, is inactivated by UV irradiation of the oocyte. *Development (Cambridge, England)*, 119(1), pp.277-85.

Hövels-Gürich, H.H., Seghaye, M.C., Däbritz, S., Messmer, B.J. & von Bernuth, G., 1997. Cardiological and general health status in preschool- and school-age children after neonatal arterial switch operation. *European journal of cardio-thoracic surgery ▪ : official journal of the European Association for Cardio-thoracic Surgery*, 12(4), pp.593-601.

Ihaka, R. & Gentleman, R., 1996. R: A Language for Data Analysis and Graphics. *Journal of Computational and Graphical Statistics*, 5(3), pp.299 - 314.

Ikeda, K., Ikeda, T., Morikawa, K. & Kamiya, R., 2007. Axonemal localization of Chlamydomonas PACRG, a homologue of the human Parkin-coregulated gene product. *Cell motility and the cytoskeleton*, 64(11), pp.814-21.

Imai, Y., Soda, M., Murakami, T., Shoji, M., Abe, K. & Takahashi, R., 2003. A product of the human gene adjacent to parkin is a component of Lewy bodies and suppresses Pael receptor-induced cell death. *The Journal of biological chemistry*, 278(51),

pp.51901-10.

Kao, K.R. & Elinson, R.P., 1989. Dorsalization of mesoderm induction by lithium. *Developmental biology*, 132(1), pp.81-90.

Kao, K.R. & Elinson, R.P., 1988. The entire mesodermal mantle behaves as Spemann's organizer in dorsoanterior enhanced Xenopus laevis embryos. *Developmental biology*, 127(1), pp.64-77.

Kartagener, M., 1933. Zur Pathogenese der Bronchiektasien. I. Mitteilung: Bronchiektasien bei Situs viscerum inversus. *Beiträge zur Klinik und Erforschung der Tuberkulose und der Lungenkrankheiten*, 83, pp.489-501.

Kawasumi, A., Nakamura, T., Iwai, N., Yashiro, K., Saijoh, Y., Belo, J.A., Shiratori, H. & Hamada, H., 2011. Left-right asymmetry in the level of active Nodal protein produced in the node is translated into left-right asymmetry in the lateral plate of mouse embryos. *Developmental biology*, 353(2), pp.321-330.

Keller, R.E., 1981. An experimental analysis of the role of bottle cells and the deep marginal zone in gastrulation of Xenopus laevis. *The Journal of experimental zoology*, 216(1), pp.81-101.

Kessler, D.S., 1997. Siamois is required for formation of Spemann's organizer. *Proceedings of the National Academy of Sciences*, 94(24), pp.13017-13022.

Khokha, M.K. et al., 2009. Rapid gynogenetic mapping of Xenopus tropicalis mutations to chromosomes. *Developmental dynamics ▪ : an official publication of the American Association of Anatomists*, 238(6), pp.1398-46.

Klein, S.L., 1987. The first cleavage furrow demarcates the dorsal-ventral axis in Xenopus embryos. *Developmental biology*, 120(1), pp.299-304.

Kramer-Zucker, A.G., Olale, F., Haycraft, C.J., Yoder, B.K., Schier, A.F. & Drummond, I. a, 2005. Cilia-driven fluid flow in the zebrafish pronephros, brain and Kupffer's vesicle is required for normal organogenesis. *Development (Cambridge, England)*, 132(8), pp.1907-21.

Kreiling, J. a, Balantac, Z.L., Crawford, A.R., Ren, Y., Toure, J., Zchut, S., Kochilas, L. & Creton, R., 2008. Suppression of the endoplasmic reticulum calcium pump during zebrafish gastrulation affects left-right asymmetry of the heart and brain. *Mechanisms of development*, 125(5-6), pp.396-410.

Kuroda, R., Endo, B., Abe, M. & Shimizu, M., 2009. Chiral blastomere arrangement dictates zygotic left-right asymmetry pathway in snails. *Nature*, 462(7274), pp.790-4.

Landesman, Y., Goodenough, D. a & Paul, D.L., 2000. Gap junctional communication in the early Xenopus embryo. *The Journal of cell biology*, 150(4), pp.929-36.

Lane, M.C. & Keller, R., 1997. Microtubule disruption reveals that Spemann's organizer is subdivided into two domains by the vegetal alignment zone. *Development (Cambridge, England)*, 124(4), pp.895-906.

Lauder, J.M., Wallace, J.A. & Krebs, H., 1981. Roles for serotonin in neuroembryogenesis. *Advances in experimental medicine and biology*, 133, pp.477-506.

Lee, J.-Y. & Harland, R.M., 2007. Actomyosin contractility and microtubules drive apical constriction in Xenopus bottle cells. *Developmental biology*, 311(1), pp.40-52.

Lee, J.-Y. & Harland, R.M., 2010. Endocytosis is required for efficient apical constriction during Xenopus gastrulation. *Current biology ▪ : CB*, 20(3), pp.253-8.

Lemaire, P. & Kodjabachian, L., 1996. The vertebrate organizer: structure and molecules. *Trends in genetics ▪ : TIG*, 12(12), pp.525-31.

Levin, M., 2003. Motor protein control of ion flux is an early step in embryonic left-right asymmetry. *BioEssays ▪ : news and reviews in molecular, cellular and developmental biology*, 25(10), pp.1002-10.

Levin, M. & Mercola, M., 1998. Gap junctions are involved in the early generation of left-right asymmetry. *Developmental biology*, 203(1), pp.90-105.

Levin, M., Buznikov, G. a & Lauder, J.M., 2006. Of minds and embryos: left-right asymmetry and the serotonergic controls of pre-neural morphogenesis. *Developmental neuroscience*, 28(3), pp.171-85.

Levin, M., Johnson, R., Sterna, C. & Kuehn, M., 1995. A molecular pathway determining left-right asymmetry in chick embryogenesis. *Cell*, 82, pp.803-814.

Levin, M., Roberts, D.J., Holmes, L.B. & Tabin, C., 1996. Laterality defects in conjoined twins. *Nature*, 384(6607), p.321.

Lohr, J.L., Danos, M.C. & Yost, H.J., 1997. Left-right asymmetry of a nodal-related gene is regulated by dorsoanterior midline structures during Xenopus development. *Development (Cambridge, England)*, 124(8), pp.1465-72.

Long, S., Ahmad, N. & Rebagliati, M., 2003. The zebrafish nodal-related gene southpaw is required for visceral and diencephalic left-right asymmetry. *Development*, 130(11), pp.2303-2316.

Lorenzetti, D., Bishop, C.E. & Justice, M.J., 2004. Deletion of the Parkin coregulated gene causes male sterility in the quaking(viable) mouse mutant. *Proceedings of the National Academy of Sciences of the United States of America*, 101(22), pp.8402-7.

Lowe, L., Supp, D., Sampath, K. & Yokoyama, T., 1996. Conserved left–right asymmetry of nodal expression and alterations in murine situs inversus. *Nature*.

Maisonneuve, C., Guilleret, I., Vick, P., Weber, T., Andre, P., Beyer, T., Blum, M. & Constam, D.B., 2009. Bicaudal C, a novel regulator of Dvl signaling abutting RNA-processing bodies, controls cilia orientation and leftward flow. *Development (Cambridge, England)*, 136(17), pp.3019-30.

Marjoram, L. & Wright, C., 2011. Rapid differential transport of Nodal and Lefty on sulfated proteoglycan-rich extracellular matrix regulates left-right asymmetry in Xenopus. *Development (Cambridge, England)*, 138(3), pp.475-85.

Marques, S., Borges, A.C., Silva, A.C., Freitas, S., Cordenonsi, M. & Belo, J.A., 2004. The activity of the Nodal antagonist Cerl-2 in the mouse node is required for correct L/R body axis. *Genes & development*, 18(19), pp.2342-7.

Marshall, W.F. & Rosenbaum, J.L., 2001. Intraflagellar transport balances continuous turnover of outer doublet microtubules: implications for flagellar length control. *The Journal of cell biology*, 155(3), pp.405-14.

Masho, R., 1990. Close correlation between the first cleavage plane and the body axis in early Xenopus embryos. *Development, growth & differentiation*, 32(1), pp.57–64.

McGrath, J., Somlo, S., Makova, S., Tian, X. & Brueckner, M., 2003. Two populations of node monocilia initiate left-right asymmetry in the mouse. *Cell*, 114(1), pp.61-73.

Meno, C., Saijoh, Y., Fujii, H., Ikeda, M., Yokoyama, T., Yokoyama, M., Toyoda, Y. & Hamada, H., 1996. Left–right asymmetric expression of the TGFβ-family member lefty in mouse embryos. *Nature*, 381(6578), pp.151–155.

Mitchell, B., Stubbs, J.L., Huisman, F., Taborek, P., Yu, C. & Kintner, C., 2009. The PCP pathway instructs the planar orientation of ciliated cells in the Xenopus larval skin. *Current Biology*, 19(11), pp.924–929.

Mogi, K., Goto, M., Ohno, E., Azumi, Y., Takeuchi, S. & Toyoizumi, R., 2003. Xenopus neurula left-right asymmetry is respeficied by microinjecting TGF-beta5 protein. *The International journal of developmental biology*, 47(1), pp.15-29.

Moon, R.T. & Kimelman, D., 1998. From cortical rotation to organizer gene expression: toward a molecular explanation of axis specification in Xenopus. *BioEssays ▪ : news and reviews in molecular, cellular and developmental biology*, 20(7), pp.536-45.

Morel, N., 2003. Neurotransmitter release: the dark side of the vacuolar-H+ATPase. *Biology of the Cell*, 95(7), pp.453-457.

Nace, G.W., Richards, C.M. & Asher, J.H.J., 1970. Parthenogenesis and Genetic Variability. I. Linkage and Inbreeding Estimations in the Frog, RANA PIPIENS. *Genetics*, 66, pp.349-368.

Nance, J., 2005. PAR proteins and the establishment of cell polarity during C. elegans development. *BioEssays ▪ : news and reviews in molecular, cellular and developmental biology*, 27(2), pp.126-35.

Nascone, N. & Mercola, M., 1997. Organizer induction determines left-right asymmetry in Xenopus. *Developmental biology*, 189(1), pp.68-78.

Nebigil, C.G. et al., 2001. Ablation of serotonin 5-HT(2B) receptors in mice leads to abnormal cardiac structure and function. *Circulation*, 103(24), pp.2973-9.

Newport, J. & Kirschner, M., 1982. A major developmental transition in early Xenopus embryos: I. characterization and timing of

cellular changes at the midblastula stage. *Cell*, 30(3), pp.675-86.

Nguyen, T., Chin, W.C., O'Brien, J. a, Verdugo, P. & Berger, a J., 2001. Intracellular pathways regulating ciliary beating of rat brain ependymal cells. *The Journal of physiology*, 531(Pt 1), pp.131-40.

Niesler, B., 2011. 5-HT(3) receptors: potential of individual isoforms for personalised therapy. *Current opinion in pharmacology*, 11(1), pp.81-86.

Nieuwkoop, P.D. & Faber, J., 1967. *Normal table of Xenopus laevis (Daudin)* 2nd ed., Utrecht: North-Holland Publishing Co.

Nonaka, S., Shiratori, H., Saijoh, Y. & Hamada, H., 2002. Determination of left-right patterning of the mouse embryo by artificial nodal flow. *Nature*, 418(6893), pp.96-9.

Nonaka, S., Tanaka, Y., Okada, Y., Takeda, S., Harada, A., Kanai, Y., Kido, M. & Hirokawa, N., 1998. Randomization of left-right asymmetry due to loss of nodal cilia generating leftward flow of extraembryonic fluid in mice lacking KIF3B motor protein. *Cell*, 95(6), pp.829-37.

Nonaka, S., Yoshiba, S., Watanabe, D., Ikeuchi, S., Goto, T., Marshall, W.F. & Hamada, H., 2005. De novo formation of left-right asymmetry by posterior tilt of nodal cilia. *PLoS biology*, 3(8), p.e268.

Noramly, S., Zimmerman, L., Cox, A., Aloise, R., Fisher, M. & Grainger, R.M., 2005. A gynogenetic screen to isolate naturally occurring recessive mutations in Xenopus tropicalis. *Mechanisms of development*, 122(3), pp.273-87.

Ohi, Y. & Wright, C.V.E., 2007. Anteriorward shifting of asymmetric Xnr1 expression and contralateral communication in left-right specification in Xenopus. *Developmental biology*, 301(2), pp.447-63.

Okada, Y., Nonaka, S., Tanaka, Y., Saijoh, Y., Hamada, H. & Hirokawa, N., 1999. Abnormal nodal flow precedes situs inversus in iv and inv mice. *Molecular cell*, 4(4), pp.459-68.

Okada, Y., Takeda, S., Tanaka, Y., Belmonte, J.-C.I. & Hirokawa, N., 2005. Mechanism of nodal flow: a conserved symmetry breaking event in left-right axis determination. *Cell*, 121(4), pp.633-44.

Oki, S., Kitajima, K., Marques, S., Belo, J.A., Yokoyama, T., Hamada, H. & Meno, C., 2009. Reversal of left-right asymmetry induced by aberrant Nodal signaling in the node of mouse embryos. *Development (Cambridge, England)*, 136(23), pp.3917-25.

Onuma, Y., Yeo, C.-Y. & Whitman, M., 2006. XCR2, one of three Xenopus EGF-CFC genes, has a distinct role in the regulation of left-right patterning. *Development (Cambridge, England)*, 133(2), pp.237-50.

Pennekamp, P., Karcher, C., Fischer, A., Schweickert, A., Skryabin, B., Horst, J., Blum, M. & Dworniczak, B., 2002. The ion channel polycystin-2 is required for left-right axis determination in mice. *Current biology ▪ : CB*, 12(11), pp.938-43.

Pohl, B.S. & Knöchel, W., 2004. Isolation and developmental expression of Xenopus FoxJ1 and FoxK1. *Development genes and evolution*, 214(4), pp.200-5.

Purcell, E.M., 1977. Life at Low Reynolds Numbers. *American Journal of Physics*, 45(June 1976), pp.3-11.

R Development Core Team, A., 2011. The R Project for Statistical Computing. Available at: http://www.r-project.org/.

Rodríguez, N. & Renaud, F.L., 1980. On the possible role of serotonin in the regulation of regeneration of cilia. *The Journal of cell biology*, 85(2), pp.242-7.

Ryan, a K. et al., 1998. Pitx2 determines left-right asymmetry of internal organs in vertebrates. *Nature*, 394(6693), pp.545-51.

Saijoh, Y., Oki, S., Ohishi, S. & Hamada, H., 2003. Left–right patterning of the mouse lateral plate requires nodal produced in the node. *Developmental Biology*, 256(1), pp.161-173.

Sampath, K., Cheng, a M., Frisch, a & Wright, C.V., 1997. Functional differences among Xenopus nodal-related genes in left-right axis determination. *Development (Cambridge, England)*, 124(17), pp.3293-302.

Sanger, G.J., 2008. 5-Hydroxytryptamine and the gastrointestinal tract: where next? *Trends in pharmacological sciences*, (August), pp.465-471.

Sarmah, B., Latimer, A.J., Appel, B. & Wente, S.R., 2005. Inositol polyphosphates regulate zebrafish left-right asymmetry. *Developmental cell*, 9(1), pp.133-45.

Satir, P., Pedersen, L.B. & Christensen, S.T., 2010. The primary cilium at a glance. *Journal of cell science*, 123(Pt 4), pp.499-503.

Sbalzarini, I.F. & Koumoutsakos, P., 2005. Feature point tracking and trajectory analysis for video imaging in cell biology. *Journal of structural biology*, 151(2), pp.182-95.

Scharf, S.R. & Gerhart, J.C., 1980. Determination of the dorsal-ventral axis in eggs of Xenopus laevis: complete rescue of uv-impaired eggs by oblique orientation before first cleavage. *Developmental biology*, 79(1), pp.181-98.

Schmid, A. & Salathe, M., 2011. Ciliary beat co-ordination by calcium. *Biology of the cell / under the auspices of the European Cell Biology Organization*, 103(4), pp.159-69.

Schneider, I., Houston, D.W., Rebagliati, M.R. & Slusarski, D.C., 2008. Calcium fluxes in dorsal forerunner cells antagonize beta-catenin and alter left-right patterning. *Development (Cambridge, England)*, 135(1), pp.75-84.

Schweickert, A., Vick, P., Getwan, M., Weber, T., Schneider, I., Eberhardt, M., Beyer, T., Pachur, A. & Blum, M., 2010. The Nodal Inhibitor Coco Is a Critical Target of Leftward Flow in Xenopus. *Current biology ▪ : CB*, 20(8), pp.738-743.

Schweickert, A., Weber, T., Beyer, T., Vick, P., Bogusch, S., Feistel, K. & Blum, M., 2007. Cilia-driven leftward flow determines laterality in Xenopus. *Current biology ▪ : CB*, 17(1), pp.60-6.

Shen, M.M., 2007. Nodal signaling: developmental roles and regulation. *Development (Cambridge, England)*, 134(6), pp.1023-34.

Shook, D.R., Majer, C. & Keller, R., 2004. Pattern and morphogenesis of presumptive superficial mesoderm in two closely related species, Xenopus laevis and Xenopus tropicalis. *Developmental biology*, 270(1), pp.163-85.

Simard, A., Di Giorgio, L., Amen, M., Westwood, A., Amendt, B.A. & Ryan, A.K., 2009. The Pitx2c N-terminal domain is a critical interaction domain required for asymmetric morphogenesis. *Developmental Dynamics*, 238(10), pp.2459–2470.

Sive, H.L., Grainger, R.M. & Harland, R.M., 2000. *Early Development of Xenopus Laevis: a laboratory manual*, Cold Spring Harbor Laboratory Press.

Smith, W.C., McKendry, R., Ribisi, S. & Harland, R.M., 1995. A nodal-related gene defines a physical and functional domain within the Spemann organizer. *Cell*, 82(1), pp.37–46.

Sokol, S.Y., 1996. Analysis of Dishevelled signalling pathways during Xenopus development. *Current biology ▪ : CB*, 6(11), pp.1456-67.

Song, H., Hu, J., Chen, W., Elliott, G., Andre, P., Gao, B. & Yang, Y., 2010. Planar cell polarity breaks bilateral symmetry by controlling ciliary positioning. *Nature*, pp.1-6.

Spemann, H. & Falkenberg, H., 1919. Über asymmetrische Entwicklung und Situs inversus viscerum bei Zwillingen und Doppelbildungen. *Archiv für Entwicklungsmechanik der Organismen*, 45(3), pp.371-422.

Spemann, H. & Mangold, H., 1924. Über induktion von Embryonalanlagen durch Implantation artfremder Organisatoren. *Archiv für Entwicklungsmechanik der Organismen*, 100(3), pp.599–638.

Stubbs, J.L., Oishi, I., Izpisúa Belmonte, J.C. & Kintner, C., 2008. The forkhead protein Foxj1 specifies node-like cilia in Xenopus and zebrafish embryos. *Nature genetics*, 40(12), pp.1454-60.

Supp, D.M., Witte, D.P., Potter, S.S. & Brueckner, M., 1997. Mutation of an axonemal dynein affects left-right asymmetry in inversus viscerum mice. *Nature*, 389(6654), pp.963-6.

Tabin, C.J. & Vogan, K.J., 2003. A two-cilia model for vertebrate left-right axis specification. *Genes & development*, 17(1), pp.1-6.

Tanaka, Y., Okada, Y. & Hirokawa, N., 2005. FGF-induced vesicular release of Sonic hedgehog and retinoic acid in leftward nodal flow is critical for left-right determination. *Nature*, 435(7039), pp.172-7.

Tao, Q. et al., 2005. Maternal wnt11 activates the canonical wnt signaling pathway required for axis formation in Xenopus embryos. *Cell*, 120(6), pp.857-71.

Thisse, C. & Thisse, B., 1999. Antivin, a novel and divergent member of the TGFbeta superfamily, negatively regulates mesoderm induction. *Development (Cambridge, England)*, 126(2), pp.229-40.

Tietze, N., 2008. *Klonierung und vergleichende Expressionsanalyse des Parkin-co-regulated Gene (PACRG) in Embryonen von Frosch , Maus , Huhn und Kaninchen.* Universität Hohenheim.

Tran, U., Pickney, L.M., Ozpolat, B.D. & Wessely, O., 2007. Xenopus Bicaudal-C is required for the differentiation of the amphibian pronephros. *Developmental biology*, 307(1), pp.152-64.

Vandenberg, L.N. & Levin, M., 2010. Consistent left-right asymmetry cannot be established by late organizers in Xenopus unless the late organizer is a conjoined twin. *Development (Cambridge, England)*, 137(7), pp.1095-105.

Vick, P., 2009. *Left-right asymmetry in Xenopus laevis: Functional dissection of leftward flow.* Universität Hohenheim.

Vick, P., Schweickert, A., Weber, T., Eberhardt, M., Mencl, S., Shcherbakov, D., Beyer, T. & Blum, M., 2009. Flow on the right side of the gastrocoel roof plate is dispensable for symmetry breakage in the frog Xenopus laevis. *Developmental biology*, 331(2), pp.281-91.

Vonica, A. & Brivanlou, A.H., 2007. The left-right axis is regulated by the interplay of Coco, Xnr1 and derrière in Xenopus embryos. *Developmental biology*, 303(1), pp.281-94.

Wada, Y., Mogami, Y. & Baba, S., 1997. Modification of ciliary beating in sea urchin larvae induced by neurotransmitters: beat-plane rotation and control of frequency fluctuation. *The Journal of experimental biology*, 200(Pt 1), pp.9-18.

Wallingford, J.B., Ewald, a J., Harland, R.M. & Fraser, S.E., 2001. Calcium signaling during convergent extension in Xenopus. *Current biology ▪ : CB*, 11(9), pp.652-61.

Weber, T., 2006. *Charakterisierung einer durch Cilien angetriebenen vektoriellen Flüssigkeitsströmung in* Xenopus laevis *zur Brechung der bilateralen Symmetrie*. Universität Hohenheim.

Wessely, O., Tran, U., Zakin, L. & Robertis, E.M.D., 2001. Identi ® cation and expression of the mammalian homologue of Bicaudal-C. *Mechanisms of Development*, 101, pp.267-270.

West, A.B., Lockhart, P.J., O'Farell, C. & Farrer, M.J., 2003. Identification of a Novel Gene Linked to Parkin via a Bi-directional Promoter. *Journal of Molecular Biology*, 326(1), pp.11-19.

Wilhelmi, H., 1921. Experimentelle Untersuchungen über Situs inversus viscerum. *Archiv für Entwicklungsmechanik der Organismen*, 48(4), pp.517-532.

Wilson, G.R., Sim, M.L.-J., Brody, K.M., Taylor, J.M., McLachlan, R.I., O'Bryan, M.K., Delatycki, M.B. & Lockhart, P.J., 2010. Molecular analysis of the PArkin co-regulated gene and association with male infertility. *Fertility and sterility*, 93(7), pp.2262-8.

Witzgall, R., 2005. New developments in the field of cystic kidney diseases. *Current molecular medicine*, 5(5), pp.455–465.

Wolpert, L., Beddington, R.S., Brockes, J., Jessell, T. & Lawrence, P., 1997. *Principles of Development*, Oxford University Press.

Yin, Y. et al., 2009. The Talpid3 gene (KIAA0586) encodes a centrosomal protein that is essential for primary cilia formation. *Development (Cambridge, England)*, 136(4), pp.655-64.

Yu, J.-K., Holland, L.Z. & Holland, N.D., 2002. An amphioxus nodal gene (AmphiNodal) with early symmetrical expression in the organizer and mesoderm and later asymmetrical expression associated with left-right axis formation. *Evolution & development*, 4(6), pp.418-25.